

# **Analysis and fate of precursors and transformation products of per- and polyfluorinated alkyl substances (PFAS)**

## **Dissertation**

der Mathematisch-Naturwissenschaftlichen Fakultät  
der Eberhard Karls Universität Tübingen  
zur Erlangung des Grades eines  
Doktors der Naturwissenschaften  
(Dr. rer. nat.)

vorgelegt von  
M.Sc. Boris Bugsel  
aus Stuttgart

Tübingen  
2021



Gedruckt mit Genehmigung der Mathematisch-Naturwissenschaftlichen Fakultät der  
Eberhard Karls Universität Tübingen.

Tag der mündlichen Qualifikation:

19.10.2021

Dekan:

Prof. Dr. Thilo Stehle

1. Berichterstatter:

Prof. Dr. Christian Zwiener

2. Berichterstatter:

Prof. Dr. Peter Grathwohl

# Contents

Abstract .....	iii
Zusammenfassung.....	v
Danksagung .....	viii
List of abbreviations .....	x
List of publications and author contributions .....	xii
1 Introduction .....	1
1.1 An Introduction to per- and polyfluoroalkyl substances (PFAS) .....	1
1.2 Subsets of PFAS discussed in this thesis .....	2
1.3 Synthesis of PFAS .....	4
1.4 Analytical chemistry of PFAS .....	4
1.5 Rastatt case .....	6
1.6 Remediation approaches .....	6
1.7 Photochemistry .....	7
1.8 Biodegradation .....	9
1.9 Electrochemistry to mimic metabolism and TP formation.....	9
2 Aim of this Thesis.....	11
3 Material & Methods .....	13
3.1 Screening approach .....	13
3.2 Photochemical degradation experiments .....	16
3.3 Electrochemical degradation experiments .....	17
4 Results .....	19
5 Summary & Discussion .....	27
6 Outlook & Further Needs .....	29
7 Bibliography .....	31
8 LC-MS screening of poly- and perfluoroalkyl substances in contaminated soil by Kendrick mass analysis.....	38
8.1 Abstract.....	39
8.2 Abbreviations .....	39
8.3 Introduction .....	40
8.4 Materials and methods.....	42
8.5 Results and discussion .....	45
8.6 Conclusions.....	53
8.7 References.....	54

9	LC-HRMS screening of per- and polyfluorinated alkyl substances (PFAS) in impregnated paper samples and contaminated soils .....	60
9.1	Abstract.....	61
9.2	Introduction .....	61
9.3	Material & Methods .....	63
9.4	Results & Discussion .....	66
9.5	References.....	75
9.6	Supporting Information.....	80
10	Electrochemical oxidation of 6:2 polyfluoroalkyl phosphate diester – transformation products and reactions kinetics with hydroxyl radicals .....	94
10.1	Abstract.....	95
10.2	Introduction .....	97
10.3	Materials & Methods .....	99
10.4	Results & Discussion .....	103
10.5	Implications.....	111
10.6	References .....	114
10.7	Supporting Information.....	120
11	Photochemical degradation of the perfluoroalkyl carboxylic acid precursor 6:2 polyfluorinated dialkylated phosphate diester (6:2 diPAP) on mineral surfaces .....	134
11.1	Abstract.....	135
11.2	Introduction .....	135
11.3	Material & Methods .....	137
11.4	Results & Discussion .....	142
11.5	References .....	149
11.6	Supporting Information.....	153

## Abstract

Per- and polyfluoroalkyl substances (PFAS) are a man-made substance class consisting of about 4700 known individual representatives. PFAS have a wide range of applications from industrial processes to consumer products. A typical industrial application is, for example, the use of PFAS in aqueous fire fighting foams (AFFFs). However, PFAS are also used in everyday products such as water-, oil- and dirt-repellent textiles, food packaging paper and non-stick cookware. Due to their high thermal and chemical stability, PFAS are highly durable. The combination of their wide range of applications and their longevity has led to the detection of PFAS in various environmental compartments worldwide. Although some PFAS can be considered as degradable in the environment (so-called precursors), they form further poly- and perfluorinated degradation products (TPs). The final products are often perfluorinated carboxylic acids (PFCAs) or perfluorinated sulfonic acids (PFSA) which are rather persistent.

In a current case in the Rastatt / Baden-Baden region in southwest Germany, a PFAS contamination of more than 10 km<sup>2</sup> of agricultural land has occurred. The application of compost and paper sludge contaminated with PFAS presumably led to the contamination. Since no precise information is available on the identity of the individual contaminants and it is also unknown which transformation products may be formed over time, analytical screening approaches must be used to identify the contaminants.

The goals of this work therefore were to a) identify so far unknown PFAS that cause the contamination and b) to evaluate the transformation potential of the revealed contamination. This is particularly important since TPs are often mobile and can lead to contaminated plants, groundwater and drinking water.

Therefore, in the first part of this work, a screening method optimized for PFAS was developed to detect previously unknown PFAS contaminants in the fields of Rastatt / Baden-Baden. In particular, dialkylated polyfluorinated alkyl phosphates (diPAPs) of chain length 4:2 / 6:2 up to 12:2 / 14:2, N-Ethyl perfluorooctane sulfonamide ethanol-based phosphate diester (diSAmPAP) as well as TP of these two substance classes could be detected in four soil samples. Through cooperation with the organic chemistry working group (Prof. Dr. Martin E. Maier, Universität Tübingen), a reference standard

of 6:2 fluorotelomer mercapto alkyl phosphate (FTMAP) was synthesized. This standard confirmed the occurrence of 6:2 FTMAP in one soil sample, the screening suggested further homologues (6:2 / 8:2; 8:2 / 8:2; 8:2 / 10:2; 10:2 / 10:2). The established screening method was then extended to a total of 13 soil samples from the Rastatt / Baden-Baden region. Furthermore, 13 PFAS impregnated paper samples which were collected during the period when the contamination occurred were provided by project partners. They were also screened for PFAS and compared to the 13 soil samples. It could be shown that PFAS impregnated papers were based either on diPAPs or FTMAPs. By comparing the chain lengths of PFAS in the soil samples with the chain lengths of PFAS in the paper samples, it was shown that the contamination on the agricultural land could be explained by PFAS impregnated papers.

In the second part of this work, the major contaminant 6:2 diPAP was used for photochemical as well as electrochemical degradation experiments. The aim was to investigate the degradation potential of the precursor and to evaluate the potential to release mobile TPs. Since radical chemical processes involving hydroxyl radicals ( $\bullet\text{OH}$ ) are expected in both photochemistry and electrochemistry, terephthalic acid was used as a  $\bullet\text{OH}$  probe in both experimental setups to determine the steady-state concentration of  $\bullet\text{OH}$ . In the photochemical degradation experiments, the mineral phases  $\text{SiO}_2$ ,  $\text{TiO}_2$  (crystal forms rutile as well as anatase) and  $\text{FeOOH}$  were used and coated with 6:2 diPAP. Subsequently, aqueous suspensions with the mineral phases were irradiated under artificial sunlight. In all mineral phases, 6:2 fluorotelomer carboxylic acid (6:2 FTCA) was found to be the most important intermediate. After 6 hours of irradiation, it was shown for anatase that 84% of the originally spiked 6:2 diPAP was transformed to PFCAs. In electrochemical degradation experiments, PFCAs, especially perfluoroheptanoic acid (PFHpA), were also shown to be the main degradation products. Experiments at different pH values also showed that the formation of PFHpA was strongly dependent on the steady-state  $\bullet\text{OH}$  concentration. With this relationship, the bimolecular rate constant  $k_{\bullet\text{OH}, \text{diPAP}}^{\text{form PFHpA}} = 9.4 (\pm 1.4) \cdot 10^7 \text{ M}^{-1} \text{ s}^{-1}$  could be determined. This constant can be used to estimate the half-life of 6:2 diPAP when the  $\bullet\text{OH}$  equilibrium concentration is known.

## Zusammenfassung

Bei per- und polyfluorierten Alkylsubstanzen (PFAS) handelt es sich um eine menschengemachte Stoffklasse, die aus rund 4700 bekannten Einzelvertretern besteht. PFAS besitzen einen breit gestreuten Anwendungsbereich, der von industriellen Prozessen bis hin zu Verbraucherprodukten reicht. Eine typische industrielle Anwendung ist beispielsweise die Verwendung von PFAS in Feuerlöschschäumen. PFAS finden aber insbesondere auch in alltäglichen Produkten wie wasser-, fett- und schmutzabweisenden Textilien sowie Lebensmittelverpackungspapieren oder antihaftbeschichteten Kochutensilien ihre Anwendung. Durch ihre hohe thermische sowie chemische Stabilität sind PFAS dabei besonders langlebig. Die Kombination aus großer Anwendungsbreite sowie Langlebigkeit der Substanzen hat dazu geführt, dass PFAS weltweit in unterschiedlichen Umweltkompartimenten nachgewiesen wurden. Zwar können einige PFAS als in der Umwelt abbaubar betrachtet werden (sogenannte Präkursoren), allerdings bilden sie dabei weitere PFAS als Transformationsprodukte (TP). Am Ende dieser Abbaukette stehen häufig perfluorierte Carbonsäuren (PFCA) oder perfluorierte Sulfonsäuren (PFSA), die unter Umweltbedingungen als persistent betrachtet werden.

In einem gegenwärtigen Fall in der Region Rastatt / Baden-Baden liegt eine PFAS Kontamination von mehr als 10 km<sup>2</sup> landwirtschaftlich genutzter Flächen vor. Die Ausbringung von Kompost und Papierschlämmen, die mit PFAS verunreinigt waren, hat mutmaßlich zu der Belastung geführt. Da über die Identität der einzelnen Kontaminanten keine genauen Informationen vorliegen und dementsprechend ebenso wenig bekannt ist, welche Transformationsprodukte im Laufe der Zeit gebildet werden können, müssen analytische Screening-Ansätze zur Identifizierung der Kontaminanten verwendet werden.

Die Ziele der Arbeit bestanden darin, a) bislang unbekannte PFAS die die Kontamination verursachen zu identifizieren und b) das Abbaupotential der identifizierten Kontamination zu evaluieren. Dies ist insbesondere wichtig, da TP häufig mobil sind und zu Kontaminationen in Pflanzen, Grundwasser und Trinkwasser führen können.



Im ersten Teil der Arbeit wurde daher eine für PFAS optimierte Screening Methode entwickelt, mit der vorher unbekannte PFAS Kontaminanten auf den Feldern von Rastatt / Baden-Baden aufgedeckt werden konnten. Dabei konnten in vier Bodenproben insbesondere dialkylierte polyfluorierte Alkylphosphate (diPAP) der Kettenlänge 4:2 / 6:2 bis hin zu 12:2 / 14:2, dialkylierte Sulfonamidoperfluoralkylphosphate (diSAmPAP) sowie TP dieser beiden Stoffklassen nachgewiesen werden. Durch Kooperation mit der Arbeitsgruppe der organischen Chemie (Prof. Dr. Martin E. Maier, Universität Tübingen) konnte ein Referenzstandard von 6:2 Fluortelomer mercapto Alkylphosphate (FTMAP) synthetisiert werden, der das Auftreten von 6:2 FTMAP in einer Bodenprobe nachgewiesen hat und weitere Homologe (6:2 / 8:2; 8:2 / 8:2; 8:2 / 10:2; 10:2 / 10:2) nahelegt. Die etablierte Screeningmethode wurde anschließend auf insgesamt 13 Bodenproben aus der Region Rastatt / Baden-Baden ausgeweitet. Außerdem wurden 13 PFAS imprägnierte Papierproben, die im Zeitraum der Entstehung der Kontamination gesammelt wurden, durch Projektpartner zur Verfügung gestellt. Diese wurden auch auf einem Screening auf PFAS unterzogen und mit den 13 Bodenproben verglichen. Dabei konnte gezeigt werden, dass PFAS beschichtete Papiere entweder mit diPAP oder FTMAP imprägniert waren. Durch einen Vergleich der Kettenlängen der PFAS in den Bodenproben mit den Kettenlängen der PFAS in den Papierproben konnte gezeigt werden, dass die Kontamination auf den landwirtschaftlichen Flächen durch PFAS imprägnierte Papiere erklärbar ist.

Im zweiten Teil der Arbeit wurde das 6:2 diPAP, ein wesentlicher Kontaminant, als Ausgangssubstanz für photochemische sowie elektrochemische Abbauprobversuche verwendet. Dabei war es das Ziel, das Abbaupotential des Präkursors zu untersuchen und das Freisetzungspotential für mobile TP besser beurteilen zu können. Da sowohl in der Photochemie als auch in der Elektrochemie radikalchemische Prozesse mit Hydroxylradikalen ( $\bullet\text{OH}$ ) zu erwarten sind, wurde in beiden Versuchsaufbauten Terephthalsäure als  $\bullet\text{OH}$  Sonde verwendet um die Gleichgewichtskonzentration von  $\bullet\text{OH}$  zu bestimmen. Bei den photochemischen Abbauprobversuchen wurden dazu die Mineralphasen  $\text{SiO}_2$ ,  $\text{TiO}_2$  (Kristallformen Rutil sowie Anatas) sowie  $\text{FeOOH}$  verwendet und mit 6:2 diPAP beaufschlagt. In wässriger Suspension fand anschließend eine Bestrahlung unter simuliertem Sonnenlicht statt. Dabei konnte bei allen Mineralphasen die 6:2 Fluortelomercarbonsäure (6:2 FTCA) als wichtigstes

Zwischenprodukt gefunden werden. Nach einer Bestrahlung von 6 Stunden konnte für Anatas gezeigt werden, dass 84 % der ursprünglich eingesetzten 6:2 diPAP in PFCA umgewandelt wurde. Auch in den elektrochemischen Abbauversuchen konnten PFCA, insbesondere Perfluorheptansäure (PFHpA), als Hauptabbauprodukte gezeigt werden. Versuche bei unterschiedlichen pH-Werten haben darüber hinaus gezeigt, dass die Bildung von PFHpA stark von der  $\bullet\text{OH}$  Gleichgewichtskonzentration abhängig ist. Durch diesen Zusammenhang konnte die bimolekulare Reaktionskonstante  $k_{\bullet\text{OH}, \text{diPAP}}^{\text{form PFHpA}} = 9.4 (\pm 1.4) \cdot 10^7 \text{M}^{-1} \text{s}^{-1}$  ermittelt werden. Diese Konstante kann dazu verwendet werden, um bei bekannter  $\bullet\text{OH}$  Gleichgewichtskonzentration die Halbwertszeit von 6:2 diPAP abzuschätzen.

## Danksagung

An erster Stelle möchte ich meinem Doktorvater Prof. Dr. Christian Zwiener für das Ermöglichen dieser Arbeit danken. Seine überwältigende langjährige Expertise, seine stetige Unterstützung sowie die vielen fruchtbaren Diskussionen haben die Arbeit möglich gemacht und maßgeblich geformt. Für das entgegengebrachte Vertrauen in meine Arbeit möchte ich ihm außerdem ausdrücklich meinen Dank aussprechen.

Weiterhin danke ich Prof. Dr. Peter Grathwohl für die Rolle des Zweitbetreuers sowie Prof. Dr. Stefan Haderlein und Prof. Dr. Jens Bange für die Verfügbarkeit als weitere Prüfer.

Bedanken möchte ich mich beim Land Baden-Württemberg für die Förderung der EOFplus sowie FluorTECH Projekte sowie den Projektpartnern aus diesen Projekten, die ebenso zum Erfolg dieser Arbeit beigetragen haben.

Dr. Markus Schmitt möchte ich ganz herzlich für die außerordentliche Unterstützung bei der Interpretation vieler Messdaten danken. Auf seine fachliche Kompetenz war zu jeder Zeit Verlass. Ebenso danke ich Dr. Martina Werneburg, die mir in meinen Anfängen wertvolles Wissen insbesondere zu den Messgeräten vermittelt hat.

Für das angenehme Arbeitsklima danke ich weiterhin allen weiteren aktuellen sowie ehemaligen Kolleginnen und Kollegen: Vielen Dank an Jonathan Zweigle und Oliver Nied für die Abschlussarbeiten, die einen großen Teil zu dieser Arbeit beitragen haben. Vielen Dank an Stephanie Nowak für die vielen ermutigenden Gespräche sowie die stetige Unterstützung im Labor, danke an Dr. Sylvain Merel, Dr. Sascha Lege, Dr. Maximilian Müller, Dr. Selina Tisler, Rebecca Bauer, sowie Zi Wang, die für Unterstützung immer zur Verfügung standen. Klaus Röhler danke ich dabei besonders sowohl für die langjährige private sowie fachliche Unterstützung als auch für die notwendigen Ablenkungen. Dr. László Tölgyesi danke ich für detaillierte Informationen zu Messgeräten und Software sowie die Messungen in Waldbronn, die ein Teil der ersten Publikation waren. Herzlichen Dank außerdem an Prof. Dr. Martin E. Maier sowie Florian Herrmann für die Synthese von 6:2 FTMAP.

In besonderer Weise möchte ich mich bei meinen Eltern bedanken, die mich zu jeder Zeit unterstützt haben und immer beiseite standen. Zuletzt bedanke ich mich

außerordentlich bei Han-Fang Hsueh, die mich auch weit über diese Arbeit hinaus unterstützt und insbesondere in der Schreibphase eine unermessliche Hilfe war.

## List of abbreviations

•OH	hydroxyl radicals
AFFF	aqueous fire-fighting foams
BDD	boron-doped diamond (electrode)
CYP 450	cytochrome P450
Da	Dalton
diPAP	polyfluorinated dialkylated phosphate ester
diSAmPAP	N-ethyl perfluorooctane sulfonamide ethanol– based phosphate diester
EOF	extractable organic fluorine
ESI	electrospray ionization
EtFASA	N-ethyl perfluoroalkanesulfonamide
EtFASAA	N-ethylperfluoro-1-alkynesulfonamidoacetic acid
FASA	perfluoroalkanesulfonamide
FOSA	perfluorooctanesulfonamide
FTCA	fluorotelomer carboxylic acid
FTMAP	fluorotelomer mercapto alkyl phosphate
FTOH	fluorotelomer alcohol
FTUCA	fluorotelomer unsaturated carboxylic acid
HO <sub>2</sub> •	hydroperoxyl radicals
HPLC	high-performance liquid chromatography
HRMS	high-resolution mass spectrometry
IVV	Fraunhofer-Institut für Verfahrenstechnik und Verpackung
KMD	Kendrick mass defect
LTZ	Landwirtschaftliches Technologiezentrum Augustenberg
m/z	mass-to-charge ratio
MeFASA	N-methyl perfluoroalkanesulfonamide
MeOH	methanol
MFE	molecular feature extraction
MS	mass spectrometer / mass spectrometry
NMR	nuclear magnetic resonance
NADPH	nicotinamide adenine dinucleotide phosphate
O <sub>2</sub> • <sup>-</sup>	superoxide
PEEK	polyether ether ketone
PFAA	perfluoroalkyl acid
PFAS	per- and polyfluorinated alkyl substances
PFCA	perfluorinated carboxylic acid
PFOA	perfluorooctanoic acid
PFOS	perfluorooctane sulfonic acid
PFSA	perfluorinated sulfonic acid
POP	persistent organic pollutant
PP	polypropylene
QqQ	triple quadrupole

Q-TOF	quadrupole time-of-flight
rcf	relative centrifugal force
ROS	reactive oxygen species
RT	retention time
TOP	total oxidizable precursor
TP	transformation product
TPA	terephthalic acid
TZW	Technologiezentrum Wasser
UV	ultraviolet

## List of publications and author contributions

This thesis includes published, submitted and unpublished papers and manuscripts, respectively. Chapter 8 presents the published article “LC-MS screening of poly- and perfluoroalkyl substances in contaminated soil by Kendrick mass analysis” by Bugsel & Zwiener (2020). In chapter 9, the submitted article “LC-HRMS screening of per- and polyfluorinated alkyl substances (PFAS) in impregnated paper samples and contaminated soils” by Bugsel et al. is presented. Chapter 10 presents the submitted article “Electrochemical oxidation of 6:2 polyfluoroalkyl phosphate diester – transformation products and reaction kinetics with hydroxyl radicals” by Zweigle et al. In chapter 11, the unpublished article “Photochemical degradation of the perfluoroalkyl carboxylic acid precursor 6:2 polyfluorinated dialkylated phosphate diester (6:2 diPAP) on mineral surfaces” by Bugsel et al. is presented. The contents of chapters 9, 10 and 11 were already submitted or are planned to be submitted to scientific journals and might therefore be published with modifications.

### Chapter 8

**Bugsel, Boris**, and Zwiener, Christian. “LC-MS screening of poly-and perfluoroalkyl substances in contaminated soil by Kendrick mass analysis.” *Analytical and Bioanalytical Chemistry* (2020), 412, 4797-4805.

#### *Author contributions*

Boris Bugsel and Christian Zwiener planned the study. Boris Bugsel performed the experimental and analytical work, evaluated the data, programmed the Matlab code and had the main role in writing and revising the manuscript. Christian Zwiener provided constructive criticism and helped shape the research and manuscript.

### Chapter 9

**Bugsel, Boris**; Bauer, Rebecca; Herrmann, Florian; Maier, Martin E.; Zwiener, Christian. “LC-HRMS screening of per- and polyfluorinated alkyl substances (PFAS) in impregnated paper samples and contaminated soils”. Submitted for publication to: *Analytical and Bioanalytical Chemistry* (in review).

### *Author contributions*

Boris Bugsel and Christian Zwiener planned the study. Boris Bugsel and Rebecca Bauer performed the experimental and analytical work. Boris Bugsel had the main role in evaluating the data, writing and revising the manuscript. Florian Herrmann and Martin E. Maier synthesized the 6:2 fluorotelomer mercaptoalkyl phosphate standard, performed the NMR measurements and interpreted the spectra. All authors provided constructive criticism and helped shape the research and manuscript.

### **Chapter 10**

Zweigle, Jonathan; **Bugsel, Boris**; Schmitt, Markus; Zwiener, Christian. “Electrochemical oxidation of 6:2 polyfluoroalkyl phosphate diester – transformation products and reaction kinetics with hydroxyl radicals”. Submitted for publication to: *Environmental Science & Technology* (in review).

### *Author contributions*

All authors planned the study. Jonathan Zweigle had the main role in writing the manuscript and performing the electrochemical degradation experiments. Markus Schmitt had the primary role in setting up the models. All authors provided constructive criticism and helped shape the research and manuscript.

### **Chapter 11**

**Bugsel, Boris**; Schmitt, Markus; Nied, Oliver; Zwiener, Christian. “Photochemical degradation of the perfluoroalkyl carboxylic acid precursor 6:2 polyfluorinated dialkylated phosphate diester (6:2 diPAP) on mineral surfaces”. Unpublished manuscript.

### *Author contributions*

Boris Bugsel, Markus Schmitt and Christian Zwiener planned the study. Boris Bugsel had the main role in writing the manuscript and performing the photochemical degradation experiments except for experiments with goethite which were performed by Oliver Nied. Boris Bugsel, Markus Schmitt and Christian Zwiener provided constructive criticism and helped shape the research and manuscript.



# 1 Introduction

## 1.1 An Introduction to per- and polyfluoroalkyl substances (PFAS)

Per- and polyfluoroalkyl substances (PFAS) are an entirely manmade substance group of about 4700 individual compounds (OECD, 2018). PFAS are generally characterized by a carbon backbone where hydrogen atoms (H) have been replaced by fluorine atoms (F), either fully which results in perfluoroalkyl substances or partially which results in polyfluoroalkyl substances. This substitution renders PFAS unique physicochemical properties such as high thermal and chemical stability, hydrophobicity and lipophobicity (Buck et al., 2011).

The history of PFAS already begins in the 1938 with the discovery of polytetrafluoroethylene (“Teflon”) (Trier et al., 2018). Ever since then, the exceptional properties of PFAS have turned this substance class into an indispensable part in many areas of the industry and household products. For example, they are used in textiles such as carpets (Gremmel et al., 2016; Rewerts et al., 2018; Robel et al., 2017; van der Veen et al., 2020), nonstick cookware (Sinclair et al., 2007), cosmetics (Fujii et al., 2013), aqueous fire-fighting foams (AFFF) (Barzen-Hanson et al., 2017; Dubocq et al., 2019) and food packaging (Begley et al., 2008; Trier et al., 2011a; Trier et al., 2018). However, their longevity and widespread use have resulted in a worldwide distribution in the environment across air, soil, water and biota (Dreyer et al., 2009; Giesy & Kannan, 2001; Pan et al., 2018; Rankin et al., 2016; Yamashita et al., 2008). The global spreading of PFAS in combination with their toxicity (Dennis et al., 2020; Kim et al., 2013) and ability to cause endocrine disruptions (Hurley et al., 2018) is alarming. In the recent years, PFAS have continuously gained attention by scientists as a result of their environmental fate.

Arguably the two most-known PFAS, perfluorooctanoic acid (PFOA) and perfluorooctanesulfonic acid (PFOS), are thus now listed as persistent organic pollutants (POPs) in the Stockholm Convention (United Nations Environment Programme, 2001). PFOA is listed under annex A, meaning that “parties must take measures to eliminate the production and use” (United Nations Environment Programme, 2001). PFOS is listed in annex B, forcing parties to “take measures to

restrict the production and use” (United Nations Environment Programme, 2001). Already in 2002, the primary U.S. manufacturer has voluntarily phased out the production of PFOS (United States Environmental Protection Agency, 2007). While these measures did undoubtedly reduce the production volume and, as a result, the PFOS concentrations in human plasma (Yeung et al., 2013) and biota (Rigét et al., 2019), other PFAS have replaced PFOA and PFOS. As alternatives, polyfluorinated compounds have substituted perfluorinated compounds such as PFOA and PFOS (Wang et al., 2013). However, research has shown that these polyfluorinated alternatives can break down in the environment and form perfluorinated substances (Benskin et al., 2013; Chen et al., 2020; Wang et al., 2011a; Wang et al., 2009; Zhao et al., 2019).

Nowadays, more and more novel PFAS are used and detected in the environment, including anionic and zwitterionic PFAS (Nakayama et al., 2019). The sheer number of PFAS with more and more substitutes being on the market continues to pose new challenges regarding the analysis and environmental monitoring. Since the structures of novel PFAS are often secrets of the manufacturing companies (Wang et al., 2013), advanced analytical techniques are of continuously increasing importance.

In December 2020, a new EU drinking water directive was published, regulating the maximum allowed concentrations of PFAS in drinking water in two parameter values. The first parameter, “PFAS total”, allows a maximum concentration of 0.1 µg/L for the sum of 20 selected PFAS (all 20 PFAS are perfluorinated carboxylic acids (PFCAs) and perfluorinated sulfonic acids (PFSAs)). The second parameter, “Sum of PFAS”, allows a maximum concentration of 0.5 µg/L for the totality of all PFAS. EU member states have to implement this directive into national regulation within two years. From then on, it is the decision of the member states to use both or only one of the parameters (Lippitsch, 2020).


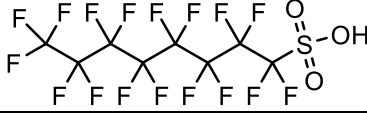
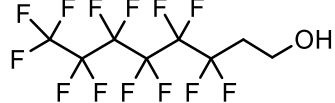
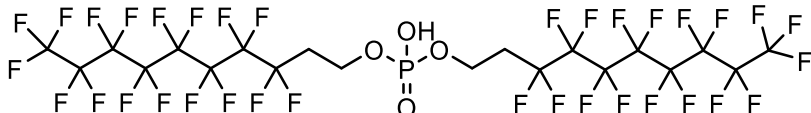
## 1.2 Subsets of PFAS discussed in this thesis

The term PFAS comprises substances with either a perfluorinated or a polyfluorinated carbon chain. They hence generally contain a  $C_nF_{2n+1}$  moiety (Buck et al., 2011). The extremely strong and stable C-F bond leads to a high stability of the compounds (Kissa, 2001). The majority of all PFAS bear a polar headgroup in addition to their

$C_nF_{2n+1}$  moiety. Common polar functional groups for example include carboxyl acids, sulfonic acids, alcohols and phosphoric acid esters (Buck et al., 2011). If all hydrogen atoms (H) in the carbon chain are substituted with fluorine atoms (F), the compound is classified as perfluorinated substance. If the compound bears single hydrogen atoms or  $CH_2$  groups within the carbon chain, it is classified as polyfluorinated substance (Buck et al., 2011).

Perfluorinated substances such as PFCAs and PFSA were commonly used PFAS in the industry until their phase out (Martin et al., 2004; Renner, 2001). Nowadays, they still occur from the transformation of other PFAS and are often referred to as “dead-end products” (Janda et al., 2019a; Janda et al., 2019b; Rewerts et al., 2018) because no further degradation in the environment is expected to occur. Two main groups of PFAS discussed in this thesis are 1) so-called precursor compounds, i.e. compounds that can break down in the environment and 2) transformation products (TPs) which are formed as an intermediate or dead-end product from the transformation of a precursor. The structure, name and acronym of selected PFAS which are discussed in this thesis are shown in Table 1.

Table 1: The structures and names of selected PFAS. PFOA and PFOS were commercially used PFAS until their phase out (Martin et al., 2004; Renner, 2001) but can also occur as typical dead-end compounds whereas 8:2 FTOH and 8:2 diPAP are precursor compounds (Benskin et al., 2013; Wang et al., 2009; Zabaleta et al., 2017).

Structure	Name (Abbreviation)
	Perfluorooctanoic acid (PFOA)
	Perfluorooctanesulfonic acid (PFOS)
	6:2 Fluorotelomer alcohol (8:2 FTOH)
	8:2 Polyfluorinated dialkylated phosphate ester (8:2 diPAP)

### 1.3 Synthesis of PFAS

For the synthesis of PFAS, two different reaction mechanisms can be used, those are electrochemical fluorination and telomerization (Martin et al., 2004). In the electrochemical fluorination process, an organic compound is dissolved in liquid hydrogen fluoride. When an electric current is applied, hydrogen is generated at the cathode and the organic compound is fluorinated (Kissa, 2001). This process leads to a mixture of both linear and branched isomers (Martin et al., 2004).

In the telomerization process, the reaction of a telogen (pentafluoroethyl iodide) with a taxogen (tetrafluoroethylene) produces isomers of the general formula  $C_2F_5(C_2F_4)_nI$ . The telomerization process therefore produces linear isomers with an even-numbered carbon chain length. In a second step,  $C_2F_5(C_2F_4)_nI$  is reacted further with ethylene to yield  $C_2F_5(C_2F_4)_nCH_2CH_2I$  (Kissa, 2001). The number of fluorinated carbon atoms and hydrogenated carbon atoms are characteristic for the nomenclature of PFAS which are produced in the telomerization process: For example, 8:2 FTOH bears 8 fully fluorinated carbon atoms and 2 hydrogenated carbon atoms. In compound classes which bear two fluorinated carbon chains such as the polyfluorinated phosphate diesters (diPAPs), these two chains can either be of the same length (e.g. 6:2 / 6:2 diPAP) or of different length (e.g. 6:2 / 8:2 diPAP) (Buck et al., 2011).

### 1.4 Analytical chemistry of PFAS

A modern technique to reliably qualify and quantify environmental contaminants is by coupling high performance liquid chromatography (HPLC) with mass spectrometry (MS). With HPLC, a mixture of compounds can be separated into its individual components by the interactions of analytes with a stationary phase. Liquid chromatography can be performed as normal phase (unpolar mobile phase, polar stationary phase) or reversed phase (polar mobile phase, unpolar stationary phase) chromatography. Typically, the majority of the applications use reversed phase chromatography (Moldoveanu & David, 2013).

After the separation of the analytes by liquid chromatography, their mass can be measured by mass spectrometry. Target screening approaches, i.e. the detection and typically quantification of selected analytes is usually performed by coupling HPLC

with a triple quadrupole (QqQ) mass spectrometer. For the correct quantification of target analytes, the development of target methods and the use of reference substances are crucial. QqQ type mass spectrometers are designed to achieve low detection limits, their drawback however is a low resolution (unit resolution) which requires the selection of analytes prior to the measurement. This drawback can be overcome by high-resolution mass spectrometry (HRMS) types such as quadrupole time-of-flight (Q-TOF) type instruments which offer high resolving power (usually in the low ppm range). The high resolving power and mass accuracy allows the deduction of possible chemical formulas from a measured accurate mass. Q-TOF instruments can hence be used for the screening of analytes (“Non-Target Screening”), i.e. the detection of analytes that are unknown prior to the measurement.

In the past years, the focus of PFAS analysis in environmental samples from routine laboratories was mostly put on PFCAs, PFSA and few selected other PFAS as given in methods provided by the environmental protection agency (Shoemaker & Tettenhorst, 2018) or the *Deutsches Institut für Normung* (DIN 38414-14:2011-08, 2018). While these methods are sensitive towards the target analytes, other PFAS which are not covered by the used method are not captured and may be missed completely. Target methods of course are not limited to the compounds provided by the methods mentioned above, they are however limited by the availability of the reference compounds which are inalienable for use of target analysis. Since reference compounds do not exist for many PFAS, the use of HRMS is crucial in the detection of complex PFAS patterns.

To estimate the extent of PFAS contaminations without information on the identity of the compounds, sum parameters such as the EOF (extractable organic fluorine) or the TOP (total oxidizable precursor) assay were developed (Houtz & Sedlak, 2012; Janda et al., 2019b; Kaiser et al., 2020). The principle behind both techniques is the transformation of unknown substances to known, measurable compounds. Briefly, EOF works by separating the inorganic fluorine from the organic fluorine. The organic fluorine can subsequently be measured via combustion ion chromatography (Kaiser et al., 2020). The TOP assay on the other hand is specific for compounds with perfluoroalkyl moieties and works by an oxidation with peroxodisulfate. As a result, the perfluoroalkyl moieties are oxidized to PFCAs which can then be quantified by HPLC-

QqQ (Janda et al., 2019b). Both of these techniques can estimate the overall concentration of PFAS in a sample, however, they do not provide information on the identity of the compounds.

## 1.5 Rastatt case

A prominent case is the “Rastatt case” in Baden-Württemberg in southwest Germany. In 2013, PFAS were detected in a drinking water well in Rastatt (Regierungspräsidium Karlsruhe, 2018). Further research showed that this contamination supposedly originated from the application of PFAS contaminated compost mixed with paper fibers on agricultural land (Biegel-Engler et al., 2017). In total, 10.45 km<sup>2</sup> of land were found to be contaminated with PFAS from the application of compost (Regierungspräsidium Karlsruhe, 2020). The application of pure, uncontaminated paper fibers on soil normally is unproblematic and can serve as organic amendment (Bellamy et al., 1995). In this particular case study however, the paper was supposedly impregnated with PFAS (Biegel-Engler et al., 2017). Over time, precursors on the paper have presumably been transformed to perfluoroalkyl acids (PFAAs) which are mobile and have hence led to polluted groundwater and also polluted plants (Brendel et al., 2018). As a result, the water works needed to upgrade their facilities with charcoal filters and crops which exceeded the thresholds of maximum allowed concentrations could not be used as food (Brendel et al., 2018). In the top soil layer (0 cm – 30 cm), 6:2 / 6:2 diPAP, 8:2 / 8:2 diPAP, N-ethyl perfluorooctane sulfonamide ethanol-based phosphate diester (diSAmPAP) and PFAAs were identified as contaminants in the year 2018 (Söhlmann et al., 2018). The gap between the sum concentration of these contaminants and the EOF was estimated to be between 52 % and 75 % (Söhlmann et al., 2018).

## 1.6 Remediation approaches

The remediation of contaminated soil can be divided into *in situ* and *ex situ* treatment technologies. *In situ* corresponding to the treatment of the soil within its original place while for an *ex situ* remediation, the soil is excavated and not treated in its original place. Soil washing is one possible *ex situ* treatment method where the contaminated soil is excavated and then washed with water in a tank. The wash water and soil are

then separated and the water then needs to be treated separately. Stabilization of contaminants is another possible method and describes the binding by both physical and chemical methods and immobilization of contaminants and can be performed both *in situ* and *ex situ* (Environmental Protection Agency, 2007). For example, activated carbon as immobilizing agent reduces both mobility and bioavailability of PFAS and therefore reduces the transfer of PFAS to plants and leaching to potable water (Bolan et al., 2021).

Another conventional treatment method for instance is the replacement of the contaminated soil with new, clean soil. This treatment however brings up the challenge to treat the contaminated soil without producing secondary pollutions (Sharma et al., 2018).

Studies particularly for PFAS have furthermore for example suggested thermal desorption as one possibility (Söregård et al., 2020). In bench-scale experiments, Söregård et al. (2020) found that at 550 °C more than 70 % of PFAS from contaminated soil could be removed by thermal desorption. However, the applicability on a large field scale as in Rastatt is highly questionable. According to Söregård et al. (2020), energy costs will be the limiting factor. Another technique which is discussed is so-called phytoremediation, i.e. the enrichment and removal of contaminants in plants (Gobelius et al., 2017). However, with investigated removal rates for PFAS in the low  $\text{g} \cdot \text{a}^{-1} \cdot \text{ha}^{-1}$  range, the removal by plants is slow and only a solution on the long term.

For both contaminated groundwater and drinking water, activated carbon can be applied to remove PFAS from the water by sorption onto the carbon (McCleaf et al., 2017; McGregor, 2018). Furthermore, membrane filtration techniques such as nanofiltration were shown to effectively remove PFAS from water (Franke et al., 2019).

## 1.7 Photochemistry

Photodegradation processes generally can be divided into direct photolysis and indirect photolysis. For direct photolysis, the target compound needs to absorb light of sufficient energy which finally leads to photolysis. Indirect photolysis describes the process when light is absorbed by a sensitizer which finally can transfer the excitation

energy directly to the target compound or can produce reactive intermediates which finally react with the target compound (Georgiou et al., 2015).

In order to undergo direct photolysis under environmental conditions, a compound needs to absorb light from the solar spectrum which reaches the earth's surface. This is typically in the range from 290 to 600 nm (Schwarzenbach et al., 2016). Absorbance in this range typically occurs in molecules with delocalized  $\pi$ -electron system, i.e. molecules with aromatic rings and conjugated double bonds. If a compound absorbs light in the mentioned range, electrons from bonding or non-bonding orbitals may get excited to antibonding orbitals ( $\pi^*$ ). When that happens, the molecule is in an excited state where its reactivity is increased. Subsequent reactions from the excited state may include heat transfer, luminescence and fragmentation (Schwarzenbach et al., 2016). Since the majority of PFAS typically neither contain aromatic rings nor conjugated double bonds, they are not expected to be susceptible to direct photolysis (see selected PFAS in Table 1).

In indirect photolysis, compounds other than the compound of interest absorb light and, as a result of their excitement, can form various reactive species such as superoxide radicals ( $\text{HO}_2^\bullet$ ), superoxide anions ( $\text{O}_2^{\bullet-}$ ) or hydroxyl radicals ( $\bullet\text{OH}$ ). Reactive species with oxygen are often summarized as reactive oxygen species (ROS). Typical naturally occurring compounds which may induce indirect photolysis include dissolved organic matter, nitrate and various iron complexes. Typically, organic pollutants can be oxidized by transient photooxidants like ROS. Since ROS are constantly produced and removed by rather fast reactions, their steady-state concentrations are typically low and can be measured by reactions with suitable probe molecules that selectively react with ROS and form specific TPs (Schwarzenbach et al., 2016). For example, terephthalate (TPA) was found to be a suitable probe molecule for  $\bullet\text{OH}$  (Page et al., 2010). Page et al. (2010) found that TPA reacts selectively with  $\bullet\text{OH}$  under the formation of hydroxyterephthalate as shown in Figure 1. Since TPA does not undergo direct photolysis, it is a suitable probe molecule for the detection of  $\bullet\text{OH}$ .



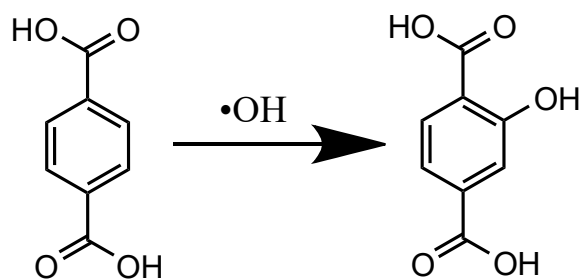


Figure 1: Formation of hydroxyterephthalic acid from terephthalic acid with •OH

## 1.8 Biodegradation

In the environment, biotransformation can play a significant role in the fate of micropollutants as also shown for PFAS precursors (Harding-Marjanovic et al., 2015; Mejia-Avendaño et al., 2016; Yi et al., 2018). Biotransformation can generally be divided into phase I and phase II metabolism (Gibson & Skett, 2013). Phase I metabolism includes oxidation, reduction, hydrolysis, hydration, dethioacetylation and isomerization, phase II metabolism includes sulfation, methylation and acetylation among other reactions (Gibson & Skett, 2013). Enzyme catalyzed oxidations are the most important phase I metabolism pathways, among which cytochrome P450 (CYP450) is the most important enzyme which performs these oxidations (Johansson et al., 2007). CYP450 enzymes are monooxygenases which means that the incorporation of a single oxygen atom from O<sub>2</sub> into substrates is catalyzed by those enzymes. The other oxygen atom is reduced by two electrons from nicotinamide adenine dinucleotide phosphate (NADPH) and yields H<sub>2</sub>O (Johansson et al., 2007).

## 1.9 Electrochemistry to mimic metabolism and TP formation

Electrochemistry has, to a limited extent, been shown to be able to mimic catalyzed oxidations performed by CYP450 (Jurva et al., 2003). This shows that electrochemistry hence can be used as a practical tool to mimic biological transformation processes in a controlled environment in the laboratory.

A typical electrochemical setup consists of the electrochemical cell with an anode, a cathode and a reference electrode. This is schematically shown in Figure 2. Boron-

doped diamond (BDD) electrodes are widely used as anode material as they showed effective transformation of compounds (Barisci & Suri, 2020; Carter & Farrell, 2008; Ochiai et al., 2011). By applying a potential, two different reaction pathways are possible: 1) on the BDD surface,  $\bullet\text{OH}$  are generated and can be released into the bulk solution where they can react with organic substances; 2) organic substances can directly be oxidized on the BDD surface (Martinez-Huitle & Ferro, 2006).

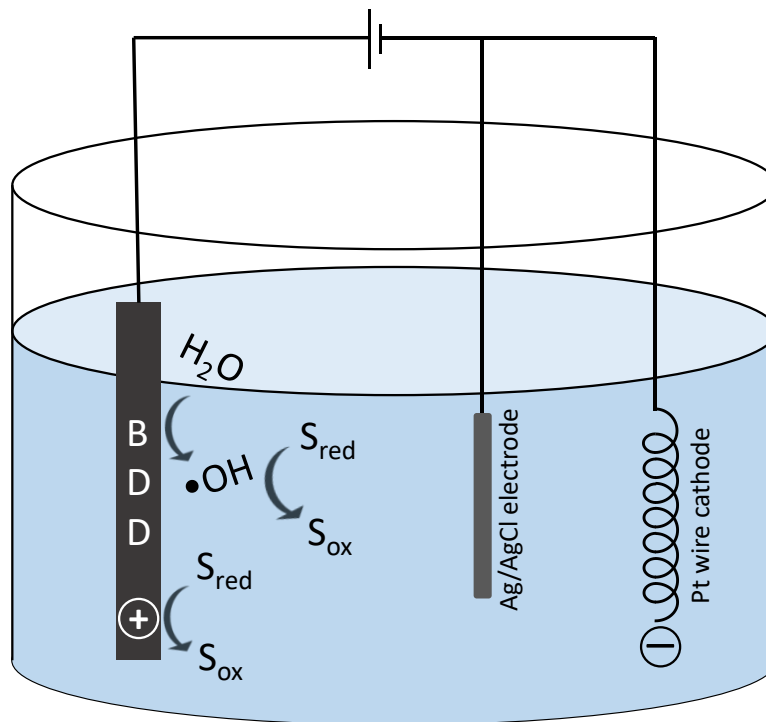


Figure 2: A typical setup of an electrochemical cell. A BDD electrode acts as anode material, a platinum wire as counter cathode and a Ag/AgCl electrode as reference electrode. Reduced organic substances ( $S_{\text{red}}$ ) can be oxidized ( $S_{\text{ox}}$ ) by either direct oxidation on the BDD surface or by reaction with  $\bullet\text{OH}$ .

## 2 Aim of this Thesis

The contaminated field site in Rastatt / Baden-Baden is a major concern for people in the affected area. The disposal of PFAS contaminated paper sludge on agricultural land has presumably led to the contamination. However, the identity and the mass of a large fraction of PFAS is still unknown. Furthermore, there are still open questions on the sources of the contamination. Environmental processes can transform precursor PFAS, the resulting TPs such as PFCAs are typically more mobile which has led to contaminations in plants, groundwater and drinking water. This opens up questions on the identity of TPs which are formed from precursors by environmental processes, on the relevance and kinetics of the processes which form these TPs and on their transport behavior in the underground.

Sum parameters such as the EOF or TOP assay are able to estimate the overall PFAS contamination in different matrices, but are not able to deliver answers on the chemical structures of contaminants. Large gaps between the EOF parameter and the sum of the concentrations known from target analysis raised questions on the identity and occurrence of further PFAS which are not considered by target analysis so far.

To be able to estimate the impacts on both the environment and people in the region of Rastatt / Baden-Baden, a more detailed characterization of the contamination is crucial. As described earlier, the fate of PFAS in the environment is greatly affected by compound properties and structure. For example, PFOA tends to be much more mobile than its precursor 8:2 diPAP (both shown in Table 1) and has led to polluted groundwater whereas 8:2 diPAP was only detected in the top soil layer (Söhlmann et al., 2018). This demonstrates that in order to assess and predict issues associated with this environmental scandal in Rastatt / Baden-Baden, detailed information on the identity of the contaminants and their fate are crucial.

The major aims of this thesis therefore were to

- a) characterize the PFAS contamination by screening approaches using LC coupled to HRMS. This provides accurate mass information on the analytes and can be used for the identification of contaminants.

- b) use electrochemistry to characterize PFAS and their potential to form environmentally relevant mobile TPs which may contribute to the contamination of groundwater, drinking water and plants. The screening method using HRMS is applied here to identify intermediate and final TPs.
- c) identify possible sources of the PFAS contamination by a characterization of PFAS patterns (classes and individual homologues) in soil samples and to compare these patterns to those from PFAS impregnated paper products. This comparison tests the hypothesis that PFAS contaminated paper sludge has caused the contamination.
- d) test the hypothesis that photodegradation is a relevant environmental process in the transformation of PFAS. The important process parameters, relevant intermediate and final TPs are investigated.

## 3 Material & Methods

### 3.1 Screening approach

In this section, the applied procedure in the detection of previously unknown contaminants is described. All used soils were kindly supplied by the Landwirtschaftliches Technologiezentrum Augustenberg (LTZ), the paper samples were provided by the Fraunhofer-Institut für Verfahrenstechnik und Verpackung (IVV). In order to detect a large variety of possible compounds, a generic extraction method for the samples needed to be applied. Therefore, methanol (MeOH) was used as an extraction solvent since MeOH has shown to be a suitable extraction solvent for PFAS (Ahmadireskety et al., 2021). Detailed information on the exact procedure of the extractions are given in chapters 8 and 9. In order to apply a screening of the extracted samples, they were measured by HPLC (1260 and 1290, Agilent Technologies, Waldbronn, Germany) coupled to a Q-TOF instrument (6550, Agilent Technologies, Santa Clara, USA).

All samples were measured in scan mode with a wide mass-to-charge ( $m/z$ ) ratio window between 100 and 1700. This was done in order to ensure that also long chained PFAS are covered by the screening method. The screening method was also performed in both positive and negative ionization mode (ESI). As mobile phase, a mixture of water and MeOH as solvent was used (bottle A: 95/5 H<sub>2</sub>O/MeOH (v/v), bottle B: 95/5 MeOH/H<sub>2</sub>O (v/v)). Ammonium acetate was used as buffer additive in both the aqueous and organic mobile phase. For detailed information on MS settings, buffer concentration, used columns and chromatographic separation, see the respective chapters 8, 9, 10 and 11. After the measurement of the samples via LC-HRMS, a molecular feature extraction (MFE) was applied. This algorithm automatically deconvolutes the data and proposes compounds (so-called features) to be present in the measured samples. Information on the compounds supplied by the MFE algorithm include their  $m/z$ , peak area and retention time. The identity of the features however remains undetermined. In this work, various techniques to discover the identity of the compounds suggested by the MFE are applied.

In order to detect PFAS in the samples, two characteristics of PFAS were used. The first characteristic is their occurrence in so-called homologous series. This means that PFAS, as the name already suggests, are substances with functional groups and varying length of the alkyl chain. For example, the compound class PFCAs consists of a carboxylic acid functional group and a  $F_3C-(CF_2)_n$ - alkyl chain. Typically, PFAS do not occur as single substance but they mutually occur with varying numbers of the repeating unit  $n$ . Since the masses of the individual compounds of the PFCAs substance class therefore all vary by 49.9968 Da (the exact mass of  $CF_2$ ), the dataset gained from the MFE algorithm can be examined for compounds with mass differences of 49.9968 Da.

This procedure was already applied on hydrocarbons by Edward Kendrick decades ago (Kendrick, 1963). To facilitate the detection of these homologous series, Kendrick suggested the use of “Kendrick masses” for molecules which are modified from the exact masses used in the periodic table. These Kendrick masses are calculated as shown in Equation 1.

$$\text{Kendrick mass} = \text{observed mass} \cdot \frac{\text{nominal mass (repeating unit)}}{\text{exact mass (repeating unit)}} \quad (1)$$

where the observed mass is the accurate mass measured by HRMS, exact mass (repeating unit) is the mass of the repeating unit as it can be deduced from the periodic table (in the case of  $CF_2$ :  $12.0000 \text{ Da} + 2 \cdot 18.9984 \text{ Da} = 49.9968 \text{ Da}$ ) and nominal mass (repeating unit) is the to the next integer rounded mass (in the case of  $CF_2$ : 50 Da). In a second step, a Kendrick mass defect (KMD) can be calculated from the Kendrick masses as shown in Equation 2.

$$\text{Kendrick mass defect} = \text{Kendrick mass} - \text{nominal Kendrick mass} \quad (2)$$

where nominal Kendrick mass is the to the nearest integer rounded calculated Kendrick mass. When these calculations are applied to all features obtained from the MFE, compounds whose masses only differ by the mass of the repeating unit become visible: For example, the four homologues perfluorohexanoic, -heptanoic, -octanoic

and -nonanoic acid all have a KMD of  $-1.96 \cdot 10^{-4}$ . When these features are now plotted in a  $m/z$  vs KMD graph, all compounds that have the same KMD value – i.e. compounds that only vary by the number of their repeating units – align horizontally. This is shown in Figure 3 as an example for various homologues of PFCAs, diPAPs, PFSA and FTOHs.

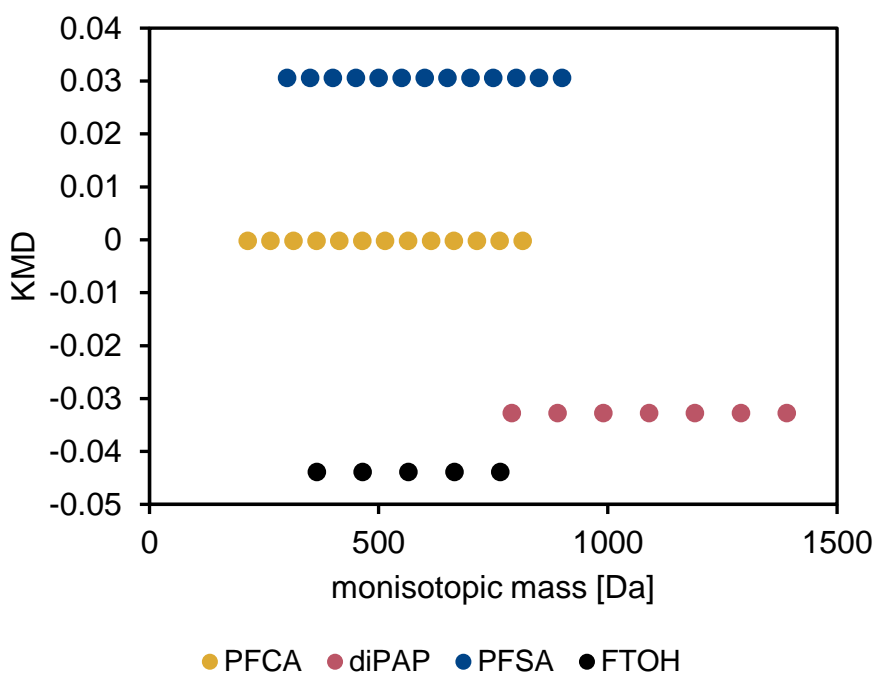


Figure 3: A Kendrick mass defect plot of the four different compound classes PFCAs ( $C_4 - C_{16}$ ), diPAPs ( $6:2 / 6:2 - 12:2 / 12:2$ ), PFSA ( $C_4 - C_{16}$ ) and FTOHs ( $6:2 - 14:2$ ). A horizontal alignment in the plot indicates compounds from the same compound classes.

Furthermore, for every  $CF_2$  unit which is added to the molecule, the hydrophobicity is increased. This is expected to result in an increasing chromatographic retention time (RT) with an increasing  $m/z$  ratio.

The second telltale characteristic of PFAS is their negative mass defect. The mass defect of compounds is the difference between their exact mass and the nominal mass. In PFAS, this negative mass defect typically arises from the high number of fluorine atoms (18.9984 Da). Typically, a positive mass defect is due to hydrogen atoms (1.0078 Da). In PFAS however, hydrogen atoms are largely or entirely substituted by fluorine atoms. Since carbon (12.0000 Da) does not contribute to the mass defect, the overall mass defect is largely influenced from the fluorine atoms and, as a result, often negative (Trier et al., 2011b). To exclude unwanted features (false

positives or compounds other than PFAS) the features from the MFE can be reduced by applying a mass defect filter between - 0.25 Da and + 0.1 Da. This range can be justified by the curated OECD database for PFAS where 92.8 % of all entries lie in that range (Alygizakis, 2019). The term curated means that this database only contains entries which are relevant for mass spectrometry, i.e. compound mixtures and different salts such as ammonium, sodium or potassium salts of the same compound are removed from this database.

While the feature list can rather easily be filtered for negative mass defect features with the software (Qualitative Analysis B.07.00, B.08.00 and 10.0) provided from Agilent Technologies, the screening for homologous series including an identification of the compounds is more challenging. To accomplish this task, a code "FindSeries" was programmed with Matlab (MathWorks, Natick, USA). This code automatically 1) calculates the KMD for all features, 2) sorts all features in clusters according to identical KMD (including a tolerance which can be defined by the user; 3 mDa were used for this work), and 3) suggests the identity of the features by comparing their measured accurate mass with exact masses from the curated OECD database.

### 3.2 Photochemical degradation experiments

All photochemical degradation experiments were performed in an artificial sunlight chamber (UVACUBE 400, Hoenle UV Technology, Gräfelfing, Germany) equipped with a SOL 500 RF2 solar simulator and an H2 filter glass. To investigate the photochemical behavior of precursor compounds, a traditional setup where the investigated compound is prepared as aqueous solution is not applicable. This is due to the fact that precursor compounds tend to be highly hydrophobic and are poorly soluble in water (for example, around 1 µg/L for 6:2 / 6:2 diPAP (Wang et al., 2011b)). Instead of introducing the precursor in the aqueous phase, typically occurring mineral phases in soils were coated with the precursor. The coating was performed by mixing the mineral phase (100 mg silicium dioxide, 20 mg titanium dioxide in both anatase and rutile crystalline form, 20 mg goethite) with 20 mL of a methanolic solution which contained 50 µg of the precursor 6:2 / 6:2 diPAP in a glass vessel. A subsequent evaporation of the solvent under constant sonication then left the precursor as a coating on the particles.



The dried, coated particles were then mixed with ultrapure water (100 mL) and spiked with TPA (10 mM) as a probe for photochemically generated  $\bullet\text{OH}$ . The resulting suspension was then placed in the artificial sunlight chamber and constantly stirred with a battery powered magnetic stirrer. The evaporated water due to elevated temperatures (up to 29 °C) in the chamber was measured gravimetrically and refilled before every sampling. For PFAS samples, 100  $\mu\text{L}$  of the suspension were taken and mixed with 900  $\mu\text{L}$  MeOH in a 2 mL polypropylene (PP) tube. After the last sample, the glass vessels with the suspensions were fully dried overnight by placing them in an oven at 70 °C. The dried particles were then extracted with 100 mL of a 90/10 MeOH/H<sub>2</sub>O (v/v) mixture by placing them in an ultrasonic bath for 60 min. The vessels were sealed with aluminum foil to prevent evaporation of the solvent, a potential loss was measured gravimetrically. After sonication, another sample was taken from the suspension to determine the leftover 6:2 / 6:2 diPAP concentration.

For TPA samples, 180  $\mu\text{L}$  of the suspension were taken and mixed with 20  $\mu\text{L}$  10 mM NaH<sub>2</sub>PO<sub>4</sub> in a glass vial in order to ensure a full desorption of potentially sorbed TPA. Both sample types were mixed at maximum available speed (13.000 rpm for PP tubes, 8.300 rpm for glass vials, 15 minutes each). TPA samples were analyzed by HPLC-UV (for details, see chapter 11), PFAS samples were analyzed by both HPLC-QqQ for target analysis and HPLC-QTOF for screening. The Matlab code FindSeries was used to screen for potentially generated TPs which were not covered by the target method. Further details on LC-MS parameters can be found in chapter 11.

### 3.3 Electrochemical degradation experiments

In blank pre-studies which were performed in a polyether ether ketone (PEEK) cell supplied by the manufacturer (Condias, Itzehoe, Germany), the formation of various PFAS such as perfluorooctane sulfonamide (FOSA) was observed. This led to the assumption that the electrochemical cell is not made out of pure PEEK, but rather PEEK with either intentional or unintentional contents of PFAS. In all following experiments, glass beakers were used as electrochemical cell. To maintain the electrode spacing between the experiments, a cover for the beaker with holes for the

electrodes was used. Here, blank experiments did not show the production of PFAS which confirms the suitability of glass beakers for the experiments.

An electrochemical cell is typically filled with an aqueous solution with the compound to be investigated. Similar to the photochemical degradation experiments, a pure aqueous solution cannot be used for PFAS precursors due to their low water solubility. Therefore, the same procedure as in the photochemical degradation experiments was applied where the precursor was first sorbed on particles which served as carrier. 40 µg of the precursor 6:2 / 6:2 diPAP in 20 mL MeOH were mixed with 100 mg silica gel (SiO<sub>2</sub>) in a 100 mL beaker. The same beaker was later on used as the electrochemical cell. Under constant stirring, the MeOH was evaporated, which left the precursor 6:2 diPAP sorbed on the silica gel. The dried particles were then mixed with 40 mL 20 mM ammonium formate buffer made from LC-MS grade water. Depending on the experiment, the pH was adjusted to 6, 9.5 or 12 with H<sub>3</sub>PO<sub>4</sub> and NaOH. Prior to the electrochemical oxidation, the suspension was spiked with TPA (10 mM) as an •OH probe.

Electrochemical degradation experiments were performed using an Autolab PGSTAT 101 potentiostat (Metrohm, Herisau, Switzerland) at 2 V, 2.5 V and 3 V. A BDD (Condias, Itzehoe) with an area of 4.4 cm<sup>2</sup> and 10 µm diamond layer on niobium base was used as working electrode. A 0.5 mm platinum spiral wire was used as counter electrode and an Ag/AgCl electrode as reference electrode. All potentials were referenced against Ag/AgCl, the electrode spacing was 2.5 cm. For PFAS samples, 200 µL were withdrawn from the suspension and mixed with 200 µL MeOH in a PP vial. For TPA samples, 200 µL were withdrawn in a glass microinlet vial. Both sample types were centrifuged at 1800 rcf (relative centrifugal force) for 15 min.

## 4 Results

This chapter summarizes the individual papers and manuscripts in chapter 8, 9, 10 and 11. In **chapter 8**, the goal was to identify previously unknown contaminants in the contaminated region in Rastatt / Baden-Baden. Therefore, a screening of four different soil samples from the contaminated region in Rastatt / Baden-Baden was performed. In total, 61 individual PFAS from twelve different compound classes could be identified with negative ESI. The identification was performed based on accurate mass measurements including comparisons with PFAS databases, as well as the detection of homologous series based on Kendrick mass analysis with the Matlab code "FindSeries". Homologous series were manually verified by the retention time trend. No compounds were confirmed in positive ESI. Among the identified substances are multiple homologues of the diPAPs (4:2 / 6:2 up to 12:2 / 14:2) and three homologues of the diSAmPAPs (C<sub>7</sub>/C<sub>8</sub>, C<sub>8</sub>/C<sub>8</sub>, C<sub>8</sub>/C<sub>9</sub>), with 98 % estimated to be C<sub>8</sub>/C<sub>8</sub> based. Both of these substance classes are known to be used as paper impregnation agents (Trier et al., 2011a). Furthermore, various transformation products of the two precursor classes could be found. Detected TPs of the diPAPs include fluorotelomer unsaturated carboxylic acids (n:2 FTUCAs), n:3 perfluoroalkyl carboxylic acids (n:3 PFCAs) and PFCAs. Detected TPs from diSAmPAP include EtFASAA (C<sub>8</sub>), MeFASA (C<sub>8</sub>), EtFASA (C<sub>8</sub>), FASA (C<sub>8</sub>) and PFSA (C<sub>6</sub> – C<sub>10</sub>). Figure 4 shows the results for a soil sample in a KMD plot based on CF<sub>2</sub> units. Different colors of the horizontally aligned homologous series are used to distinguish them from one another. The filling of the data points goes from dark (early RT) to pale (late RT) and indicates the normalized RT.

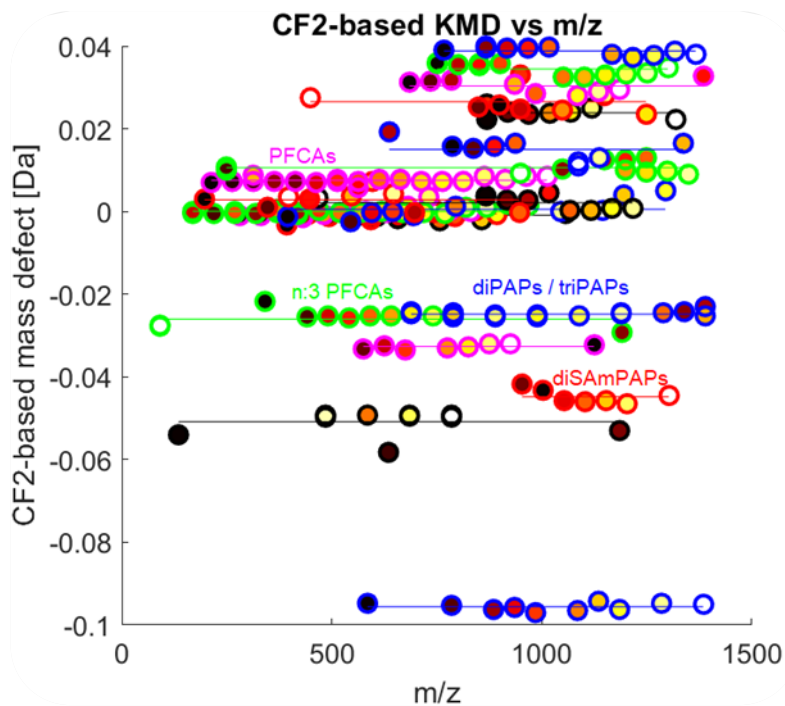


Figure 4: KMD plot for  $\text{CF}_2$  repeating units of a contaminated soil sample. Only homologous series with at least seven individual homologues are shown. Different colors of the circles represent different homologous series, the filling of the dots represents the normalized RT from dark (early RT) to pale (late RT).

The applied analytical screening approach was able to identify a much broader range of homologous diPAPs (4:2 / 6:2 up to 12:2 / 14:2) while only the 6:2 / 6:2 and 8:2 / 8:2 homologues were identified as contaminants before the screening (Söhlmann et al., 2018). Only a single authentic standard was required to identify further homologues of the same compound class based on Kendrick mass analysis and systematic RT shifts. In **additional results** which are not part of chapter 8, the response factors of 6:2 / 6:2 diPAP and 8:2 / 8:2 diPAP were used to estimate the concentrations of the newly identified homologues in one soil sample. For this particular sample, the concentrations of those two homologues were quantified (41  $\mu\text{g}/\text{kg}$  and 160  $\mu\text{g}/\text{kg}$  for 6:2 / 6:2 diPAP and 8:2 / 8:2 diPAP, respectively) and provided by the project partner Technologiezentrum Wasser (TZW), Karlsruhe. Based on the assumption that all homologues have the same response factor, a total of more than 600  $\mu\text{g}/\text{kg}$  diPAP was estimated. This is shown in Figure 5. This semi-quantitative approach was able to reduce the unknown fraction of the EOF to less than 20 %.

These results indicate that the diPAP substance class with homologues in the range from 4:2 / 6:2 up to 12:2 / 14:2 is a major contaminant in the investigated samples.

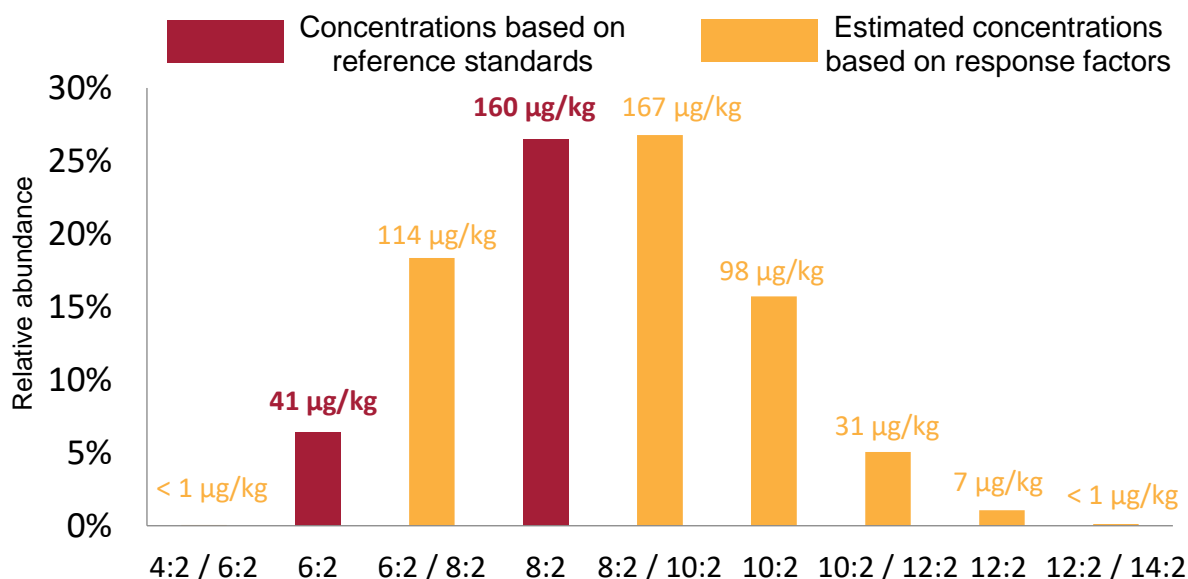


Figure 5: Relative abundances for various diPAP homologues in a contaminated soil sample from the region of Rastatt/Baden-Baden. Red bars indicate measured concentrations (measured by the Technologiezentrum Wasser (TZW), Karlsruhe), yellow bars indicate calculated concentrations for further homologues based on the assumption of the same response factor for all homologues.

In **chapter 9**, PFAS patterns (substance classes and homologues) from soil samples were compared to the patterns in PFAS impregnated paper samples. By this comparison, the hypothesis whether PFAS contaminated paper sludge can be the source of the contamination was tested. The substance class of fluorotelomer mercapto alkyl phosphates (FTMAPs) was detected as a further contaminant in one of the supplied soil samples. Due to the lack of authentic standards and the absence of FTMAPs from databases such as the curated OECD database for PFAS (Alygizakis, 2019), they were not suspected to be part of the contamination at first. However, since FTMAPs were known to be a paper impregnation agent (Trier et al., 2011a), a manual screen revealed homologous series of this compound class. An authentic standard of 6:2 / 6:2 FTMAP was kindly synthesized and provided by the working group of Prof. Dr. Martin E. Maier of the University of Tübingen. The  $^{19}\text{F}$ -NMR spectrum of the synthesized compound is shown in Figure 6. This standard confirmed the occurrence of 6:2 / 6:2 FTMAP in one soil sample and could explain previously unknown contaminants. A comparison of an MS/MS fragmentation of  $m/z$  920.9793 ( $m/z$  of 6:2 / 6:2 FTMAP) of the synthesized reference standard and the contaminated soil sample

is shown in Figure 7. Furthermore, the screening method suggests further homologues (6:2 / 8:2, 8:2 / 8:2, 8:2 / 10:2, 10:2 / 10:2) in the soil sample.

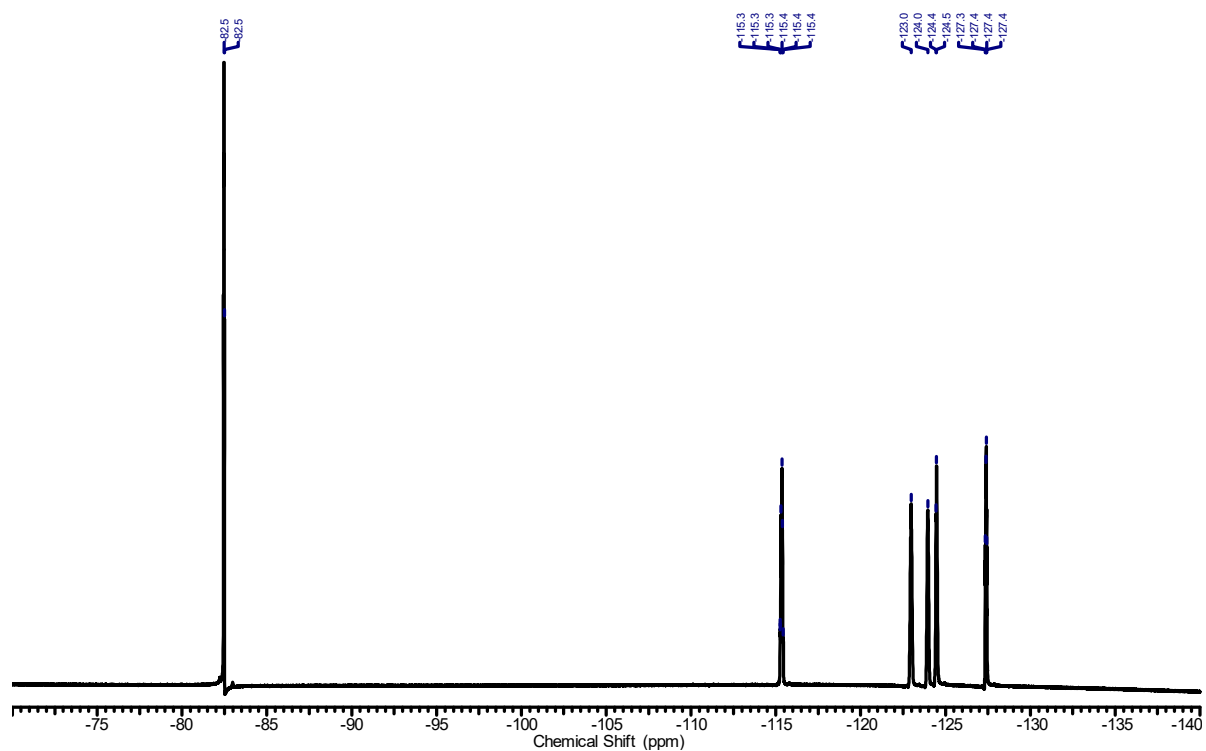


Figure 6: <sup>19</sup>F-NMR spectrum of the synthesized 6:2 / 6:2 FTMAP. Synthesis, NMR measurements and NMR evaluation were performed by the working group of Prof. Dr. Martin E. Maier, University of Tübingen.

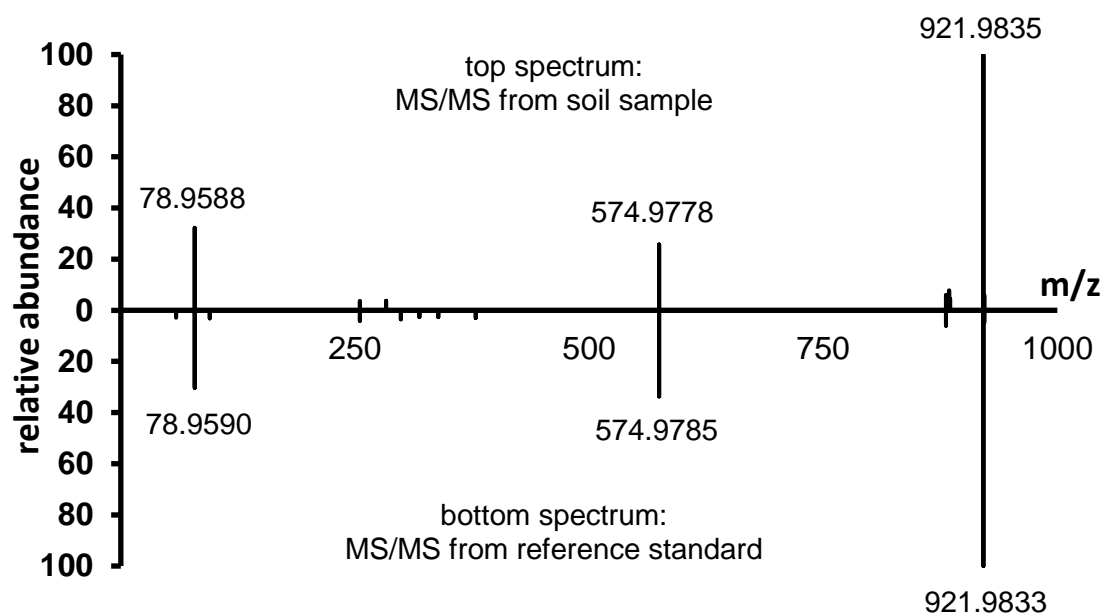


Figure 7: MS/MS spectrum of m/z 920.9793 (m/z of 6:2 FTMAP) with a collision energy of 40 eV in the soil sample (top) and the synthesized 6:2 FTMAP standard (1 mg/L, bottom). The intensities are normalized to the most abundant signal.

**Chapter 9** furthermore compares the contamination patterns in 14 different soil samples from the region of Rastatt / Baden-Baden with 14 impregnated paper samples which were collected in a time span in which the contamination is expected to have occurred. It was shown that paper samples are suspected to be either impregnated with FTMAPs or with diPAPs. Furthermore, a comparison of the carbon chain length distribution of diPAP, FTMAP, PFCA and fluorotelomer sulfonic acid (FTSA) homologues (PFCAs and FTSA are possible TPs of diPAPs and FTMAPs, respectively) showed that the chain lengths of the precursor compounds diPAP and FTMAP are similar in paper samples and soil samples. The chain lengths of PFCAs and FTSA in soil samples were shifted to longer chained homologues compared to paper samples. The comparison of the intensity weighted average carbon chain length is demonstrated in Figure 8. This was suspected to be a result of selective leaching in soil which is in good agreement with the finding by Higgins & Luthy (2006) who found increasing sorption with increasing carbon chain length (Higgins & Luthy, 2006). In turn, shorter homologues have a higher water solubility and can leach more easily (Gellrich & Knepper, 2012). This results in an enrichment of long chained homologues in soil and therefore a shift to longer homologues of the average carbon chain length.

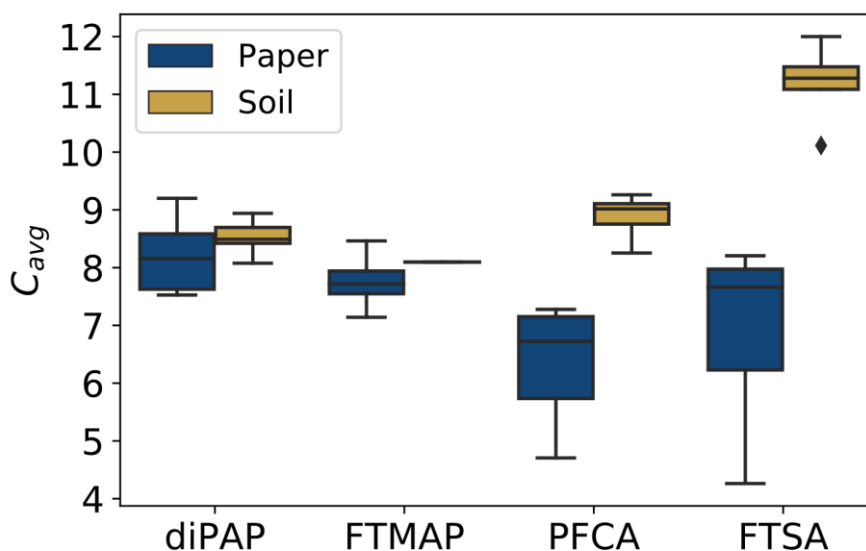


Figure 8: Box-Whisker-Plot for the weighted average lengths of the perfluorinated carbon chain  $C_{avg}$  of diPAPs, FTMAPs, PFCAs, and FTSA in 14 soil and 14 paper samples. For diPAPs and FTMAPs which bear two fluorotelomer carbon chains only the average carbon length of one side chain was considered. The box represents 25, 75 percentiles and the median, whiskers show the minimum and maximum values, the diamond indicates an outlier.

In **chapter 10**, the aim was to electrochemically degrade PFAS precursors in a controlled environment in the laboratory. This controlled production of TPs was used to generate and identify TPs that may also play an important role in the contaminated soils. Furthermore, the goal was to characterize PFAS precursors from their produced TPs. As a representative PFAS precursor, the electrochemical oxidation behavior of 6:2 / 6:2 diPAP was studied. This compound was selected as model compound due to a) the significance of the diPAP class in the PFAS contamination case in Rastatt / Baden-Baden and b) the availability of authentic standards for this particular homologue. Optimum degradation parameters were evaluated to be pH 6, 20 mM ammonium formate buffer in ultrapure water, a potential of 3 V and a duration of 18 h. The electrochemical oxidation of 6:2 / 6:2 diPAP yielded  $C_5$ - $C_7$  PFCAs and the two intermediate products 6:2 FTUCA and 6:2 FTCA. This indicates that these are relevant TPs from 6:2 diPAP. The major TP was PFHpA and formed with a pseudo-first order reaction from 6:2 / 6:2 diPAP. The formation of PFHpA as a major metabolite shows that the chain length of the dominantly produced TP is indicative for the precursor carbon chain length. This can be used as a means to estimate the precursor carbon chain length. Experiments at pH 6, 9.5 and 12 showed a decreasing formation rate of



PFHpA with increasing pH value. Similarly, the steady-state  $\bullet\text{OH}$  concentration decreased with increasing pH value. A linear relationship of steady-state  $\bullet\text{OH}$  and formation rate of PFHpA could be shown. Furthermore, the addition of a radical quencher, 2-propanol, led to a decreased steady-state  $\bullet\text{OH}$  concentration and decreased formation rate of PFHpA. This indicated that 6:2 / 6:2 diPAP is oxidized to PFHpA via  $\bullet\text{OH}$ . The relationship of steady-state  $\bullet\text{OH}$  concentration and formation rate of PFHpA was used to estimate a bimolecular rate constant of  $k_{\bullet\text{OH}, \text{diPAP}}^{\text{form PFHpA}} = 9.4 (\pm 1.4) \cdot 10^7 \text{ M}^{-1} \text{ s}^{-1}$  for the reaction of 6:2 diPAP with  $\bullet\text{OH}$  to form PFHpA. This constant can be used in order to estimate the reaction kinetics of 6:2 / 6:2 diPAP when the steady-state  $\bullet\text{OH}$  concentration is known. To the best of the authors knowledge, this constant is reported for the first time for 6:2 / 6:2 diPAP.

The goal of **chapter 11** was to investigate if photochemical degradation is expected to be a relevant environmental process in the transformation of PFAS. The chapter focuses on the formation of TPs via the photochemical oxidation of the precursor compound 6:2 / 6:2 diPAP on different mineral phases which typically occur in soils. Titanium dioxide (both anatase and rutile), goethite and silicium dioxide were selected and all showed 6:2 FTCA as a major intermediate product. A further but less important intermediate was 6:2 FTUCA. In the case of goethite (20 mg), the addition of oxalate (500  $\mu\text{M}$ ) was necessary to initiate the photo-Fenton process which produces various ROS. Without the addition of oxalate, no transformation of the precursor was observed. The intermediate 6:2 FTCA was further oxidized to a so-far unknown product.

The classical photocatalysts anatase and rutile (20 mg each) showed rather high transformation rates of the precursor: After 2 hours of irradiation in the artificial sunlight chamber, a complete transformation to 6:2 FTCA was observed. The subsequent reaction of 6:2 FTCA however varied between both titanium dioxide crystalline types. Rutile showed a slow and incomplete transformation of 6:2 FTCA to PFCAs over the experiment duration of 6 hours, anatase showed an almost complete transformation (94 %) to subsequent TPs within 2 hours.  $\text{C}_5\text{-C}_7$  PFCAs were generated as stable end products in both titanium dioxide phases. After an irradiation time of 6 h, 84 % of the initially spiked 6:2 / 6:2 diPAP was transformed to PFCAs which indicates that photochemistry can play an important role in the environmental transformation of

PFAS precursors to mobile PFCAs. An experiment with PFHpA as starting substance in combination with anatase revealed that no shortening of the  $\text{CF}_2$  chain occurs for PFCAs, the detected  $\text{C}_5\text{-C}_7$  PFCAs therefore needed to be a result of an individual transformation pathway from 6:2 FTCA. Therefore, photochemical oxidation of PFAS on anatase was proposed as a characterization method for unknown precursors.

Silicium dioxide particles (100 mg) showed a rather slow transformation of 6:2 / 6:2 diPAP to 6:2 FTCA (about 40 % transformation after 6 hours of irradiation). The addition of 10 mM  $\text{H}_2\text{O}_2$  significantly increased the steady-state  $\bullet\text{OH}$  concentration by a factor of 100 but did not have any significant effect on neither the formation nor the degradation of 6:2 FTCA.

## 5 Summary & Discussion

A detailed characterization of environmental contaminations is crucial in order to estimate further impacts. The aim of this study was to characterize the PFAS contamination in the region of Rastatt / Baden-Baden in more detail and to estimate the potential to produce mobile transformation products. By the use of screening methods, photochemical and electrochemical degradation experiments, this aim was achieved. The most important findings are summarized below.

- A screening of various contaminated soil and paper samples revealed that paper impregnation agents diPAPs (4:2 / 6:2 up to 12:2 / 14:2), diSAmPAP (C<sub>8</sub>/C<sub>8</sub>) and FTMAPs (6:2 / 6:2 up to 10:2 / 10:2) cause the main contamination. With 7 newly identified diPAP homologues and the newly identified substance class of FTMAPs, we could identify the main contaminants.
- PFAS impregnated papers which were collected in the time span when the contamination occurred were shown to be either impregnated with diPAPs or with FTMAPs and can explain the contamination in the investigated soil samples.
- Over time, degradation of those precursors led to transformation to multiple substance classes which generally are more mobile than their precursors. This has caused an enrichment of long-chained homologues in the upper soil layers whereas short-chained homologues are more mobile and have been leached to deeper soil layers and finally to groundwater.
- Photochemical degradation experiments showed that photochemistry can play a role in the transformation of PFAS precursors. Experiments on typical soil minerals with 6:2 / 6:2 diPAP showed 6:2 FTCA as a major intermediate product and PFCAs, in particular PFHpA, as major dead-end TPs.

- Electrochemical degradation experiments were used to characterize precursor PFAS and investigate environmental relevant TPs. Electrochemical experiments with 6:2 diPAP showed mostly PFCAs, in particular PFHpA, as TPs. Experiments at three different pH values showed a clear relationship of the steady-state  $\bullet\text{OH}$  concentration and the formation rate of PFHpA. This relationship was used to estimate the bimolecular rate constant  $k_{\bullet\text{OH}, \text{diPAP}}^{\text{form PFHpA}} = 9.4 (\pm 1.4) \cdot 10^7 \text{ M}^{-1} \text{ s}^{-1}$  which describes the reaction of 6:2 / 6:2 diPAP with  $\bullet\text{OH}$  to form PFHpA.
- Both photochemical and electrochemical degradation experiments suggested PFCAs to be major transformation products. PFCAs have shown to be more mobile than their precursors and can lead to pollutions in different compartments via leaching.

## 6 Outlook & Further Needs

This work significantly improves the understanding of the characterization of the contaminants in the Region of Rastatt / Baden-Baden and the fate of the detected contaminants. In order to better understand and assess the risks associated with PFAS in the environment, following steps are proposed as follow up of this work.

- The results of this work showed that the present contamination in the soil is expected to produce mobile TPs in the future. Since these mobile transformation products can migrate into other compartments such as groundwater, drinking water and plants, a close monitoring of all potentially affected compartments is crucial. In particular, this monitoring is of high relevance for drinking water and crops.
- Electrochemical degradation experiments should be performed with contaminated soil samples from the field to get data on TPs and formation kinetics which are representative for environmentally relevant processes. This increases the complexity of the experimental parameters and the data interpretation.
- Photochemical degradation experiments should also be performed with contaminated soil samples. This could for example be done with pure soil particles instead of coated mineral phases, with pure soil particles mixed with mineral phases such as anatase to possibly produce TPs more rapidly or with a contaminated soil extract which could be coated on pure mineral phases.
- The degradation studies which were performed for 6:2 / 6:2 diPAP should be extended to further contaminant classes which play a major role in contamination. Degradation studies using the other two major paper impregnation agents which were identified, diSAmPAP and FTMAPs, can reveal the potential to release further mobile TPs. This is especially the case for the FTMAPs since no information on the degradation potential of this substance class was published yet.

- To quantify the contaminants in screening analysis, authentic standards of all individual homologues would be needed. However, since many of the standards are not available commercially, organic synthesis of missing reference standards should be considered. The additional availability of isotope labelled authentic standards would be ideal. Without standards, only rough estimations on concentrations can be done. This inhibits the complete characterization of the source term of the contamination and a more comprehensive risk assessment.
- A major issue of environmental forensics is detailed missing information on production and application areas of commercially produced and applied products. In some cases, also the identity of compounds and their formulations in products are not adequately clarified. This is also the case for PFAS products. A close cooperation of manufacturers and regulation authorities should improve these knowledge gaps.
- Since PFAS are very stable in the environment and in most treatment processes, they are sometimes referred to as “forever chemicals” (Miner et al., 2021). Ideally, the production volume and usage of PFAS therefore needs to be decreased as much as possible in order to protect the environment. The usage of PFAS should be limited to absolutely necessary applications. This is attempted by the European Commission where only “essential uses” of PFAS should be allowed (European Commission, 2020). An example from the document for an essential PFAS use is protection clothing with oil repelling properties for some workers, whereas for consumer uses, this would not be considered essential (European Commission, 2020).

## 7 Bibliography

- Ahmadireskety, A., Da Silva, B. F., Townsend, T. G., Yost, R. A., Solo-Gabriele, H. M., & Bowden, J. A. (2021). Evaluation of extraction workflows for quantitative analysis of per- and polyfluoroalkyl substances: A case study using soil adjacent to a landfill. *Science of The Total Environment*, 760, 143944.
- Alygizakis, N. (2019). PFAS|NORMAN: List of PFAS from the OECD Curated by Nikiforos Alygizakis. Retrieved from [https://comptox.epa.gov/dashboard/chemical\\_lists/PFASOECDNA](https://comptox.epa.gov/dashboard/chemical_lists/PFASOECDNA). Accessed 04.06.2021.
- Barisci, S., & Suri, R. (2020). Electrooxidation of short and long chain perfluorocarboxylic acids using boron doped diamond electrodes. *Chemosphere*, 243, 125349.
- Barzen-Hanson, K. A., Roberts, S. C., Choyke, S., Oetjen, K., McAlees, A., Riddell, N., McCrindle, R., Ferguson, P. L., Higgins, C. P., & Field, J. A. (2017). Discovery of 40 Classes of Per- and Polyfluoroalkyl Substances in Historical Aqueous Film-Forming Foams (AFFFs) and AFFF-Impacted Groundwater. *Environmental Science & Technology*, 51(4), 2047-2057.
- Begley, T., Hsu, W., Noonan, G., & Diachenko, G. (2008). Migration of fluorochemical paper additives from food-contact paper into foods and food simulants. *Food Additives and Contaminants*, 25(3), 384-390.
- Bellamy, K., Chong, C., & Cline, R. (1995). Paper sludge utilization in agriculture and container nursery culture. *Journal of Environmental Quality*, 24(6), 1074-1082.
- Benskin, J. P., Ikonomou, M. G., Gobas, F. A., Begley, T. H., Woudneh, M. B., & Cosgrove, J. R. (2013). Biodegradation of N-ethyl perfluorooctane sulfonamido ethanol (EtFOSE) and EtFOSE-based phosphate diester (SAmPAP diester) in marine sediments. *Environmental Science & Technology*, 47(3), 1381-1389.
- Biegel-Engler, A., Vierke, L., Apel, P., Fetter, E., & Staude, C. (2017). Mitteilungen des Umweltbundesamtes zu per- und polyfluorierten Chemikalien (PFC) in Trinkwasser. *Bundesgesundheitsblatt Gesundheitsforschung Gesundheitsschutz*, 60(3), 341-346.
- Bolan, N., Sarkar, B., Yan, Y., Li, Q., Wijesekara, H., Kannan, K., Tsang, D. C., Schauerte, M., Bosch, J., & Noll, H. (2021). Remediation of poly- and perfluoroalkyl substances (PFAS) contaminated soils—To mobilize or to immobilize or to degrade? *Journal of hazardous materials*, 401, 123892.
- Brendel, S., Fetter, E., Staude, C., Vierke, L., & Biegel-Engler, A. (2018). Short-chain perfluoroalkyl acids: environmental concerns and a regulatory strategy under REACH. *Environmental Sciences Europe*, 30(1), 9.
- Buck, R. C., Franklin, J., Berger, U., Conder, J. M., Cousins, I. T., de Voogt, P., Jensen, A. A., Kannan, K., Mabury, S. A., & van Leeuwen, S. P. (2011). Perfluoroalkyl and polyfluoroalkyl substances in the environment: terminology, classification, and origins. *Integrated Environmental Assessment and Management*, 7(4), 513-541.
- Carter, K. E., & Farrell, J. (2008). Oxidative Destruction of Perfluorooctane Sulfonate Using Boron-Doped Diamond Film Electrodes. *Environmental Science & Technology*, 42(15), 6111-6115.
- Chen, H., Liu, M., Munoz, G., Duy, S. V., Sauv e, S. b., Yao, Y., Sun, H., & Liu, J. (2020). Fast Generation of Perfluoroalkyl Acids from Polyfluoroalkyl Amine Oxides in Aerobic Soils. *Environmental Science & Technology Letters*, 7(10), 714-720.

- Dennis, N. M., Karnjanapiboonwong, A., Subbiah, S., Rewerts, J. N., Field, J. A., McCarthy, C., Salice, C. J., & Anderson, T. A. (2020). Chronic Reproductive Toxicity of Perfluorooctane Sulfonic Acid and a Simple Mixture of Perfluorooctane Sulfonic Acid and Perfluorohexane Sulfonic Acid to Northern Bobwhite Quail (*Colinus virginianus*). *Environmental Toxicology and Chemistry*, 39(5), 1101-1111.
- DIN 38414-14:2011-08. (2018). Deutsche Einheitsverfahren zur Wasser-, Abwasser- und Schlammuntersuchung - Schlamm und Sedimente (Gruppe S) - Teil 14: Bestimmung ausgewählter polyfluorierter Verbindungen (PFC) in Schlamm, Kompost und Boden - Verfahren mittels Hochleistungs-Flüssigkeitschromatographie und massenspektrometrischer Detektion (HPLC-MS/MS) (S 14) *Beuth Verlag, Berlin*.
- Dreyer, A., Weinberg, I. T., C., & Ebinghaus, R. (2009). Polyfluorinated Compounds in the Atmosphere of the Atlantic and Southern Oceans: Evidence for a Global Distribution. *Environmental Science & Technology*, 43(17), 6507-6514.
- Dubocq, F., Wang, T., Yeung, L. W., Sjöberg, V., & Kärrman, A. (2019). Characterization of the Chemical Contents of Fluorinated and Fluorine-Free Firefighting Foams Using a Novel Workflow Combining Nontarget Screening and Total Fluorine Analysis. *Environmental Science & Technology*, 54(1), 245-254.
- Environmental Protection Agency. (2007). Treatment Technologies for Site Cleanup: Annual Status Report. Twelfth Edition.
- European Commission. (2020). COMMISSION STAFF WORKING DOCUMENT. Poly-and perfluoroalkyl substances (PFAS). Accompanying the document: COMMUNICATION FROM THE COMMISSION TO THE EUROPEAN PARLIAMENT, THE COUNCIL, THE EUROPEAN ECONOMIC AND SOCIAL COMMITTEE AND THE COMMITTEE OF THE REGIONS. Retrieved from [https://ec.europa.eu/environment/pdf/chemicals/2020/10/SWD\\_PFAS.pdf](https://ec.europa.eu/environment/pdf/chemicals/2020/10/SWD_PFAS.pdf). Accessed 09.05.2021.
- Franke, V., McCleaf, P., Lindegren, K., & Ahrens, L. (2019). Efficient removal of per- and polyfluoroalkyl substances (PFASs) in drinking water treatment: nanofiltration combined with active carbon or anion exchange. *Environmental Science: Water Research & Technology*, 5(11), 1836-1843.
- Fujii, Y., Harada, K. H., & Koizumi, A. (2013). Occurrence of perfluorinated carboxylic acids (PFCAs) in personal care products and compounding agents. *Chemosphere*, 93(3), 538-544.
- Gellrich, V., & Knepper, T. P. (2012). Sorption and leaching behavior of perfluorinated compounds in soil. In *Polyfluorinated Chemicals and Transformation Products* (pp. 63-72): Springer.
- Georgiou, C. D., Sun, H. J., McKay, C. P., Grintzalis, K., Papapostolou, I., Zisimopoulos, D., Panagiotidis, K., Zhang, G., Koutsopoulou, E., & Christidis, G. E. (2015). Evidence for photochemical production of reactive oxygen species in desert soils. *Nature Communications*, 6, 7100.
- Gibson, G. G., & Skett, P. (2013). *Introduction to drug metabolism*: Springer.
- Giesy, J. P., & Kannan, K. (2001). Global Distribution of Perfluorooctane Sulfonate in Wildlife. *Environmental Science & Technology*, 35(7), 1339-1342.
- Gobelius, L., Lewis, J., & Ahrens, L. (2017). Plant uptake of per- and polyfluoroalkyl substances at a contaminated fire training facility to evaluate the



- phytoremediation potential of various plant species. *Environmental Science & Technology*, 51(21), 12602-12610.
- Gremmel, C., Frömel, T., & Knepper, T. P. (2016). Systematic Determination of Perfluoroalkyl and Polyfluoroalkyl Substances (PFASs) in Outdoor Jackets. *Chemosphere*, 160, 173-180.
- Harding-Marjanovic, K. C., Houtz, E. F., Yi, S., Field, J. A., Sedlak, D. L., & Alvarez-Cohen, L. (2015). Aerobic biotransformation of fluorotelomer thioether amido sulfonate (Lodyne) in AFFF-amended microcosms. *Environmental Science & Technology*, 49(13), 7666-7674.
- Higgins, C. P., & Luthy, R. G. (2006). Sorption of perfluorinated surfactants on sediments. *Environmental Science & Technology*, 40(23), 7251-7256.
- Houtz, E. F., & Sedlak, D. L. (2012). Oxidative conversion as a means of detecting precursors to perfluoroalkyl acids in urban runoff. *Environmental Science & Technology*, 46(17), 9342-9349.
- Hurley, S., Goldberg, D., Wang, M., Park, J.-S., Petreas, M., Bernstein, L., Anton-Culver, H., Nelson, D. O., & Reynolds, P. (2018). Breast cancer risk and serum levels of per- and poly-fluoroalkyl substances: a case-control study nested in the California Teachers Study. *Environmental Health*, 17(1), 1-19.
- Janda, J., Nödler, K., Brauch, H.-J., Zwiener, C., & Lange, F. T. (2019a). Robust trace analysis of polar (C 2-C 8) perfluorinated carboxylic acids by liquid chromatography-tandem mass spectrometry: method development and application to surface water, groundwater and drinking water. *Environmental Science and Pollution Research*, 26(8), 7326-7336.
- Janda, J., Nödler, K., Scheurer, M., Happel, O., Nurenberg, G., Zwiener, C., & Lange, F. T. (2019b). Closing the gap - inclusion of ultrashort-chain perfluoroalkyl carboxylic acids in the total oxidizable precursor (TOP) assay protocol. *Environmental Science: Processes & Impacts*, 21.11, 1926-1935.
- Johansson, T., Weidolf, L., & Jurva, U. (2007). Mimicry of phase I drug metabolism--novel methods for metabolite characterization and synthesis. *Rapid Communications in Mass Spectrometry*, 21(14), 2323-2331.
- Jurva, U., Wikström, H. V., Weidolf, L., & Bruins, A. P. (2003). Comparison between electrochemistry/mass spectrometry and cytochrome P450 catalyzed oxidation reactions. *Rapid Communications in Mass Spectrometry*, 17(8), 800-810.
- Kaiser, A.-M., Aro, R., Kärrman, A., Weiss, S., Hartmann, C., Uhl, M., Forsthuber, M., Gundacker, C., & Yeung, L. W. (2020). Comparison of extraction methods for per- and polyfluoroalkyl substances (PFAS) in human serum and placenta samples—insights into extractable organic fluorine (EOF). *Analytical and Bioanalytical Chemistry*, 1-12.
- Kendrick, E. (1963). A Mass Scale Based on CH<sub>2</sub>= 14.0000 for High Resolution Mass Spectrometry of Organic Compounds. *Analytical Chemistry*, 35(13), 2146-2154.
- Kim, M., Son, J., Park, M. S., Ji, Y., Chae, S., Jun, C., Bae, J.-S., Kwon, T. K., Choo, Y.-S., & Yoon, H. (2013). In vivo evaluation and comparison of developmental toxicity and teratogenicity of perfluoroalkyl compounds using *Xenopus* embryos. *Chemosphere*, 93(6), 1153-1160.
- Kissa, E. (2001). *Fluorinated surfactants and repellents* (Vol. 97): CRC Press.
- Lippitsch, C. (2020). Die neue EU-Trinkwasserrichtlinie. *Österreichische Wasser- und Abfallwirtschaft*, 72(11), 498-500.

- Martin, J. W., Kannan, K., Berger, U., Voogt, P. D., Field, J., Franklin, J., Giesy, J. P., Harner, T., Muir, D. C., & Scott, B. (2004). Analytical challenges hamper perfluoroalkyl research. *Environmental Science & Technology*, 38(13), 248A-255A.
- Martinez-Huitle, C. A., & Ferro, S. (2006). Electrochemical oxidation of organic pollutants for the wastewater treatment: direct and indirect processes. *Chemical Society Reviews*, 35(12), 1324-1340.
- McCleaf, P., Englund, S., Östlund, A., Lindegren, K., Wiberg, K., & Ahrens, L. (2017). Removal efficiency of multiple poly-and perfluoroalkyl substances (PFASs) in drinking water using granular activated carbon (GAC) and anion exchange (AE) column tests. *Water research*, 120, 77-87.
- McGregor, R. (2018). In situ treatment of PFAS-impacted groundwater using colloidal activated carbon. *Remediation Journal*, 28(3), 33-41.
- Mejia-Avendaño, S., Vo Duy, S., Sauvé, S. b., & Liu, J. (2016). Generation of perfluoroalkyl acids from aerobic biotransformation of quaternary ammonium polyfluoroalkyl surfactants. *Environmental Science & Technology*, 50(18), 9923-9932.
- Miner, K., Clifford, H., Taruscio, T., Potocki, M., Solomon, G., Ritari, M., Napper, I., Gajurel, A., & Mayewski, P. (2021). Deposition of PFAS 'forever chemicals' on Mt. Everest. *Science of The Total Environment*, 759, 144421.
- Moldoveanu, S., & David, V. (2013). Essentials in Modern HPLC Separations. *Waltham, MA: Elsevier*.
- Nakayama, S. F., Yoshikane, M., Onoda, Y., Nishihama, Y., Iwai-Shimada, M., Takagi, M., Kobayashi, Y., & Isobe, T. (2019). Worldwide trends in tracing poly-and perfluoroalkyl substances (PFAS) in the environment. *Trends in Analytical Chemistry*, 121, 115410.
- Ochiai, T., Iizuka, Y., Nakata, K., Murakami, T., Tryk, D. A., Fujishima, A., Koide, Y., & Morito, Y. (2011). Efficient electrochemical decomposition of perfluorocarboxylic acids by the use of a boron-doped diamond electrode. *Diamond and Related Materials*, 20(2), 64-67.
- OECD. (2018). Toward a New Comprehensive Global Database of Per- and Polyfluoroalkyl Substances (PFASs). Retrieved from <http://www.oecd.org/chemicalsafety/risk-management/global-database-of-per-and-polyfluoroalkyl-substances.xlsx>. Accessed 01.07.2020.
- Page, S. E., Arnold, W. A., & McNeill, K. (2010). Terephthalate as a probe for photochemically generated hydroxyl radical. *Journal of Environmental Monitoring*, 12(9), 1658-1665.
- Pan, Y., Zhang, H., Cui, Q., Sheng, N., Yeung, L. W. Y., Sun, Y., Guo, Y., & Dai, J. (2018). Worldwide Distribution of Novel Perfluoroether Carboxylic and Sulfonic Acids in Surface Water. *Environmental Science & Technology*, 52(14), 7621-7629.
- Rankin, K., Mabury, S. A., Jenkins, T. M., & Washington, J. W. (2016). A North American and global survey of perfluoroalkyl substances in surface soils: Distribution patterns and mode of occurrence. *Chemosphere*, 161, 333-341.
- Regierungspräsidium Karlsruhe. (2018). PFC-Problematik: Zwischenbilanz und Ausblick. Retrieved from [https://rp.baden-wuerttemberg.de/rpk/Abt5/Ref541/PFC/Seiten/pfc\\_buergerinfo.aspx](https://rp.baden-wuerttemberg.de/rpk/Abt5/Ref541/PFC/Seiten/pfc_buergerinfo.aspx). Accessed 19.04.2021.

- Regierungspräsidium Karlsruhe. (2020). PFC-Problematik in Nord- und Mittelbaden: Statusbericht. Berichtszeitraum Januar bis Juni 2020. Retrieved from [https://rp.baden-wuerttemberg.de/fileadmin/RP-Internet/Karlsruhe/Abteilung\\_5/Referat\\_54.1/Stabsstelle\\_PFC/DocumentLibraries/Documents/Statusbericht\\_1\\_HJ\\_2020.pdf](https://rp.baden-wuerttemberg.de/fileadmin/RP-Internet/Karlsruhe/Abteilung_5/Referat_54.1/Stabsstelle_PFC/DocumentLibraries/Documents/Statusbericht_1_HJ_2020.pdf). Accessed 31.05.2021.
- Renner, R. (2001). Growing concern over perfluorinated chemicals. *Environmental Science & Technology*, 35(7), 154A-160A.
- Rewerts, J. N., Morré, J. T., Massey Simonich, S. L., & Field, J. A. (2018). In-Vial Extraction Large Volume Gas Chromatography Mass Spectrometry for Analysis of Volatile PFASs on Papers and Textiles. *Environmental Science & Technology*, 52(18), 10609-10616.
- Rigét, F., Bignert, A., Braune, B., Dam, M., Dietz, R., Evans, M., Green, N., Gunnlaugsdóttir, H., Hoydal, K. S., & Kucklick, J. (2019). Temporal trends of persistent organic pollutants in Arctic marine and freshwater biota. *Science of The Total Environment*, 649, 99-110.
- Robel, A. E., Marshall, K., Dickinson, M., Lunderberg, D., Butt, C., Peaslee, G., Stapleton, H. M., & Field, J. A. (2017). Closing the mass balance on fluorine on papers and textiles. *Environmental Science & Technology*, 51(16), 9022-9032.
- Schwarzenbach, R. P., Gschwend, P. M., & Imboden, D. M. (2016). *Environmental Organic Chemistry*. John Wiley & Sons.
- Sharma, S., Tiwari, S., Hasan, A., Saxena, V., & Pandey, L. M. (2018). Recent advances in conventional and contemporary methods for remediation of heavy metal-contaminated soils. *3 Biotech*, 8(4), 1-18.
- Shoemaker, J., & Tettenhorst, D. (2018). Method 537.1: determination of selected per- and polyfluorinated alkyl substances in drinking water by solid phase extraction and liquid chromatography/tandem mass spectrometry (LC/MS/MS). *US Environmental Protection Agency, Office of Research and Development*.
- Sinclair, W., Kim, S. K., Akinleye, H. B., & Kannan, K. (2007). Quantitation of Gas-Phase Perfluoroalkyl Surfactants and Fluorotelomer Alcohols Released from Nonstick Cookware and Microwave Popcorn Bags. *Environmental Science & Technology*, 41(4), 1180-1185.
- Söhlmann, R., Striegel, G., & Lange, F. T. (2018). Die Anwendung der Summenparameter EOF und AOF bei der Untersuchung der Tiefenverlagerung von Perfluoralkyl- und Polyfluoralkylverbindungen (PFAS) in belasteten Böden in Mittelbaden. *Mitteilungen der Fachgruppe Umweltchemie und Ökotoxikologie, 24. Jahrg. 2018/ Nr.4*, 89-91.
- Söregård, M., Lindh, A., & Ahrens, L. (2020). Thermal desorption as a high removal remediation technique for soils contaminated with per- and polyfluoroalkyl substances (PFASs). *PLOS ONE*, 15(6), e0234476.
- Trier, X., Granby, K., & Christensen, J. H. (2011a). Polyfluorinated surfactants (PFS) in paper and board coatings for food packaging. *Environmental Science and Pollution Research*, 18(7), 1108-1120.
- Trier, X., Granby, K., & Christensen, J. H. (2011b). Tools to discover anionic and nonionic polyfluorinated alkyl surfactants by liquid chromatography electrospray ionisation mass spectrometry. *Journal of Chromatography A*, 1218(40), 7094-7104.
- Trier, X., Taxvig, C., Rosenmai, A. K., & Pedersen, G. A. (2018). *PFAS in paper and board for food contact: Options for risk management of poly- and perfluorinated substances*: Nordic Council of Ministers.

- United Nations Environment Programme. (2001). Stockholm Convention on Persistent Organic Pollutants (Annex A and B). Retrieved from <http://www.pops.int/TheConvention/ThePOPs/AllPOPs/tabid/2509/Default.aspx>. Accessed 10.03.2021.
- United States Environmental Protection Agency. (2007). Technical Fact Sheet – Perfluorooctane Sulfonate (PFOS) and Perfluorooctanoic Acid (PFOA). Retrieved from [https://www.epa.gov/sites/production/files/2017-12/documents/ffrrofactsheet\\_contaminants\\_pfos\\_pfoa\\_11-20-17\\_508\\_0.pdf](https://www.epa.gov/sites/production/files/2017-12/documents/ffrrofactsheet_contaminants_pfos_pfoa_11-20-17_508_0.pdf). Accessed 12.03.2021.
- van der Veen, I., Hanning, A.-C., Stare, A., Leonards, P. E., de Boer, J., & Weiss, J. M. (2020). The effect of weathering on per- and polyfluoroalkyl substances (PFASs) from durable water repellent (DWR) clothing. *Chemosphere*, *249*, 126100.
- Wang, N., Liu, J., Buck, R. C., Korzeniowski, S. H., Wolstenholme, B. W., Folsom, P. W., & Sulecki, L. M. (2011a). 6:2 fluorotelomer sulfonate aerobic biotransformation in activated sludge of waste water treatment plants. *Chemosphere*, *82*(6), 853-858.
- Wang, N., Szostek, B., Buck, R. C., Folsom, P. W., Sulecki, L. M., & Gannon, J. T. (2009). 8-2 fluorotelomer alcohol aerobic soil biodegradation: pathways, metabolites, and metabolite yields. *Chemosphere*, *75*(8), 1089-1096.
- Wang, Z., Cousins, I. T., Scheringer, M., & Hungerbühler, K. (2013). Fluorinated alternatives to long-chain perfluoroalkyl carboxylic acids (PFCAs), perfluoroalkane sulfonic acids (PFSA) and their potential precursors. *Environment International*, *60*, 242-248.
- Wang, Z., MacLeod, M., Cousins, I. T., Scheringer, M., & Hungerbühler, K. (2011b). Using COSMOtherm to predict physicochemical properties of poly- and perfluorinated alkyl substances (PFASs). *Environmental Chemistry*, *8*(4), 389-398.
- Yamashita, N., Taniyasu, S., Petrick, G., Wei, S., Gamo, T., Lam, P. K. S., & Kannan, K. (2008). Perfluorinated Acids As Novel Chemical Tracers of Global Circulation of Ocean Waters. *Chemosphere*, *70*(7), 1247-1255.
- Yeung, L. W., Robinson, S. J., Koschorreck, J., & Mabury, S. A. (2013). Part II. A temporal study of PFOS and its precursors in human plasma from two German cities in 1982–2009. *Environmental Science & Technology*, *47*(8), 3875-3882.
- Yi, S., Harding-Marjanovic, K. C., Houtz, E. F., Gao, Y., Lawrence, J. E., Nichiporuk, R. V., Iavarone, A. T., Zhuang, W.-Q., Hansen, M., & Field, J. A. (2018). Biotransformation of AFFF component 6: 2 fluorotelomer thioether amido sulfonate generates 6: 2 fluorotelomer thioether carboxylate under sulfate-reducing conditions. *Environmental Science & Technology Letters*, *5*(5), 283-288.
- Zabaleta, I., Bizkarguenaga, E., Izagirre, U., Negreira, N., Covaci, A., Benskin, J. P., Prieto, A., & Zuloaga, O. (2017). Biotransformation of 8:2 polyfluoroalkyl phosphate diester in gilthead bream (*Sparus aurata*). *Science of The Total Environment*, *609*, 1085-1092.
- Zhao, S., Liang, T., Zhu, L., Yang, L., Liu, T., Fu, J., Wang, B., Zhan, J., & Liu, L. (2019). Fate of 6: 2 fluorotelomer sulfonic acid in pumpkin (*Cucurbita maxima* L.) based on hydroponic culture: Uptake, translocation and biotransformation. *Environmental Pollution*, *252*, 804-812.

**Chapter 8 – personal contribution**

<b>Author</b>	<b>Author position</b>	<b>Scientific ideas %</b>	<b>Data generation %</b>	<b>Analysis &amp; interpretation %</b>	<b>Paper writing %</b>
Boris Bugsel	1	80	80	90	80
Christian Zwiener	2	20	0	10	20
Title of paper:		LC-MS screening of poly- and perfluoroalkyl substances in contaminated soil by Kendrick mass analysis			
Status in publication process:		Published (DOI: 10.1007/s00216-019-02358-0)			

## 8 LC-MS screening of poly- and perfluoroalkyl substances in contaminated soil by Kendrick mass analysis

Boris Bugsel<sup>1</sup>, Christian Zwiener<sup>1</sup> (2020)

<sup>1</sup> Environmental Analytical Chemistry, Center for Applied Geoscience, University of Tübingen, Hölderlinstraße 12, 72074, Tübingen

*Analytical and Bioanalytical Chemistry* (412: 4797-4805)

DOI: 10.1007/s00216-019-02358-0

The Electronic Supplementary is published “Open Access” and available on <https://doi.org/10.1007/s00216-019-02358-0>

## 8.1 Abstract

The application of contaminated paper sludge on arable land in southwest Germany caused the occurrence of a broad range of poly- and perfluoroalkyl substances (PFASs) on soil. Recently, the dead-end transformation products (TPs) perfluorooctanoic acid and perfluorooctanesulfonic acid were detected in groundwater and drinking water. The precursors and other transformation products mostly remained unknown. Therefore, HRMS screening by Kendrick mass analysis and assignment of homologous series in combination with suspect screening were applied to identify original PFASs and their TPs in four different soil samples from sites where contaminated paper sludge was applied. In total, twelve compound classes comprising more than 61 PFASs could be fully or tentatively identified. The data reveal that contamination mainly originates from polyfluorinated dialkylated phosphate esters (from 4:2/6:2 to 12:2/14:2), N-ethyl perfluorooctane sulfonamide ethanol-based phosphate diesters (only C8/ C8) and transformation products of these precursors. Contamination patterns can be attributed to PFASs used for paper impregnation and can vary slightly from site to site.

## 8.2 Abbreviations

AIF	All-ion fragmentation
Da	Dalton
diPAP	Polyfluorinated dialkylated phosphate ester
diSAmPAP	N-ethyl perfluorooctane sulfonamide ethanol-based phosphate diester
EIC	Extracted Ion Chromatogram
ESI	Electrospray Ionization
EtFASA	N-ethyl perfluoroalkanesulfonamide
EtFASAA	N-ethylperfluoro-1-alkanesulfonamidoacetic acid
EtFOSAA	N-ethylperfluoro-1-octanesulfonamidoacetic acid
FASA	Perfluoroalkanesulfonamide
FOSA	Perfluorooctanesulfonamide
FTOH	Fluorotelomer alcohol
FTSA	Fluorotelomer sulfonic acid
FTUCA	Fluorotelomer unsaturated carboxylic acid
GenX	Ammonium 2,3,3,3-tetrafluoro-2-(heptafluoropropoxy) propanoate
HRMS	High resolution mass spectrometry
HS	Homologous series
KM	Kendrick mass
KMD	Kendrick mass defect
LC	Liquid Chromatography
LTZ	Landwirtschaftliches Technologiezentrum Augustenberg

MeFASA	N-Methyl perfluoroalkanesulfonamide
MeOH	Methanol
MFE	Molecular feature extraction
NH <sub>4</sub> Ac	Ammonium acetate
OM	Observed mass
PFAAs	Perfluoroalkyl acids
PFASs	Poly- and perfluorinated alkylated substances
PFCAs	Perfluorocarboxylic acids
PFHpA	Perfluoroheptanoic acid
PFOA	Perfluorooctanoic acid
PFNA	Perfluorononanoic acid
PFOS	Perfluorooctanesulfonic acid
PFPIA	Perfluorinated phosphinic acid
PFSAAs	Perfluorosulfonic acids
PP	Polypropylene
rcf	Relative centrifugal force
RT	Retention time
TP	Transformation product
triPAP	Polyfluorinated trialkylated phosphate ester

### 8.3 Introduction

Poly- and perfluorinated alkylated substances (PFASs) are anthropogenic compounds with an increasing environmental significance [1]. They comprise a family of more than 4700 single compounds [2]. Due to their unique, both water- and grease-repelling properties, their fields of applications are textiles such as clothing and carpets [3], nonstick cookware [4], food packaging [5, 6], cosmetics [7], and firefighting foams [8, 9]. The widespread use of PFASs has led to a global distribution in biota [10], air [11], soil [12], and water where they were even proposed as novel tracers [13]. While the characteristics of PFASs render them desirable for the industry, their negative impacts on both environment and health are beyond question. Two of the best studied PFASs, perfluorooctanoic acid (PFOA) and perfluorooctanesulfonic acid (PFOS), accumulate in the liver, lung, and kidney of rats and are proposed to be a big threat to humans and biota [14, 15]. Their major manufacturer 3M has hence phased out the production of these two substances between 2000 and 2002 [1], yet other PFASs such as ammonium 2, 3,3,3- tetrafluoro-2-(heptafluoropropoxy)-propanoate (GenX) have replaced these compounds [16]. Studies performed by Gomis et al. [17] and Sun et al. [18] even indicate a higher toxicity and a lower sorption on activated carbon for GenX than for PFOA, highlighting the importance of both legacy and novel PFASs. Liquid



chromatography coupled to mass spectrometry has earlier been used in the identification and determination of PFASs [5, 8, 19–22]. The use of high-resolution mass spectrometry (HRMS) reveals valuable accurate mass information which can be used in the identification of unknown contaminants. The nature of PFASs typically is their occurrence in multiple homologues, a beneficial characteristic in their identification. Coupling HRMS with homologous series (HS) detection has a variety of useful applications such as the detection of surfactants or polymers [23, 24] and PFASs [25, 26].

In summer 2013, a routine sampling has revealed PFAS contamination of a drinking water well near Rastatt (Baden Württemberg, Germany) [27]. Further research showed that soil contamination on agricultural land has led to groundwater pollution. Compost mixed with paper sludge containing PFASs was applied to about 7.8 Mio m<sup>2</sup> agricultural soil [28, 29]. A large variety of both anionic and non-ionic PFASs is known to be applied to food packaging paper and board in order to grant oil and water repellency [6]. Schaidler et al. [30] found that 46% out of roughly 400 food contact papers showed detectable levels of fluorinated substances. Typically, these PFAS paper impregnation agents can contain multiple alkyl chains and functional groups [6]. Lab experiments revealed that the original PFAS paper impregnation products (precursors) are slowly degrading to short single-chain perfluoroalkyl acids (PFAAs) such as perfluorocarboxylic acids (PFCAs) and perfluorosulfonic acids (PFSAs) [31, 32]. The transformation products (TPs) are more mobile, migrate to groundwater, and can be taken up by plants [33, 34]. To evaluate the exposure of the population which received contaminated drinking water, blood tests were conducted. Results of the contaminated area showed increased blood levels of PFASs of the exposed people (e.g., 15.7 µg/L PFOA) compared to controls (1.7 µg/L PFOA) [35]. In other regions, PFOA blood concentrations of exposed people are also about 10-fold higher than those of control population [36]. In the present case study, information on the identity and amount of technical products used and discharged is very limited. These precursors are typically not included in target methods. The aim of the present work hence is the characterization and identification of the original contamination and its TPs. Here, we used a non-target approach with LC-high-resolution mass spectrometry and Kendrick mass analysis.

## 8.4 Materials and methods

### Chemicals and reagents

Optima LC-MS grade methanol (MeOH), ammonium acetate (NH<sub>4</sub>Ac), and water were purchased from Fisher Scientific. Authentic reference standards of sodium (1H,1H,2H,2H,perfluorooctyl-1H,1H,2H,2H-perfluorodecyl)phosphate (6:2/ 8:2 diPAP), N-ethyl perfluorooctane sulfonamide ethanol– based phosphate diester (diSAmPAP), 2H-perfluoro-2decenoic acid (8:2 FTUCA), N-ethylperfluoro-1-octanesulfonamidoacetic acid (EtFOSAA), sodium perfluoro-1-octanesulfonate (PFOS), 3-perfluoroheptyl propanoic acid (7:3 PFCA), 2H-perfluoro-2-decenoic acid (8:2 PFCA), and sodium 1H,1H,2H,2H-perfluorooctane sulfonate (6:2 FTSA) were obtained from Wellington Laboratories, Inc. (Guelph, Ontario, Canada). Tris(1H,1H,2H,2H-perfluorohexyl) phosphate (6:2 polyfluorinated trialkylated phosphate ester, triPAP) was purchased from Chiron AS (Trondheim, Norway). Bis(perfluorohexyl)phosphonic acid (perfluorinated phosphonic acid, PFPIA) was purchased from Toronto Research Chemicals (North York, Ontario, Canada). PFOA was obtained from ABCR (Karlsruhe, Germany). Perfluorooctanesulfonamide (FOSA) was obtained from SynQuest Laboratories (Alachua, FL, USA).

### Sample collection and preparation

The homogenized, freeze-dried soil samples from the contaminated area in Germany were collected in 2017 and provided by the Landwirtschaftliches Technologiezentrum Augustenberg (LTZ) (Karlsruhe, Germany). Sample 1 originated from Hügelsheim and samples 2, 3, and 4 from the area around Mannheim. Five grams of the soil samples was weighed in a 50-mL polypropylene (PP) tube, and 10 mL MeOH was added. The mixture was thoroughly vortexed for 2 min, sonicated for 10 min, and then put on a horizontal shaker for 24 h. After centrifuging (10 min, 4000 relative centrifugal force (rcf)), the supernatant was transferred to a 20-mL PP vessel using a glass pipette. The extraction was repeated with 10 mL MeOH as described. The supernatants were combined, heated to 40 °C, and evaporated to less than 1 mL with a gentle stream of nitrogen. Pure MeOH was used to adjust the volume to 1 mL. The concentrate was transferred into a PP vial and centrifuged (10 min, 4000 rcf) prior to analysis.

## **Instrumental analysis**

Samples were analyzed by LC-MS using a 1290 HPLC (Agilent Technologies, Waldbronn, Germany) coupled to a 6550 QTOF mass spectrometer (Agilent Technologies, Santa Clara, USA). An Agilent C18 column (Poroshell 120 EC-C18, 2.1 mm × 100 mm, particle size 2.7 μm) was used to separate the analytes, and the flow rate was set to 0.4 mL/min and the temperature to 40°C. Eluent A (95:5 H<sub>2</sub>O/MeOH) and eluent B (5:95 H<sub>2</sub>O/MeOH), both with 2 mM NH<sub>4</sub>Ac, were used for gradient elution. The gradient started with 25% B, followed by a linear increase to 85% B within 2 min and to 100% B within 2.5 min, and kept isocratic for another 12 min. Initial conditions were reset at 12.1 min with a subsequent equilibration time of 15 min. The injection volume of the sample was 20 μL. The electrospray ionization (ESI) source, equipped with the Agilent Jet Stream technology, was operated in negative ionization mode. The MS measurements were performed in scan mode for screening and in both targeted MS/MS mode and all-ion fragmentation (AIF) for further structural information. AIF measurements were performed at collision energies of 0 eV, 20 eV, and 40 eV. Instrumental parameters for MS/MS measurements are given in Electronic Supplementary Material (ESM) 1 (section targeted MS/MS measurements). To validate the extraction method, targeted MS/MS measurements were performed with uncontaminated soil spiked with 10 ng of several PFASs (diSAmPAP, 8:2 PFCA, EtFOSAA, 6:2 FTSA) each. Original uncontaminated and spiked soil samples were extracted in the same way as the contaminated samples 1–4. The results are shown in the ESM (Figs. S1.42 to S1.45).

## **Data analysis and HS detection**

The recorded data were processed using the molecular feature extraction (MFE) algorithm of the MassHunter software (versions B.07.00 and 10.0; Agilent Technologies). Features were narrowed down to mass defects between - 0.25 and + 0.1 Da as well as an intensity of at least 1000 counts. To validate the mass defect filtering, we used the curated Organisation for Economic Co-operation and Development (OECD) PFAS list (list of acronym PFASOECDNA, available from the EPA dashboard) and calculated the mass defect of all entries. Out of a total of 3213 PFASs, 2982 substances had a mass defect between - 0.25 and + 0.1, showing that an application of this filter covers 92.8% of all PFASs within this database. The

resulting compounds after filtering are hydrocarbon compounds with chemical formulae containing more or less elements with negative mass defects (e.g., F, Cl, Br, I, O, P, S).

The selected features were exported as a CSV file which could then be imported to Matlab (MathWorks, Natick, USA) to automatically be processed by FindSeries, a code which was written in-house for Kendrick mass defect (KMD) analysis of PFAS. As proposed in 1963 by Edward Kendrick [37], the KMD was calculated according to Eqs. (1) and (2). By normalizing the observed mass (OM) of a compound by the integer mass of the repeating unit (e.g., 50:49.9968 in the case of CF<sub>2</sub>), all homologue compounds with the same core structure but varying numbers of the repeating unit reveal the same KMD. For example, perfluoroheptanoic acid (PFHpA), PFOA, and perfluorononanoic acid (PFNA) have the exact masses 363.9769, 413.9737, and 463.9705, respectively. They all bear a carboxylic acid group as a common structural moiety and are only distinguished by the number of the repeating units (CF<sub>2</sub> with an exact mass of 49.9968). For example, the KMD for PFHpA is  $1.96 \cdot 10^{-4}$  (Eq. 3) and exactly the same number for PFOA and PFNA or even larger PFCAs like perfluorohexadecanoic acid (C<sub>16</sub>HF<sub>31</sub>O<sub>2</sub>).

Detected HS are further visualized by plotting the KMD vs. m/z where compounds from the same compound class align horizontally.

$$KM = OM \cdot \frac{\text{nominal mass (repeating unit)}}{\text{exact mass (repeating unit)}} \quad (1)$$

$$KMD = \text{nominal KM} - \text{exact KM} \quad (2)$$

$$KMD = 364 - 363.9769 \cdot \frac{50}{49.9968} = 1.96 \cdot 10^{-4} \quad (3)$$

where KM is the Kendrick mass, OM is the accurate observed mass of the compound, and KMD is the Kendrick mass defect.

In step 1, FindSeries further compares the measured accurate masses with a database containing exact masses of known PFASs (curated OECD PFAS list, available online at EPA dashboard) [38] using a tolerance of 3 mDa. Matching masses are exported, including the respective name, yielding a list of potentially occurring PFASs in the sample. In step 2, FindSeries performs a Kendrick mass analysis for different repeating units such as –CF<sub>2</sub>–, –CF<sub>2</sub>O–, or –C<sub>2</sub>F<sub>4</sub>O– using a tolerance of 5

mDa. This higher tolerance is chosen in step 2 because unlike in step 1, there is no reference mass value from a database, and all members from one HS need to deviate less than the applied tolerance from one another. The resulting HS are subsequently validated by a manual inspection of the chromatographic peaks (Gaussian peak shape, signal-to-noise ratio > 10) and a systematic retention time (RT) shift. The RT difference between the first members of a HS defines a RT shift, and the following homologues need to be in the same range. With increasing mass, a decreasing retention time shift has to be observed due to the increasing elution strength of the LC gradient. For example, four consecutive members of a HS with RT 3 min, 4 min, 4.1 min, and 6 min would be discarded (vastly different time shifts with no clear trend). In turn, four consecutive members of a HS with RT 3 min, 3.6 min, 4.1 min, and 4.5 min would be considered for further evaluation (plausible RT shift trend).

If available, one authentic standard per HS was purchased and used for confirmation of the compound identity. According to the scheme of identification confidence from Schymanski et al. [39], detected PFASs were classified by defined confidence levels. For level 1, the structure was confirmed by an authentic standard based on accurate mass and RT. Level 2a was used for members of a HS if one candidate was successfully confirmed by a reference standard and the other candidates exhibited the previously mentioned systematic mass and RT shifts. For level 2b, members of a HS with a systematic RT shift were detected and structures were validated with fragmentation patterns. Single features not belonging to a HS were classified as level 3, and compound identifications were tentatively proposed based on accurate mass and matching with the OECD database.

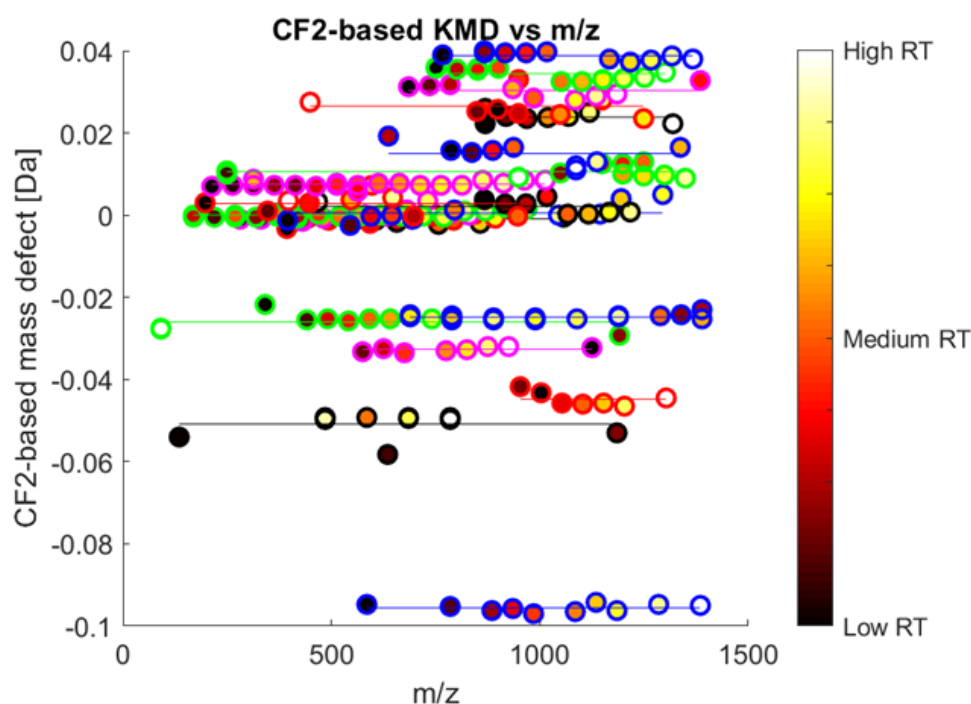
## 8.5 Results and discussion

Highly contaminated soil samples were analyzed for PFAS precursors and TPs by LC-QTOF-MS. The procedure of the data evaluation is shown in detail for sample 1. Further results for samples 2, 3, and 4 are presented subsequently using the same work flow. For readability, only integer masses are shown in the result tables. The corresponding accurate masses are shown in Tables S1–S6 (see ESM). Accurate mass scans showed in total 4837 features in the contaminated soil sample 1, 1940 of those had negative mass defects in the range between  $-0.25$  and  $+0.1$  Da, which

typically characterize compounds with a high number of elements with negative mass defects, such as fluorine, chlorine, bromine, oxygen, phosphorus, or sulfur, and with a low number of hydrogen atoms with a positive mass defect. The mass defect filter considerably reduced the dataset, even though not all features with negative mass defects can be attributed to highly fluorinated compounds. Accurate mass data have been evaluated by Kendrick mass analysis for compounds characterized by HS with CF<sub>2</sub>, CF<sub>2</sub>O, and C<sub>2</sub>F<sub>4</sub>O repeating units.

### Data evaluation of sample 1

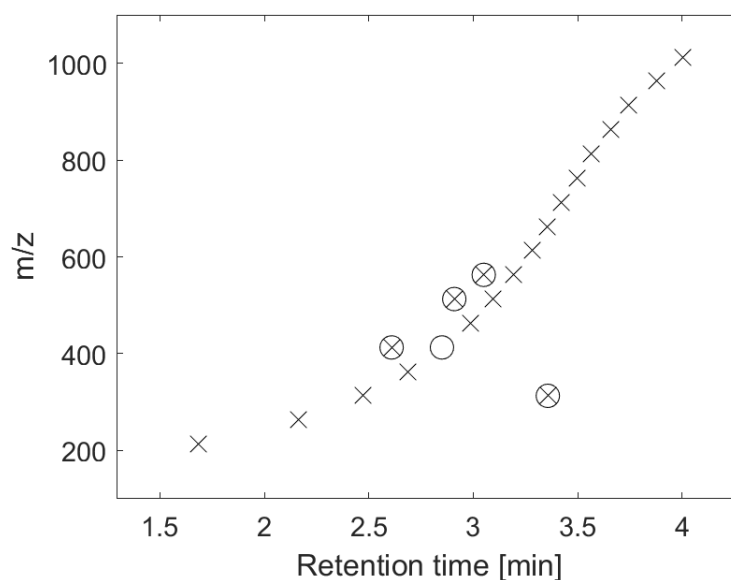
FindSeries revealed the occurrence of 329 HS based on CF<sub>2</sub> repeating units (see ESM Table S1). This still includes HS with only two compounds. Reducing this list to HS with at least three individual compounds condensed this dataset to 133 HS (see ESM Table S2). Visualization in a CF<sub>2</sub>-based Kendrick mass defect plot (Fig. 1) easily allows a first overview on the data. Compounds belonging to the same class are aligned horizontally. As a second criterion, increasing retention time with increasing mass is used to identify members of a true HS. This is visualized by color code of the data points in Fig. 1 from dark to white for increasing retention times.



**Fig. 1** Kendrick mass defect for CF<sub>2</sub> repeating units vs. mass-to-charge ratio. Only selected HS with at least 7 homologues are shown. Each feature is represented by a circle in different colors to distinguish HS. The color code of the dot filling corresponds to the normalized RT and therefore comprises the full range for each HS from dark to white for short to long RT

Finally, 70 HS fulfilled the criteria of HS detection with at least 3 homologues and systematic RT shifts. They are marked in green in ESM Table S2. This reduced list of the accurate masses is matched with the OECD database (available in ESM Table S3) for a first tentative identification. For example, HS 82 consists of 20 single features (see ESM Table S1). Plotting these features in a  $m/z$  vs. RT diagram (see Fig. 2) shows a clear RT shift for most of the features. Four features obviously differ from the clear trend (marked with encircled multiplication sign), and another feature with  $m/z$  413 at the correct RT is missing (marked with empty circle). The absence of a signal may be due to missing of the compound, low signal intensity, or mismatch in the feature finding algorithm MFE. All features of this HS could be matched with at least one compound of the OECD PFAS database. The number of matches is indicated in the "Presence" row. The lowest  $m/z$  in this HS,  $m/z$  212.9793, was matched with the two isomeric PFCAs heptafluorobutyric acid (CAS number 375-224) and heptafluoroisobutyric acid (CAS number 335-10-4). Also, all other homologues of HS 82 could be assigned to PFCAs. Next, the extracted ion chromatograms (EICs) of the features were checked manually at a mass accuracy of 10 ppm (ESM Fig. S1). Since the MFE algorithm could always miss single features, also missing members of the HS were included and confirmed, for example the presence of the previously discussed missing feature at  $m/z$  413. Since some peaks exhibit shoulders or not well separated peaks in front ( $m/z$  412.9664), the MFE algorithm registered two peaks which were marked with encircled multiplication sign in Fig. 2.  $m/z$  412.9664 (also a fronting peak) was integrated once with a rather short RT and therefore explains the missing feature in Fig. 2. Identification of  $m/z$  412.9664 as PFOA could be confirmed by an authentic standard (ESM Fig. S1.1). The other PFCA homologues of HS 82 could be identified with confidence level 2a. This procedure was repeated for each of the 70 HS which are marked in green in ESM Table S2. This resulted in the identification of the following substance classes: PFSAs, diSAmPAPs, FTUCAs, diPAPs, and  $n:3$  PFCAs. Identification based on standards for these evaluated substance classes is shown in Figs. S1.2 to S1.8 (see ESM). Further identifications based on matches with the OECD PFAS database with only one homologue are shown in ESM Table S3. For example,  $m/z$  497.9457 (line 153 in ESM Table S3) was assigned to FOSA and finally confirmed by an authentic standard (ESM Fig. S1.3).

Chromatograms were checked manually for further perfluoroalkanesulfonamide (FASA) homologues which were not detected in this case. This procedure was repeated for most compounds in ESM Table S3. Compounds are discarded which are likely to be false positives, for example if no ionization in ESI negative is expected. This procedure further identified the following substance classes: FASA, N-methyl perfluoroalkanesulfonamide (MeFASA), N-ethyl perfluoroalkanesulfonamide (EtFASA), and N-ethylperfluoro-1-alkanesulfonamidoacetic acid (EtFASAA) (one compound each). A complete list of all findings, including the identification level according to Schymanski et al. [39], is presented in Table 1, and the identified substance classes are discussed subsequently.



**Fig. 2** Systematic retention time shift for HS 82 (PFCAs). Legend: multiplication sign, feature from FindSeries following the RT shift trend; encircled multiplication sign, feature from FindSeries not following the RT shift trend; empty circle, missing feature from FindSeries (possible miss from the MFE)

### diPAPs (HS 252) and triPAPs (HS M1)

A total of 8 diPAP homologues were detected (corresponding to 4:2/6:2, 6:2/6:2, 6:2/8:2, 8:2/8:2, 8:2/10:2, 10:2/10:2, 10:2/12:2, 12:2/12:2, and 12:2/14:2) and confirmed by an authentic standard of 6:2/8:2 diPAP. diPAPs are known to be used in food contact paper to act as grease repellent [6], making their occurrence in the paper sludge that was applied on the arable land plausible. Manual inspection of the diPAP chromatograms revealed further peaks with longer retention times. However, these peaks were suspected to originate from triPAPs which are impurities in diPAP products [6]. During ESI, triPAPs are fragmented in-source by the loss of a fluorotelomer alcohol



(FTOH) group and therefore appear as diPAPs in LC-MS chromatograms [6, 40, 41]. However, from one triPAP, multiple peaks can result from in-source fragmentation (e.g., 6:2/8:2/10:2 triPAP) depending on which FTOH chain is lost. As a result, an unequivocal identification of triPAPs is challenging, also because authentic standards are not available for all homologues. Therefore, only 6:2/6:2/6:2 triPAP could be identified with an authentic standard, and the other homologues could be tentatively identified and were assigned to confidence level 3.

#### **diPAP TPs: FTUCAs (HS 40), n:3 PFCAs (HS 265), and PFCAs (HS 82)**

DiPAPs and triPAPs can be transformed into FTOHs by cleavage of the phosphate ester bonds [42], which can be further degraded to several compound classes like FTUCAs, PFCAs, or n:3 PFCAs [43].

Five homologues of FTUCAs have been detected in sample 1 (10:2, 12:2, 14:2, 16:2, and 18:2). Based on a study by Liu and Avendano [44], 8:2 FTUCA is a precursor of several PFCAs (perfluorohexanoic, perfluoroheptanoic, and perfluorooctanoic acids). Longer FTUCA homologues are hence expected to transform into longer-chain PFCAs. An authentic standard for 8:2 FTUCA was used to evaluate the mass fragmentation, which is characterized by the loss of HFCO<sub>2</sub> at a collision energy of 20 eV. The same fragments were observed for the FTUCA congeners that are found in the soil sample (data available in ESM Figs. S1.11–S1.16), and confidence level 2b was hence assigned to this HS. Further degradation of FTUCAs can produce n:3 PFCAs of which five were detected (7:3, 9:3, 11:3, 13:3, and 15:3) and confirmed by a reference standard of 7:3 PFCA. These n:3 PFCAs are suggested to further break down into PFCAs [44]. In total, 16 different PFCA homologues were found, ranging from carbon chain lengths C<sub>5</sub> up to C<sub>20</sub>. PFOA was used as reference standard. PFCAs are rather persistent compounds which will hardly be further degraded in the environment [43].

#### **diSAmPAPs (HS 17)**

Three homologues of the diSAmPAP class (C<sub>7</sub>/C<sub>8</sub>, C<sub>8</sub>/C<sub>8</sub>, and C<sub>8</sub>/C<sub>9</sub>) were detected in sample 1. C<sub>8</sub>/C<sub>8</sub> was confirmed by a standard and is with 98% of the intensity of all diSAmPAPs by far the most abundant homologue in sample 1. This points to the use of PFAS products on a C<sub>8</sub>-based chemistry. DiSAmPAP is a chemical that was used directly in food contact papers and had a high production volume until 2002 [31].

### **diSAmPAP TPs: EtFASAAs (HS M2), MeFASAAs (HS M3), EtFASAAs (HS M4), FASAAs (HS M5), and PFSAAs (HS 321)**

The degradation of diSAmPAPs in marine sediments showed several TPs like EtFASAAs, EtFASAAs, FASAAs, and PFSAAs [22], which could be confirmed in our work. MeFASA most likely is an impurity in diSAmPAP products. Identification of diSAmPAPs, EtFASAAs, FASAAs, and PFSAAs was confirmed by a C8-based reference standard of each compound class. As already expected from the dominant occurrence of C8/C8 diSAmPAP, no other homologues than C8 could be detected for EtFASAA, MeFASA, EtFASA, and FASA. The intensity of PFOS was higher than 99.5% compared to the sum of the intensities from all measured PFSAAs. This finding suggests PFOS as the degradation product of C8/C8 diSAmPAPs.

### **False positive assignments**

PFPIAs were first suggested to occur in the contaminated soil sample (see ESM Table S1, HS 4). Even though only higher homologues than the available reference standard of the C6/C6-PFPIA ( $m/z$  700.9221) were detected in the soil, the standard was used to record an MS/MS spectrum at 40 eV (ESM Fig. S1.9). Two fragments at  $m/z$  62.9638 (PO<sub>2</sub>) and  $m/z$  400.9415 (C<sub>6</sub>F<sub>14</sub>O<sub>2</sub>P) have been detected. While the fragment  $m/z$  400.9415 is dependent on the PFPIA chain length, the PO<sub>2</sub> fragment should occur for any PFPIA homologue but did not. Therefore, PFPIA homologues could not be identified (ESM Fig. S1.10).

### **Further unknown PFASs**

In addition to the identified PFASs, the data still contain many unidentified PFASs occurring in HS with CF<sub>2</sub>, CF<sub>2</sub>O, and C<sub>2</sub>F<sub>4</sub>O repeating units. FindSeries suggested 50 HS based on CF<sub>2</sub> repeating units, 23 HS based on CF<sub>2</sub>O, and 13 HS based on C<sub>2</sub>F<sub>4</sub>O, each with a minimum number of 5 individual compounds (data available in ESM Tables S5 and S6). While some of them may be false positives for example due to in-source fragmentation or adduct formation, we expect also the presence of true positives which are absent in the OECD PFAS database and may be degradation products of the original PFAS products.

**Table 1** Identified PFAS classes and their number of homologues in sample 1

HS no.	Identified as	Number of homologues	Mass range	Identification level
252	diPAPs	8	689 - 1389	Level 2a (1x Level 1*)
M1	triPAPs	>4	N/A	Level 3 (1x Level 1*)
40	FTUCAs	5	557 - 957	Level 2b
265	n:3 PFCAs	5	441 - 841	Level 2a (1x Level 1*)
82	PFCAs	16	263 - 1013	Level 2a (1x Level 1*)
17	diSAmPAPs	3	1103 - 1263	Level 2a (1x Level 1*)
M2	EtFASAs	1	584	Level 1
M3	MeFASAs	1	512	Level 3
M4	EtFASAs	1	526	Level 3
M5	FASAs	1	498	Level 1
321	PFASAs	5	399 - 599	Level 2a (1x Level 1*)

Details can be found in ESM Table S1 under the corresponding HS no. Manually detected compound classes are marked with an M. For accurate masses of all homologues, see ESM Table S4

\*For reference standards, see ESM Table S4

### Results for samples 2, 3, and 4 and comparison of all four samples

Analogous to sample 1, samples 2, 3, and 4 were evaluated and the results are summarized in Tables 2, 3, and 4. Detailed information and accurate masses are presented in ESM Table S4.

Also samples 2, 3, and 4 are characterized by the presence of diPAPs (7 to 8 homologues: 4:2/6:2, 6:2/6:2, 6:2/8:2, 8:2/ 8:2, 8:2/10:2, 10:2/10:2, 10:2/12:2, 12:2/12:2, and 12:2/14:2), C8/C8 diSAmPAP (only 1 dominating homologue), and their TPs. In all four samples, PFCAs reveal a large number of homologues between 14 and 17. n:3 PFCAs were detected only in samples 1 and 3 and FTSAAs only in samples 2 and 4. FTSAAs are not expected to be TPs of either diPAPs or diSAmPAPs. Hence, they could either occur from the degradation of another, so-far unidentified or already fully degraded, precursor.

**Table 2** Identified PFAS classes and their number of homologues in sample 2

HS no.	Identified as	Number of homologues	Mass range	Identification level
248	diPAPs	7	789 - 1389	Level 2a (1x Level 1)
M1	triPAPs	>4	N/A	Level 3 (1x Level 1)
86	PFCAs	17	213 - 1013	Level 2a (1x Level 1)
23	diSAmPAPs	1	1203	Level 1
M2	EtFASAAAs	1	584	Level 1
M3	FASAs	1	498	Level 1
312	PFSAs	7	299 - 599	Level 2a (1x Level 1)
166	FTSAs	6	427 - 927	Level 2a (1x Level 1)

Manually detected compound classes are marked with an M. For accurate masses of all homologues, see ESM Table S4

**Table 3** Identified PFAS classes and their number of homologues in sample 3

HS no.	Identified as	Number of homologues	Mass range	Identification level
250	diPAPs	8	689 - 1389	Level 2a (1x Level 1)
M1	triPAPs	>4	N/A	Level 3 (1x Level 1)
265	n:3 PFCAs	5	441 - 841	Level 2a (1x Level 1)
M2	PFCAs	15	213 - 963	Level 2a (1x Level 1)
16	diSAmPAPs	1	1203	Level 1
M3	EtFASAAAs	1	584	Level 1
M4	MeFASA	1	512	Level 3
M5	FASAs	1	498	Level 1
M6	PFSAs	4	399 - 549	Level 2a (1x Level 1)

Manually detected compound classes are marked with an M. For accurate masses of all homologues, see ESM Table S4

**Table 4** Identified PFAS classes and their number of homologues in sample 4

HS no.	Identified as	Number of homologues	Mass range	Identification level
290	diPAPs	7	789 - 1389	Level 2a (1x Level 1)
M1	triPAPs	> 4	N/A	Level 3 (1x Level 1)
M2	PFCAs	14	213 - 913	Level 2a (1x Level 1)
M3	diSAmPAPs	1	1203	Level 1
M4	EtFASAAAs	1	584	Level 1
M5	FASAs	1	498	Level 1
M6	PFSAs	4	399 - 549	Level 2a (1x Level 1)
192	FTSAs	4	627 - 927	2a

Manually detected compound classes are marked with an M. For accurate masses of all homologues, see ESM Table S4

### **Estimated concentration levels**

Based on the response factors of the authentic standards for single PFASs at one concentration level (each at 5 µg/L corresponding to 10 µg/kg soil), concentration levels of these PFASs have been estimated for the soil samples. In soil sample 1, PFOA occurred at about 60 µg/kg (ESM Fig. S1.1), PFOS at 100 µg/kg (ESM Fig. S1.4), EtFOSAA at 100 µg/kg (ESM Fig. S1.5), 6:2/8:2 diPAP at 210 µg/kg (ESM Fig. S1.7), and diSAmPAP at 630 µg/kg (ESM Fig. S1.8). In sample 2, PFOA was found at 250 µg/kg (ESM Fig. S1.46) and 6:2/8:2 diPAP at 20 µg/kg (ESM Fig. S1.47); in sample 3, PFOA was 240 µg/kg (ESM Fig. S1.48) and 6:2/8:2 diPAP 90 µg/kg (ESM Fig. S1.49); in sample 4, PFOA had 90 µg/kg (ESM Fig. S1.50) and 6:2/ 8:2 diPAP 70 µg/kg (ESM Fig. S1.51).

Based on these results, diPAPs and PFCAs are suggested to be the major contaminants in all four samples. In sample 1, diSAmPAP and its TPs (PFOS and EtFOSAA) are the dominating contaminants followed by diPAPs and its TPs.

### **8.6 Conclusions**

Paper sludge contaminated with PFAS products caused a complex contamination on agricultural soils, since different not further characterized PFAS products and a considerable number of different TPs contribute to the overall contamination. LC-high-resolution mass spectrometry (LC-HRMS) data revealed the complex contamination. The identification of homologous series (HS) of original compounds and transformation products (TPs) by Kendrick mass analysis and systematic retention time shifts was a successful strategy to confidently identify PFASs also with a very limited number of authentic standards. DiPAPs (7–8 homologues, 4:2/6:2 to 12:2/14:2) and diSAmPAP (C8/C8) have been identified as the major contaminants of the soils. These PFASs were also used in products for paper impregnation. All other major compound classes could be linked to known TPs of these products with the only exception of FTSAAs. The low availability of authentic standards and suitable database entries especially for TPs mainly limit the identification of numerous unknowns which are still in the HRMS data. The application of the proposed workflow on technical products in original form and after degradation tests is a further promising approach to increase the fraction of identified PFAS and their TPs in environmental samples.

## Acknowledgments

Open Access funding provided by Projekt DEAL. The authors thank the “Landwirtschaftliches Technologiezentrum Augustenberg” (Karlsruhe) for supplying the soil samples, “Technologiezentrum Wasser (TZW)” (Karlsruhe) for the project coordination, and Selina Tisler and Rebecca Bauer for their valuable support for the data evaluation, and the state of Baden-Württemberg for funding of the project EOFplus (L75 17012).

**Conflict of interest** The authors declare that they have no conflict of interest.

**Open Access** This article is licensed under a Creative Commons Attribution 4.0 International License, which permits use, sharing, adaptation, distribution and reproduction in any medium or format, as long as you give appropriate credit to the original author(s) and the source, provide a link to the Creative Commons licence, and indicate if changes were made. The images or other third party material in this article are included in the article's Creative Commons licence, unless indicated otherwise in a credit line to the material. If material is not included in the article's Creative Commons licence and your intended use is not permitted by statutory regulation or exceeds the permitted use, you will need to obtain permission directly from the copyright holder. To view a copy of this licence, visit <http://creativecommons.org/licenses/by/4.0/>.

## 8.7 References

1. Buck RC, Franklin J, Berger U, Conder JM, Cousins IT, deVoogt P, et al. Perfluoroalkyl and polyfluoroalkyl substances in the environment: terminology, classification, and origins. *Integr Environ Assess Manag*. 2011;7(4):513–41.
2. OECD. Toward a new comprehensive global database of per- and polyfluoroalkyl substances (PFASs). 2018. <http://www.oecd.org/chemicalsafety/risk-management/global-database-of-per-andpolyfluoroalkyl-substances.xlsx>. Accessed 22.08.2019.
3. Lang JR, Allred BM, Peaslee GF, Field JA, Barlaz MA. Release of per- and polyfluoroalkyl substances (PFASs) from carpet and clothing in model anaerobic landfill reactors. *Environ Sci Technol*. 2016;50(10):5024–32.
4. Sinclair W, Kim SK, Akinleye HB, Kannan K. Quantitation of gas phase perfluoroalkyl surfactants and fluorotelomer alcohols released from nonstick cookware and microwave popcorn bags. *Environ Sci Technol*. 2007;41(4):1180–5.

5. Zabaleta I, Negreira N, Bizkarguenaga E, Prieto A, Covaci A, Zuloaga O. Screening and identification of per- and polyfluoroalkyl substances in microwave popcorn bags. *Food Chem.* 2017;230: 497–506.
6. Trier X, Granby K, Christensen JH. Polyfluorinated surfactants (PFS) in paper and board coatings for food packaging. *Environ Sci Pollut Res.* 2011;18(7):1108–20.
7. Fujii Y, Harada KH, Koizumi A. Occurrence of perfluorinated carboxylic acids (PFCAs) in personal care products and compounding agents. *Chemosphere.* 2013;93(3):538–44.
8. Barzen-Hanson KA, Roberts SC, Choyke S, Oetjen K, McAlees A, Riddell N, et al. Discovery of 40 classes of per- and polyfluoroalkyl substances in historical aqueous film-forming foams (AFFFs) and AFFF-impacted groundwater. *Environ Sci Technol.* 2017;51(4): 2047–57.
9. Favreau P, Poncioni-Rothlisberger C, Place BJ, Bouchex-Bellomie H, Weber A, Tremp J, et al. Multianalyte profiling of per- and polyfluoroalkyl substances (PFASs) in liquid commercial products. *Chemosphere.* 2017;171:491–501.
10. Giesy JP, Kannan K. Global distribution of perfluorooctane sulfonate in wildlife. *Environ Sci Technol.* 2001;35(7):1339–42.
11. Dreyer A, Weinberg I, Temme C, Ebinghaus R. Polyfluorinated compounds in the atmosphere of the Atlantic and Southern oceans: evidence for a global distribution. *Environ Sci Technol.* 2009;43(17):6507–14.
12. Rankin K, Mabury SA, Jenkins TM, Washington JW. A North American and global survey of perfluoroalkyl substances in surface soils: distribution patterns and mode of occurrence. *Chemosphere.* 2016;161:333–41.
13. Yamashita N, Taniyasu S, Petrick G, Wei S, Gamo T, Lam PKS, et al. Perfluorinated acids as novel chemical tracers of global circulation of ocean waters. *Chemosphere.* 2008;70(7):1247–55.
14. Cui L, Zhou QF, Liao CY, Fu JJ, Jiang GB. Studies on the toxicological effects of PFOA and PFOS on rats using histological observation and chemical analysis. *Arch Environ Contam Toxicol.* 2009;56(2):338–49.
15. Shi X, Du Y, Lam PK, Wu RS, Zhou B. Developmental toxicity and alteration of gene expression in zebrafish embryos exposed to PFOS. *Toxicol Appl Pharmacol.* 2008;230(1):23–32.
16. Bao Y, Deng S, Jiang X, Qu Y, He Y, Liu L, et al. Degradation of PFOA substitute: GenX (HFPO-DA ammonium salt): oxidation with UV/persulfate or reduction with UV/sulfite? *Environ Sci Technol.* 2018;52(20):11728–34.
17. Gomis MI, Vestergren R, Borg D, Cousins IT. Comparing the toxic potency in vivo of long-chain perfluoroalkyl acids and fluorinated alternatives. *Environ Int.* 2018;113:1–9.

18. Sun M, Arevalo E, Strynar M, Lindstrom A, Richardson M, Kearns B, et al. Legacy and emerging perfluoroalkyl substances are important drinking water contaminants in the Cape Fear River watershed of North Carolina. *Environ Sci Technol.* 2016;3(12):415–9.
19. Janda J, Nödler K, Brauch H-J, Zwiener C, Lange FT. Robust trace analysis of polar (C 2-C 8) perfluorinated carboxylic acids by liquid chromatography-tandem mass spectrometry: method development and application to surface water, groundwater and drinking water. *Environ Sci Pollut Res.* 2019;26(8):7326–36.
20. Yu N, Guo H, Yang J, Jin L, Wang X, Shi W, et al. Non-target and suspect screening of per- and polyfluoroalkyl substances in airborne particulate matter in China. *Environ Sci Technol.* 2018;52(15): 8205–14.
21. Gremmel C, Frömel T, Knepper TP. Systematic determination of perfluoroalkyl and polyfluoroalkyl substances (PFASs) in outdoor jackets. *Chemosphere.* 2016;160:173–80.
22. Llorca M, Farré M, Picó Y, Müller J, Knepper TP, Barceló D. Analysis of perfluoroalkyl substances in waters from Germany and Spain. *Sci Total Environ.* 2012;431:139–50.
23. Hollender J, Schymanski EL, Singer HP, Ferguson PL. Nontarget screening with high resolution mass spectrometry in the environment: ready to go? *Environ Sci Technol.* 2017;51(20):11505–12.
24. Schymanski EL, Singer HP, Longree P, Loos M, Ruff M, Stravs MA, et al. Strategies to characterize polar organic contamination in wastewater: exploring the capability of high resolution mass spectrometry. *Environ Sci Technol.* 2014;48(3):1811–8.
25. Wang Y, Yu N, Zhu X, Guo H, Jiang J, Wang X, et al. Suspect and nontarget screening of per- and polyfluoroalkyl substances in wastewater from a fluorochemical manufacturing park. *Environ Sci Technol.* 2018;52(19):11007–16.
26. Strynar M, Dagnino S, McMahan R, Liang S, Lindstrom A, Andersen E, et al. Identification of novel perfluoroalkyl ether carboxylic acids (PFECAs) and sulfonic acids (PFESAs) in natural waters using accurate mass time-of-flight mass spectrometry (TOFMS). *Environ Sci Technol.* 2015;49(19):11622–30.
27. Regierungspräsidium Karlsruhe. PFC-Problematik: Zwischenbilanz und Ausblick. 2018. [https://rp.badenwuerttemberg.de/rpk/Abt5/Ref541/PFC/Seiten/pfc\\_buergerinfo.aspx](https://rp.badenwuerttemberg.de/rpk/Abt5/Ref541/PFC/Seiten/pfc_buergerinfo.aspx). Accessed 22.08.2019.
28. Brendel S, Fetter E, Staude C, Vierke L, Biegel-Engler A. Shortchain perfluoroalkyl acids: environmental concerns and a regulatory strategy under REACH. *Environ Sci Eur.* 2018;30(1):9.
29. Biegel-Engler A, Vierke L, Apel P, Fetter E, Staude C. Mitteilungen des Umweltbundesamtes zu per- und polyfluorierten Chemikalien (PFC) in Trinkwasser. *Bundesgesundheitsbl Gesundheitsforsch Gesundheitsschutz.* 2017;60(3):341–6.



30. Schaidler LA, Balan SA, Blum A, Andrews DQ, Strynar MJ, Dickinson ME, Lunderberg DM, Lang JR, Peaslee GF. Fluorinated compounds in US fast food packaging. *Environ Sci Technol Lett.* 2017; 4: 105–111.
31. Benskin JP, Ikonomou MG, Gobas FA, Begley TH, Woudneh MB, Cosgrove JR. Biodegradation of N-ethyl perfluorooctane sulfonamido ethanol (EtFOSE) and EtFOSE-based phosphate diester (SAmPAP diester) in marine sediments. *Environ Sci Technol.* 2013;47(3):1381–9.
32. Liu C, Liu J. Aerobic biotransformation of polyfluoroalkyl phosphate esters (PAPs) in soil. *Environ Pollut.* 2016;212:230–7.
33. Ghisi R, Vamerali T, Manzetti S. Accumulation of perfluorinated alkyl substances (PFAS) in agricultural plants: a review. *Environ Res.* 2018.
34. Bizkarguenaga E, Zabaleta I, Mijangos L, Iparraguirre A, Fernández LA, Prieto A, et al. Uptake of perfluorooctanoic acid, perfluorooctane sulfonate and perfluorooctane sulfonamide by carrot and lettuce from compost amended soil. *Sci Total Environ.* 2016;571:444–51.
35. Ministerium für Soziales und Integration (Baden-Württemberg). Erste Ergebnisse der PFC-Blutuntersuchungen im Landkreis Rastatt liegen vor. 2018. <https://sozialministerium.badenwuerttemberg.de/de/service/presse/pressemitteilung/pid/ersteergebnisse-der-pfc-blutuntersuchungen-im-landkreis-rastatt-liegenvor/>. Accessed 22.08.2019.
36. Ingelido AM, Abballe A, Gemma S, Dellatte E, Iacovella N, De Angelis G, et al. Biomonitoring of perfluorinated compounds in adults exposed to contaminated drinkingwater in the Veneto region, Italy. *Environ Int.* 2018;110:149–59.
37. Kendrick E. A mass scale based on CH<sub>2</sub>= 14.0000 for high resolution mass spectrometry of organic compounds. *Anal Chem.* 1963;35(13):2146–54.
38. Alygizakis N. PFAS|NORMAN: list of PFAS from the OECD curated by Nikiforos Alygizakis. 2019. [https://comptox.epa.gov/dashboard/chemical\\_lists/pfastrier](https://comptox.epa.gov/dashboard/chemical_lists/pfastrier). Accessed 22.08.2019.
39. Schymanski EL, Jeon J, Gulde R, Fenner K, Ruff M, Singer HP, et al. Identifying small molecules via high resolution mass spectrometry: communicating confidence. *Environ Sci Technol.* 2014;48(4):2097–8.
40. Gebbink WA, Ullah S, Sandblom S, Berger U. Polyfluoroalkyl phosphate esters and perfluoroalkyl carboxylic acids in target food samples and packaging—method development and screening. *Environ Sci Pollut Res.* 2013;20(11):7949–58.
41. Trier X, Nielsen NJ, Christensen JH. Structural isomers of polyfluorinated di- and tri-alkylated phosphate ester surfactants present in industrial blends and in microwave popcorn bags. *Environ Sci Pollut Res Int.* 2011;18(8):1422–32.

42. D'Eon J, Mabury S. Production of perfluorinated carboxylic acids (PFCAs) from the biotransformation of polyfluoroalkyl phosphate surfactants (PAPs): exploring routes of human contamination. *Environ Sci Technol*. 2007;41(13):4799–805.
43. Wang N, Szostek B, Buck RC, Folsom PW, Sulecki LM, Gannon JT. 8-2 Fluorotelomer alcohol aerobic soil biodegradation: pathways, metabolites, and metabolite yields. *Chemosphere*. 2009;75(8):1089–96.
44. Liu J, Avendano SM. Microbial degradation of polyfluoroalkyl chemicals in the environment: a review. *Environ Int*. 2013;61:98–114.

**Publisher's note** Springer Nature remains neutral with regard to jurisdictional claims in published maps and institutional affiliations.

**Chapter 9** – personal contribution

<b>Author</b>	<b>Author position</b>	<b>Scientific ideas %</b>	<b>Data generation %</b>	<b>Analysis &amp; interpretation %</b>	<b>Paper writing %</b>
Boris Bugsel	1	80	80	90	80
Rebecca Bauer	2	0	15	0	0
Florian Herrmann	3	0	5	2.5	0
Martin E. Maier	4	0	0	2.5	0
Christian Zwiener	5	20	0	5	20
Title of paper:	LC-HRMS screening of per- and polyfluorinated alkyl substances (PFAS) in impregnated paper samples and contaminated soils				
Status in publication process:	Submitted for publication to: <i>Analytical &amp; Bioanalytical Chemistry</i>				

## 9 LC-HRMS screening of per- and polyfluorinated alkyl substances (PFAS) in impregnated paper samples and contaminated soils

Boris Bugsel<sup>1</sup>, Rebecca Bauer<sup>1</sup>, Florian Herrmann<sup>2</sup>, Martin E. Maier<sup>2</sup>, Christian Zwiener<sup>1</sup>

<sup>1</sup> Environmental Analytical Chemistry, Center for Applied Geoscience, University of Tübingen, Schnarrenbergstr. 94-96, 72076, Tübingen

<sup>2</sup> Institute for Organic Chemistry, University of Tübingen, Auf der Morgenstelle 18, 72076 Tübingen

Manuscript submitted for publication to: *Analytical & Bioanalytical Chemistry*

## 9.1 Abstract

High PFAS concentrations have been detected in agricultural soils in Southwest Germany. Discharges of PFAS contaminated paper sludge and compost are suspected to be the cause of the contamination. Perfluorinated carboxylic acids (PFCAs) have been detected also in groundwater, drinking water and plants in this area. Recently, previously unknown compounds have been identified by high-resolution mass spectrometry (HRMS). Major contaminants were polyfluorinated dialkylated phosphate esters (diPAPs) and N-Ethyl perfluorooctane sulfonamide ethanol-based phosphate diester (diSAmPAP). In this study, HRMS screening for PFAS was applied to 14 soil samples from the contaminated area and 14 impregnated paper samples which were from a similar period than the contamination. The paper samples were characterized by diPAPs (from 4:2/6:2 to 12:2/12:2), fluorotelomer mercapto alkyl phosphates (FTMAPs; 6:2/6:2 to 10:2/10:2) and diSAmPAP. In soil samples, diPAPs and their transformation products (TPs) were the major contaminants, but also FTMAPs, diSAmPAP and their TPs occurred. The distribution patterns of the carbon chain lengths of the precursor PFAS in soil samples were shown to resemble those in paper samples. This supports the hypothesis that paper sludge is a major source of contamination. The presence of major degradation products like PFCAs, FTSAAs or PFOS and their distribution of carbon chain lengths indicate the activity of biotic or abiotic degradation processes and selective leaching processes from the upper soil horizons.

## 9.2 Introduction

Per- and polyfluorinated alkyl substances (PFAS) have unique properties and a broad application spectrum. Currently, PFAS comprise a family of 4730 known individual compounds [1]. They are chemically and thermally very stable compounds [2] and characterized by hydrophobic and lipophobic properties. Therefore, PFAS are advantageous compounds in many consumer products and in industrial processes. They are widely used as oil and water repellents for textiles [3], paper products [4], but also as surfactants in fire-fighting foams [5] and industrial processes like electroplating [6]. However, concerns about PFAS come from their high persistence, their potential to bioaccumulate and to cause adverse health effects in laboratory and wild animals

[7-10]. Due to the widespread and extensive use of PFAS, they are found in aquatic and terrestrial fauna, in human blood serum [11], in ground, surface and drinking water [12-17].

Many of commercially used PFAS can be partially degraded in the environment. These compounds are referred to as precursor compounds. Typical PFAS precursors that were applied to food contact paper in the past include dialkylated polyfluorinated phosphate esters (diPAPs) along with their mono- and trialkylated analogues as impurities (mono and triPAPs) as well as N-Ethyl perfluorooctane sulfonamide ethanol-based phosphate diester (diSAmPAP) [4].

Even though biotic and abiotic transformation can play a role for many precursor PFAS, perfluorocarboxylic acids (PFCAs) are typical dead-end transformation products (TPs) [18-21]. They can for example reach the environment via wastewater treatment plant effluents due to the use in consumer and personal care products [22,23], landfill leachates [3] or atmospheric deposition [24].

In a recent case in SW Germany, the “Rastatt case”, high PFAS concentrations have been detected in soil, plants, groundwater and even drinking water [25-28]. Deposition of compost mixed with waste from paper industry onto arable land between the years 2000 and 2008 is suspected to be the main cause of contamination [29]. Our earlier study on the Rastatt site [25] focused on the determination and characterization of the contamination by liquid chromatography coupled to high resolution mass spectrometry (LC-HRMS). It could be shown that diPAPs and diSAmPAP play a major role in the contamination of agricultural fields. Over time, diPAPs can degrade by cleavage of the phosphate ester bond which then results in a fluorotelomer alcohol (FTOH) [18]. Further degradation products which were detected in soil samples include n:2 fluorotelomer unsaturated carboxylic acids (FTUCAs), n:3 acids and PFCAs [30]. Also diSAmPAP TPs were detected including N-Ethyl perfluorooctane sulfonamidoacetate (EtFOSAA) and perfluorooctanesulfonate (PFOS) [31].

To understand the big picture of the sources and fate of the contamination, we tested the hypothesis that the contaminant patterns on soils can be traced back to PFAS products used for paper impregnation. Therefore, in this work we characterized PFAS and potential transformation products (TPs) from impregnated paper products from

the early 2000s and compared the results to PFAS patterns from contaminated soil samples.

### 9.3 Material & Methods

#### **Chemicals and reagents**

Optima LC-MS grade methanol (MeOH), ammonium acetate (NH<sub>4</sub>Ac) and water were purchased from Fisher Scientific. Bis[2-(perfluorohexyl)ethyl]phosphate (6:2 diPAP), 6:2 fluorotelomer sulfonic acid (6:2 FTSA), N-ethyl polyfluoroalkyloctane sulfonamidoacetic acid (EtFOSAA), N-ethyl perfluorooctane sulfonamide ethanol-based phosphate diester (diSAmPAP), linear perfluorooctane sulfonic acid (PFOS) and perfluoroheptanoic acid (PFHpA) were purchased from Wellington Laboratories, Inc. (Guelph, Ontario, Canada). Perfluorooctanesulfonamide (FOSA) was obtained from SynQuest Laboratories (Alachua, FL, USA). 6:2 fluorotelomer mercapto alkyl phosphate (6:2 FTMAP) was synthesized according to literature [32]. Further details on the identification of the synthesized FTMAP by HRMS and NMR are given in ESM 1.

#### **Sample preparation**

Homogenized, freeze-dried soil samples from the plough horizon (top 30 cm) were provided by the Agricultural Technology Center Augustenberg (Karlsruhe, Germany). 5 g were weighed into a polypropylene (PP) tube and extracted with 10 mL methanol. The mixture was sonicated for 15 min and put onto a horizontal shaker for 24 h. The polypropylene tube was subsequently centrifuged (15 min, 3000 rcf). An aliquot (1 mL) was transferred into a PP vial and centrifuged again prior to analysis (15 min, 6000 rcf).

Paper samples consisted of a variety of store-bought paper products including muffin liners (5 samples: P8, P9, P10, P12, P14) and paper plates (1 sample: P4) as well as raw papers (8 samples: P1, P2, P3, P5, P6, P7, P11, P13) used for the production of consumer products. They were provided by the Fraunhofer Institute for Process Engineering and Packaging (Freising, Germany) and collected in the time period between 2000 and 2010. The papers were cut into rectangular shapes with defined surface areas in the range of 47 cm<sup>2</sup> – 308 cm<sup>2</sup> (details in Table S1), put in 5 L beakers,

fully immersed in 100 mL MeOH and shaken overnight. The beakers were tightly sealed with transparent foil to prevent evaporation of the MeOH. The extracts were then transferred into round-bottom flasks and reduced to < 5 mL with a rotary evaporator at 40 °C and 330 mbar. The enriched extracts were transferred into 5 mL glass vials and evaporated to 1 mL with a gentle stream of nitrogen. Prior to analysis, the samples were centrifuged (15 min, 6000 rcf) and transferred to a PP vial.

### **Instrumental analysis**

For soil samples S11 – S14 and paper samples P1 – P14, an Agilent C18 column (Poroshell 120 EC-C18, 2.1 mm × 100 mm, particle size 2.7 µm) with a flow rate of 0.4 mL/min and a temperature of 40 °C was used. Eluent A (95:5 v/v H<sub>2</sub>O/MeOH) and eluent B (95:5 v/v MeOH/H<sub>2</sub>O), both with 5 mM NH<sub>4</sub>Ac, were used for gradient elution. The gradient started with 25 % B, followed by a linear increase to 85 % B within 2 min and 100 % B within 2.5 min. 100 % B was kept isocratic until 12 min, followed by an equilibration time of the initial conditions until 15 min. 20 µL were injected.

Soil samples S1-S10 were analyzed with a slightly different LC method. For soil samples S1-S10, an Acquity UPLC BEH C18 column (2.1 mm × 100 mm, particle size 1.7 µm) equipped with an Acquity UPLC BEH C18 guard column (2.1 mm × 5 mm, particle size 1.7 µm) with a flow rate of 0.4 mL/min and at a temperature of 60 °C was used. Eluent A (95:5 v/v H<sub>2</sub>O/MeOH) and eluent B (95:5 v/v MeOH/H<sub>2</sub>O), both with 2 mM NH<sub>4</sub>Ac, were used for gradient elution. The gradient started with 40 % B, followed by a linear increase to 60 % B within 1 min and 100 % B within 1.5 min. 100 % B was kept isocratic until 4.5 min, followed by an equilibration time of the initial conditions until 7 min. 10 µL were injected.

All samples were measured on a 1290 HPLC system (Agilent Technologies, Waldbronn, Germany) coupled to a 6550 QTOF (Agilent Technologies, Santa Clara, USA) operated in negative ionization mode with a scan range from m/z 100 to m/z 1700.

### **Data evaluation**

Determination and identification of suspect compounds was determined according to the method described in our previous work [25]. Briefly, samples were screened for PFAS a) by finding compounds in homologous series with CF<sub>2</sub> repeating units and b)



by comparing the accurate masses of all features with exact masses in the OECD PFAS database. This database was manually extended with PFAS from literature research. Peak integration of confirmed compounds was performed using ProFinder 10.0 from Agilent Technologies. According to Schymanski et al. (2014) [33], we assigned confidence level 1a for compound identifications that were confirmed with an authentic standard; level 1b for homologues of an identified compound (1a) with systematic retention time shifts; level 3, if only an accurate mass fit was available. No other levels were assigned. For further information on the systematic retention time shifts, see our previous publication (Bugsel & Zwiener (2020) [25]).

Python was used for statistical evaluation and plotting of the data, the heatmap was modified and degradation schemes were drawn using InkScape. Boxplots were generated using the standard settings of the seaborn package in Python.

Due to different data acquisition methods from various sampling campaigns, the relative distribution patterns of homologues within a compound class for each sample have been compared. These patterns are generally independent of the concentrations and acquisition methods and can therefore be used across all samples. Commercial PFAS products typically contain homologue patterns from the industrial synthesis which may vary depending on manufacturer and batch, and are therefore useful as a sort of fingerprint.

For each compound class with multiple homologues, the weighted average perfluorinated carbon chain length for each sample  $C_{avg}$  can be calculated according to equation 1:

$$C_{avg} = \sum_{i=1}^k \left( \frac{A_i}{\sum A_i} \cdot n_i \right) \quad (1)$$

where  $A_i$  is the peak area and  $n_i$  is the carbon chain length of the homologue  $i$ . For example, consider the detection of the three different PFCAs perfluoroheptanoic, -octanoic and -nonanoic acid with  $A_i = 0.7, 1$  and  $0.6$ , respectively. With  $\sum A_i = 2.3$  and  $n_i = (6, 7, 8)$ , the weighted average chain length would be  $C_{avg} = 6.96$ . These values may differ from the average chain length weighted with the actual concentration. However, due to the non-target screening approach and the lack of analytical

standards, we used this approach, well-aware that ionization efficiency is known to vary within one homologous series.

## 9.4 Results & Discussion

### **Occurrence of PFAS classes**

PFAS impregnated paper samples and PFAS contaminated soil samples were analyzed by LC-HRMS to compare patterns of homologous series of PFAS. A total of 31 individual compounds out of 8 different compound classes were identified in all samples using a previously described method [25]. The full result set including signal abundances, mass deviations and confidence levels of identification is given in ESM2. The compound classes PFCAs, diPAPs, diSAmPAP, EtFOSAA, FOSA, FTSA and FTMAPs were confirmed with one authentic standard for each homologous series. FOSAA was confirmed by its accurate mass with an error less than 15 ppm. Chemical structures of precursor compounds and related transformation products are shown in Figures S1, S2 and S3. A clustermap visualizes the occurrence of different compound classes and their normalized abundances for all samples and allows to compare the chemical composition of the samples (Figure 1). Clusters of samples and compounds are based on the correlation distance metric (for further information see ESM1).

### **Cluster analysis & relationship of compound classes**

Interestingly, all samples are clearly subdivided into three clusters (Figure 1): Cluster 1) consists of paper samples P2, 3, 5, 6, 7, 12 which are dominated by FTMAPs and FTSA; cluster 2) represents paper samples P1, 4, 8, 9, 10, 11, 13, 14 which are dominated by diPAPs; and cluster 3) comprises soil samples S1 – S14, which are mainly characterized by diPAPs, PFOS and PFCAs.

In cluster 1) FTMAPs range from 6:2/6:2 to 10:2/10:2 and are typically found in commercial products for paper impregnation like Lodyne P208E (Trier et al. 2011). For example, from paper P2 9 mg/m<sup>2</sup> of 6:2/6:2 FTMAP were extractable by methanol (see ESM 1 for further information). FTSA range from 6:2 to 12:2 and are suggested to be processing aids or reagents of FTMAP synthesis.

In paper samples of cluster 2) diPAPs dominate in the range between 4:2/6:2 and 12:2/12:2. They are used in commercial fluorinated impregnation products like Zonyl [34].

All soil samples in cluster 3) are dominated by diPAPs (4:2/6:2 to 12:2/12:2), PFOS and PFCAs. Especially perfluorodecanoic acid (PFDA) occurs in all soil samples (S1 - S14). PFCAs are break-down products of diPAPs [18,30], which explains their simultaneous occurrence in soil samples.

The high abundances of PFOS are suggested to originate from the biodegradation of diSAmPAP as precursor [31,25], which itself is also found in high abundances in soil samples (S4, S7, S8, S10-S14). Further TPs of diSAmPAP are EtFOSAA, FOSAA and FOSA which were also found in samples with high PFOS contamination. The co-occurrence of precursors and degradation products hint to the presence of active degradation processes, even if the kinetics may be rather slow since the precursor compounds are still being found 10 years after the last discharge. Interestingly, samples S2 - S8, S10, and S12 with high PFOS contamination show less diPAP abundance and vice versa (S1, S9, S11, S13, S14). This is a strong hint to different contamination sources on these soil plots.

The soil sample S13 which appears in the clustermap at the upper fringe of cluster 3 (Figure 1) is further characterized by the occurrence of five FTMAPs (6:2/6:2 to 10:2/10:2) and FTSAAs (6:2 to 12:2) which hint to an additional contamination source compared to other soil samples. 8:2/10:2 FTMAP was further detected in S11 and S14. To the best of our knowledge, this is the first time that FTMAPs could be detected and identified in an environmental sample. Figure 2 shows the extracted ion chromatograms of five FTMAP homologues and their characteristic retention time shifts. Their identity has been confirmed by accurate mass, accurate mass fragments and retention time of the synthesized 6:2/6:2 FTMAP (ESM1). In addition to the occurrence of FTSAAs as byproducts in paper, FTSAAs may be break-down products of FTMAPs [32], which are formed by cleavage of the carbon-sulfur bond and further oxidation of the thiol group of the fluorotelomer side chain.

## Comparison of compound patterns & homologue distribution

The results of the cluster analysis support the hypothesis that paper waste impregnated with PFAS precursors is the primary source of soil contamination which is reflected by PFAS patterns of impregnated paper products. Therefore, we compared the compound patterns in paper and soil samples in more detail and considered the distribution of homologues for the precursors diPAPs and FTMAPs, as well as for the transformation products PFCAs and FTSA by principal component analysis (PCA) (Figure 3) and boxplots demonstrating the average carbon chain lengths  $C_{avg}$  (Figure 4). In the PCA plot for diPAPs in Figure 3a) soil and paper samples show a rather broad distribution. DiPAPs in soils cluster in the lower left corner of the PCA plot and are partly separated from those in paper. Interestingly, the two paper samples P4 and P13 are well-positioned within the soil cluster, and are characterized by the abundant occurrence of 8:2/10:2 diPAP and rather low intensities of 6:2/6:2 and 6:2/8:2 diPAP. The results indicate a rather broad distribution of diPAP products used for paper impregnation and more specific, but still different input sources for soil contamination on the different soil plots. It should still be emphasized here that the diPAP patterns in soil can also be changed by environmental processes. The PCA plots for PFCAs, the major products of biodegradation, show a different picture (Figure 3b). A rather clear separation of paper vs. soil samples along component 1 reveals clear differences in the distribution pattern between the soil samples and the paper samples. Analogously, we see a similar picture for the PCA plots of FTMAPs (Figure 3c), which show a broad distribution for the paper samples but the occurrence in only one soil sample (S13). FTMAP patterns of S13 resemble well those of paper samples P2 and P5, which suggests again a rather specific source of contamination. The PCA plots of FTSA, the major degradation products of FTMAPs, show again a clear separation between the soil and paper samples (Figure 3d). The occurrence of FTSA in five soil samples (S9, S11-14) further indicate a past FTMAP contamination of which only the degradation products are still visible. But also, direct FTSA discharge or contamination of so far unidentified precursors which may also form FTSA has to be taken into consideration.

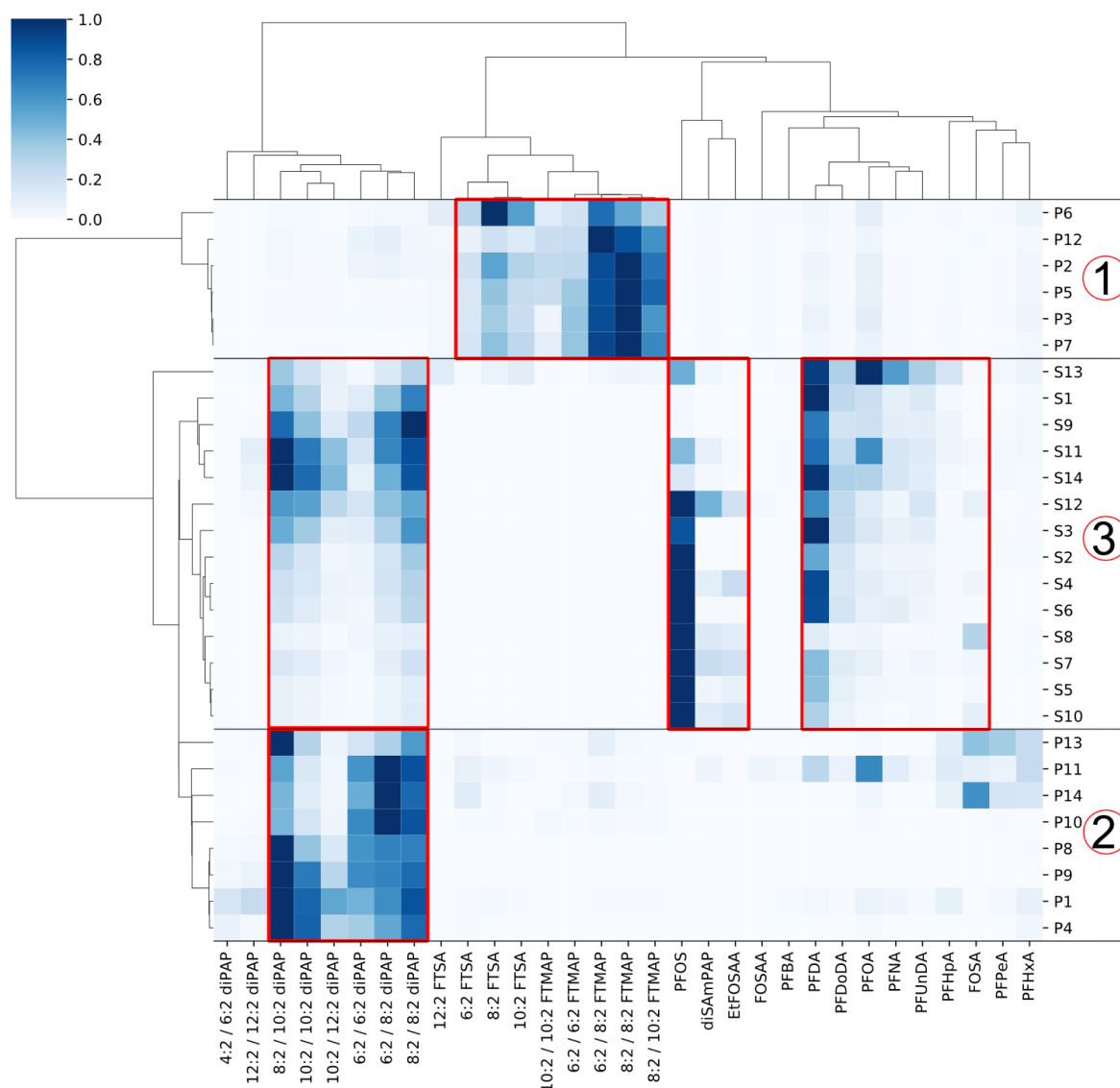
## Comparison of carbon chain lengths & environmental implications

Since various commercial PFAS products differ in their relative distribution of homologues, the differences between samples for individual compound classes can be worked out by the length of the carbon chains. We therefore plotted the weighted average length of the perfluorinated carbon chains  $C_{avg}$  for each sample in Figure 4. For diPAPs the distribution of  $C_{avg}$  in soil samples is narrower than that for paper samples, but both are still overlapping. The same applies to FTMAP which is only occurring in one soil sample. For both diPAPs and FTMAPs we see a trend to longer  $C_{avg}$  in soil samples. For the TPs PFCAs and FTSAAs, we clearly see higher  $C_{avg}$  values and therefore longer chain lengths in soil samples and a clear separation of the distribution patterns between paper and soil. The average carbon chain lengths of PFCAs in soil samples are at about 10 and for paper samples between 7 and 8, whereas for FTSAAs we found  $C_{avg}$  above 11 in soils and between 6 and 8 in papers. The data have to be interpreted against the background that the TPs can be introduced into soil via paper waste, but can also be formed in soil from the precursors diPAPs and FTMAPs by environmental processes. Therefore, we expect to find TPs with  $C_{avg}$  that fit to the original contamination of the so-far unknown input material concerning TPs and PFAS precursors. The shift of PFCAs and FTSAAs to longer chain lengths compared to their occurrence in paper and more importantly to their precursors diPAPs and FTMAPs can be explained by the fact that sorption and transport of PFAS precursors and TPs strongly depends on their carbon chain length.

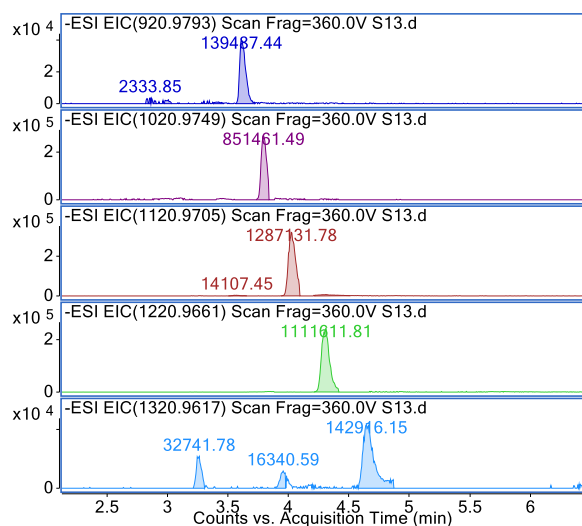
Sorption of PFAS in soils and sediments is generally increased with perfluoroalkyl chain length [35-37]. Short chain PFCAs and PFSAs with up to six carbon atoms showed early breakthrough in column leaching tests while their longer chain homologues were still retarded due to sorption to sediment [38]. This may explain the shift to long chain PFCAs and FTSAAs in the topsoil, whereas short-chain TPs have been already transported to deeper soil horizons by leachate. Since the soil-water distribution coefficients of the precursors diPAP and FTMAP which bear two polyfluorinated carbon chains are even higher than the corresponding PFCAs [37], they are expected to reside in the top soil within the plough horizon. This has been confirmed by the predominance of diPAPs in the upper 40 cm of a soil core [39] and by little or no detection in deeper soil layers (n = 14/14 in 0 cm – 30 cm deep layer

(S1-S14), n = 1/8 in 30 cm – 60 cm deep layer (S8), n = 0/7 in 60 cm – 90 cm deep layer; data of deeper soil layers not shown). Therefore, formation of PFCAs and FTSAAs has occurred from corresponding precursors in the top soils, whereas short-chain PFCAs and FTSAAs have been displaced by leachate to deeper soil horizons.

Overall, we can conclude that PFAS found in the soil samples are in good agreement with the PFAS used for paper impregnation. The paper impregnation products diPAPs, FTMAPs, and diSAmPAP and their TPs have been shown to play a major role in the soil contamination and their origin can be attributed to paper products. Differences in the patterns of TPs between paper and soil samples can be attributed mainly to sorption and leaching processes which are strongly dependent on carbon chain lengths.

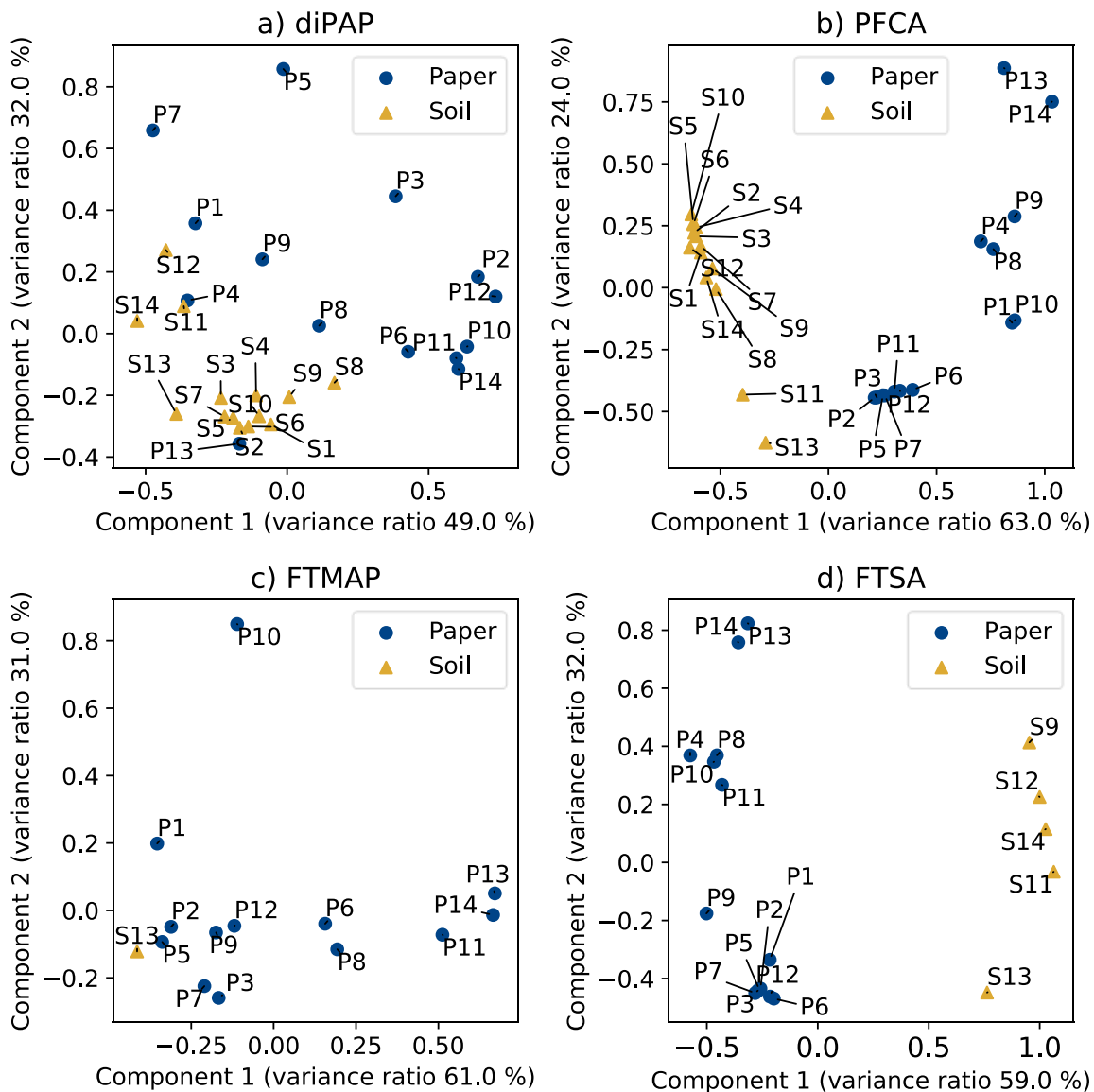


**Figure 1:** Clustermap for the occurrence and relative intensity of PFAS and potential TPs in paper (P1-14) and soil (S1-14) samples. Cluster 1) Papers dominated by FTMAPs and TPs; cluster 2) Papers with diPAPs; cluster 3) soil samples dominated by diPAPs, PFOS and PFCAs. The normalized peak intensity for each sample is color coded. Dendrograms are generated using the correlation distance metric (SI).

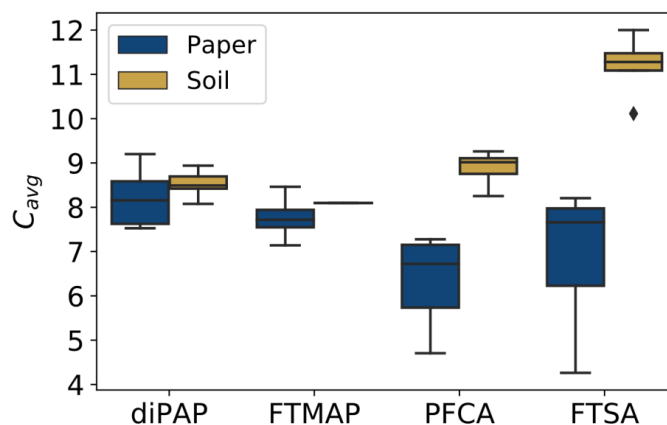


**Figure 2:** Extracted ion chromatograms (10 ppm) for five FTMAPs in soil sample S13. 6:2/6:2 FTMAP ( $m/z$  920.9812) was identified with the synthesized standard, further FTMAP homologues are characterized by the repeating unit  $C_2F_4$  ( $\Delta m/z$  99.9936).





**Figure 3:** Principal component analysis (PCA) based on the normalized chain length distribution patterns in paper and soil samples for a) diPAPs, b) PFCAs, c) FTMAPs and d) FTSA.



**Figure 4:** Box-Whisker-Plot for the weighted average lengths of the perfluorinated carbon chain  $C_{avg}$  of diPAPs, FTMAPs, PFCAs, and FTSA in 14 soil and 14 paper samples. For diPAPs and FTMAPs which bear two fluorotelomer carbon chains only the average carbon length of one side chain was considered. The box represents 25, 75 percentiles and the median, whiskers show the minimum and maximum values, the diamond indicates an outlier.

### Acknowledgement

We acknowledge funding of the project FluorTECH by the state of Baden-Württemberg (BWPFC 19010) and project coordination by F. Sacher, TZW (German Water Center), Karlsruhe. We thank M. Schlummer, Fraunhofer Institute for Process Engineering and Packaging, Freising, for paper samples and J. Breuer, Agricultural Technology Center Augustenberg, Karlsruhe, for supplying the soil samples.

## 9.5 References

1. OECD (2018) Toward a New Comprehensive Global Database of Per- and Polyfluoroalkyl Substances (PFASs). <http://www.oecd.org/chemicalsafety/risk-management/global-database-of-per-and-polyfluoroalkyl-substances.xlsx>. Accessed 01.07.2020
2. Kissa E (2001) Fluorinated surfactants and repellents, vol 97. CRC Press.
3. Lang JR, Allred BM, Peaslee GF, Field JA, Barlaz MA (2016) Release of Per- and Polyfluoroalkyl Substances (PFASs) from Carpet and Clothing in Model Anaerobic Landfill Reactors. *Environmental Science & Technology* 50 (10):5024-5032.
4. Trier X, Granby K, Christensen JH (2011) Polyfluorinated surfactants (PFS) in paper and board coatings for food packaging. *Environmental Science and Pollution Research* 18 (7):1108-1120.
5. Barzen-Hanson KA, Roberts SC, Choyke S, Oetjen K, McAlees A, Riddell N, McCrindle R, Ferguson PL, Higgins CP, Field JA (2017) Discovery of 40 Classes of Per- and Polyfluoroalkyl Substances in Historical Aqueous Film-Forming Foams (AFFFs) and AFFF-Impacted Groundwater. *Environmental Science & Technology* 51 (4):2047-2057.
6. Glüge J, Scheringer M, Cousins I, DeWitt JC, Goldenman G, Herzke D, Lohmann R, Ng C, Trier X, Wang Z (2020) An overview of the uses of per-and polyfluoroalkyl substances (PFAS). *Environmental Science: Processes & Impacts* 22.12:2345-2373.
7. Kim M, Son J, Park MS, Ji Y, Chae S, Jun C, Bae J-S, Kwon TK, Choo Y-S, Yoon H, Yoon D, Ryoo J, Kim S-H, Park M-J, Lee H-S (2013) In vivo evaluation and comparison of developmental toxicity and teratogenicity of perfluoroalkyl compounds using *Xenopus* embryos. *Chemosphere* 93 (6):1153-1160.

8. Seacat AM, Thomford PJ, Hansen KJ, Clemen LA, Eldridge SR, Elcombe CR, Butenhoff JL (2003) Sub-chronic dietary toxicity of potassium perfluorooctanesulfonate in rats. *Toxicology* 183 (1-3):117-131.
9. Dennis NM, Karnjanapiboonwong A, Subbiah S, Rewerts JN, Field JA, McCarthy C, Salice CJ, Anderson TA (2020) Chronic Reproductive Toxicity of Perfluorooctane Sulfonic Acid and a Simple Mixture of Perfluorooctane Sulfonic Acid and Perfluorohexane Sulfonic Acid to Northern Bobwhite Quail (*Colinus virginianus*). *Environmental Toxicology and Chemistry* 39 (5):1101-1111.
10. Barmantlo SH, Stel JM, van Doorn M, Eschauzier C, de Voogt P, Kraak MH (2015) Acute and chronic toxicity of short chained perfluoroalkyl substances to *Daphnia magna*. *Environmental Pollution* 198:47-53.
11. Olsen GW, Mair DC, Lange CC, Harrington LM, Church TR, Goldberg CL, Herron RM, Hanna H, Nobiletti JB, Rios JA (2017) Per- and polyfluoroalkyl substances (PFAS) in American Red Cross adult blood donors, 2000–2015. *Environmental Research* 157:87-95.
12. McCord J, Strynar M (2019) Identification of Per- and Polyfluoroalkyl Substances in the Cape Fear River by High Resolution Mass Spectrometry and Nontargeted Screening. *Environmental Science & Technology* 53 (9):4717-4727.
13. Yu N, Guo H, Yang J, Jin L, Wang X, Shi W, Zhang X, Yu H, Wei S (2018) Non-Target and Suspect Screening of Per- and Polyfluoroalkyl Substances in Airborne Particulate Matter in China. *Environmental Science & Technology* 52 (15):8205-8214.
14. Wang Y, Yu N, Zhu X, Guo H, Jiang J, Wang X, Shi W, Wu J, Yu H, Wei S (2018) Suspect and Nontarget Screening of Per- and Polyfluoroalkyl Substances in Wastewater from a Fluorochemical Manufacturing Park. *Environmental Science & Technology* 52 (19):11007-11016.

15. Pan Y, Zhang H, Cui Q, Sheng N, Yeung LWY, Sun Y, Guo Y, Dai J (2018) Worldwide Distribution of Novel Perfluoroether Carboxylic and Sulfonic Acids in Surface Water. *Environmental Science & Technology* 52 (14):7621-7629.
16. Chen H, Yao Y, Zhao Z, Wang Y, Wang Q, Ren C, Wang B, Sun H, Alder AC, Kannan K (2018) Multimedia Distribution and Transfer of Per- and Polyfluoroalkyl Substances (PFASs) Surrounding Two Fluorochemical Manufacturing Facilities in Fuxin, China. *Environmental Science & Technology* 52 (15):8263-8271.
17. Nguyen MA, Wiberg K, Ribeli E, Josefsson S, Futter M, Gustavsson J, Ahrens L (2017) Spatial distribution and source tracing of per-and polyfluoroalkyl substances (PFASs) in surface water in Northern Europe. *Environmental Pollution* 220:1438-1446.
18. D'Eon J, Mabury S (2007) Production of Perfluorinated Carboxylic Acids (PFCAs) from the Biotransformation of Polyfluoroalkyl Phosphate Surfactants (PAPs): Exploring Routes of Human Contamination. *Environmental Science & Technology* 41 (13):4799-4805.
19. Mejia Avendano S, Liu J (2015) Production of PFOS from aerobic soil biotransformation of two perfluoroalkyl sulfonamide derivatives. *Chemosphere* 119:1084-1090.
20. Wang N, Liu J, Buck RC, Korzeniowski SH, Wolstenholme BW, Folsom PW, Sulecki LM (2011) 6:2 fluorotelomer sulfonate aerobic biotransformation in activated sludge of waste water treatment plants. *Chemosphere* 82 (6):853-858.
21. Zabaleta I, Bizkarguenaga E, Izagirre U, Negreira N, Covaci A, Benskin JP, Prieto A, Zuloaga O (2017) Biotransformation of 8:2 polyfluoroalkyl phosphate diester in gilthead bream (*Sparus aurata*). *Science of The Total Environment* 609:1085-1092.
22. Fujii Y, Harada KH, Koizumi A (2013) Occurrence of perfluorinated carboxylic acids (PFCAs) in personal care products and compounding agents. *Chemosphere* 93 (3):538-544.

23. Ahrens L (2011) Polyfluoroalkyl compounds in the aquatic environment: a review of their occurrence and fate. *Journal of Environmental Monitoring* 13 (1):20-31.
24. Ellis DA, Martin JW, De Silva AO, Mabury SA, Hurley MD, Sulbaek Andersen MP, Wallington TJ (2004) Degradation of fluorotelomer alcohols: a likely atmospheric source of perfluorinated carboxylic acids. *Environmental Science & Technology* 38 (12):3316-3321.
25. Bugsel B, Zwiener C (2020) LC-MS screening of poly- and perfluoroalkyl substances in contaminated soil by Kendrick mass analysis. *Analytical and Bioanalytical Chemistry* 412:4805.
26. Muschket M, Keltsch N, Paschke H, Reemtsma T, Berger U (2020) Determination of transformation products of per- and polyfluoroalkyl substances at trace levels in agricultural plants. *Journal of Chromatography A*:461271.
27. Biegel-Engler A, Vierke L, Apel P, Fetter E, Staude C (2017) Mitteilungen des Umweltbundesamtes zu per- und polyfluorierten Chemikalien (PFC) in Trinkwasser. *Bundesgesundheitsblatt Gesundheitsforschung Gesundheitsschutz* 60 (3):341-346.
28. Janda J, Nödler K, Brauch H-J, Zwiener C, Lange FT (2019) Robust trace analysis of polar (C 2-C 8) perfluorinated carboxylic acids by liquid chromatography-tandem mass spectrometry: method development and application to surface water, groundwater and drinking water. *Environmental Science and Pollution Research* 26 (8):7326-7336.
29. Söhlmann R, Striegel G, Lange FT (2018) Die Anwendung der Summenparameter EOF und AOF bei der Untersuchung der Tiefenverlagerung von Perfluoralkyl- und Polyfluoralkylverbindungen (PFAS) in belasteten Böden in Mittelbaden. *Mitt Umweltchem Ökotox* 24. Jahrg. 2018/ Nr.4:89-91.

30. Wang N, Szostek B, Buck RC, Folsom PW, Sulecki LM, Gannon JT (2009) 8-2 fluorotelomer alcohol aerobic soil biodegradation: pathways, metabolites, and metabolite yields. *Chemosphere* 75 (8):1089-1096.
31. Benskin JP, Ikonomou MG, Gobas FA, Begley TH, Woudneh MB, Cosgrove JR (2013) Biodegradation of N-ethyl perfluorooctane sulfonamido ethanol (EtFOSE) and EtFOSE-based phosphate diester (SAmPAP diester) in marine sediments. *Environmental Science & Technology* 47 (3):1381-1389.
32. Lee H, Mabury SA (2011) A pilot survey of legacy and current commercial fluorinated chemicals in human sera from United States donors in 2009. *Environmental Science & Technology* 45 (19):8067-8074.
33. Schymanski EL, Jeon J, Gulde R, Fenner K, Ruff M, Singer HP, Hollender J (2014) Identifying small molecules via high resolution mass spectrometry: communicating confidence. *Environ Sci Technol* 48 (4):2097-2098.
34. Trier X, Nielsen NJ, Christensen JH (2011) Structural isomers of polyfluorinated di- and tri-alkylated phosphate ester surfactants present in industrial blends and in microwave popcorn bags. *Environmental Science and Pollution Research* 18 (8):1422-1432.
35. Enevoldsen R, Juhler RK (2010) Perfluorinated compounds (PFCs) in groundwater and aqueous soil extracts: using inline SPE-LC-MS/MS for screening and sorption characterisation of perfluorooctane sulphonate and related compounds. *Analytical and Bioanalytical Chemistry* 398 (3):1161-1172.
36. Higgins CP, Luthy RG (2006) Sorption of perfluorinated surfactants on sediments. *Environmental Science & Technology* 40 (23):7251-7256.
37. Lee H, Mabury SA (2017) Sorption of perfluoroalkyl phosphonates and perfluoroalkyl phosphinates in soils. *Environmental Science & Technology* 51 (6):3197-3205.

38. Vierke L, Möller A, Klitzke S (2014) Transport of perfluoroalkyl acids in a water-saturated sediment column investigated under near-natural conditions. *Environmental Pollution* 186:7-13.

39. Janda J, Nodler K, Scheurer M, Happel O, Nurenberg G, Zwiener C, Lange FT (2019) Closing the gap - inclusion of ultrashort-chain perfluoroalkyl carboxylic acids in the total oxidizable precursor (TOP) assay protocol. *Environmental Science: Processes & Impacts* 21.11:1926-1935.

## 9.6 Supporting Information

### LC-MS Operating parameters

**Table S1:** Operating parameters used for HPLC-QTOF measurements

<b>Instrument Parameters</b>	<b>6550 QTOF</b>	<b>6470 QqQ</b>
Gas Temp (°C)	150	150
Gas Flow (L/min)	16	16
Nebulizer (psig)	35	45
Sheath gas temperature (°C)	380	380
Sheath gas flow (L/min)	12	12
Capillary voltage (V)	3000	3000
Nozzle voltage (V)	300	0

### Paper extraction

**Table S2:** Paper size used for extraction.

<b>Sample ID</b>	<b>Size [cm<sup>2</sup>]</b>
P1	307
P2	307
P3	307
P4	151
P5	307
P6	307
P7	307



P8	104
P9	104
P10	82
P11	47
P12	74
P13	89
P14	79

---

### Clustermap calculation

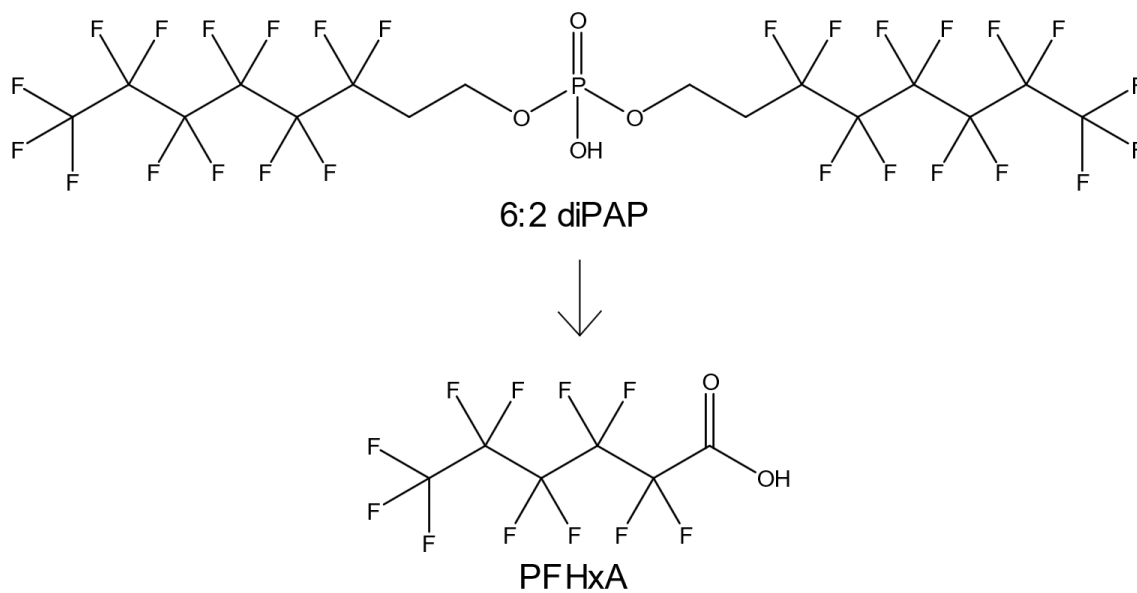
For the clustermap, distances between the samples were calculated according to the correlation distance metric which computes the correlation distance between two vectors  $u$  and  $v$  according to

$$1 - \frac{(u - \bar{u}) \cdot (v - \bar{v})}{\| (u - \bar{u}) \|_2 \| (v - \bar{v}) \|_2}$$

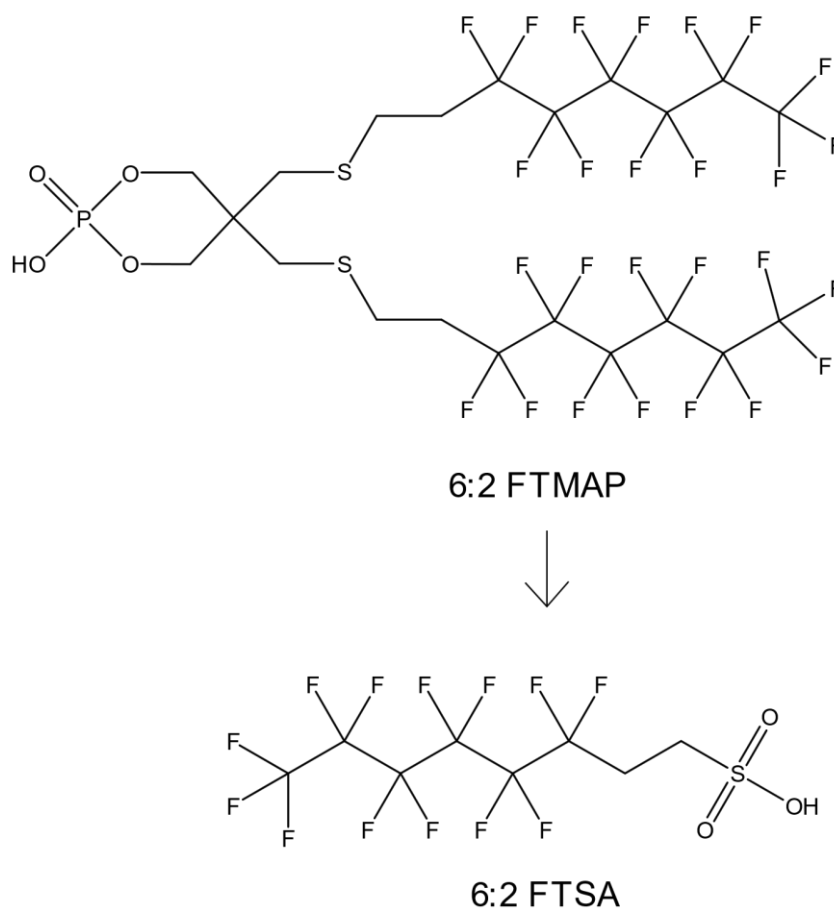
where  $\| (x) \|_p$  is the p-norm of  $x$ :

$$\| (x) \|_p := \left( \sum_{i=1}^n |x_i|^p \right)^{\frac{1}{p}}$$

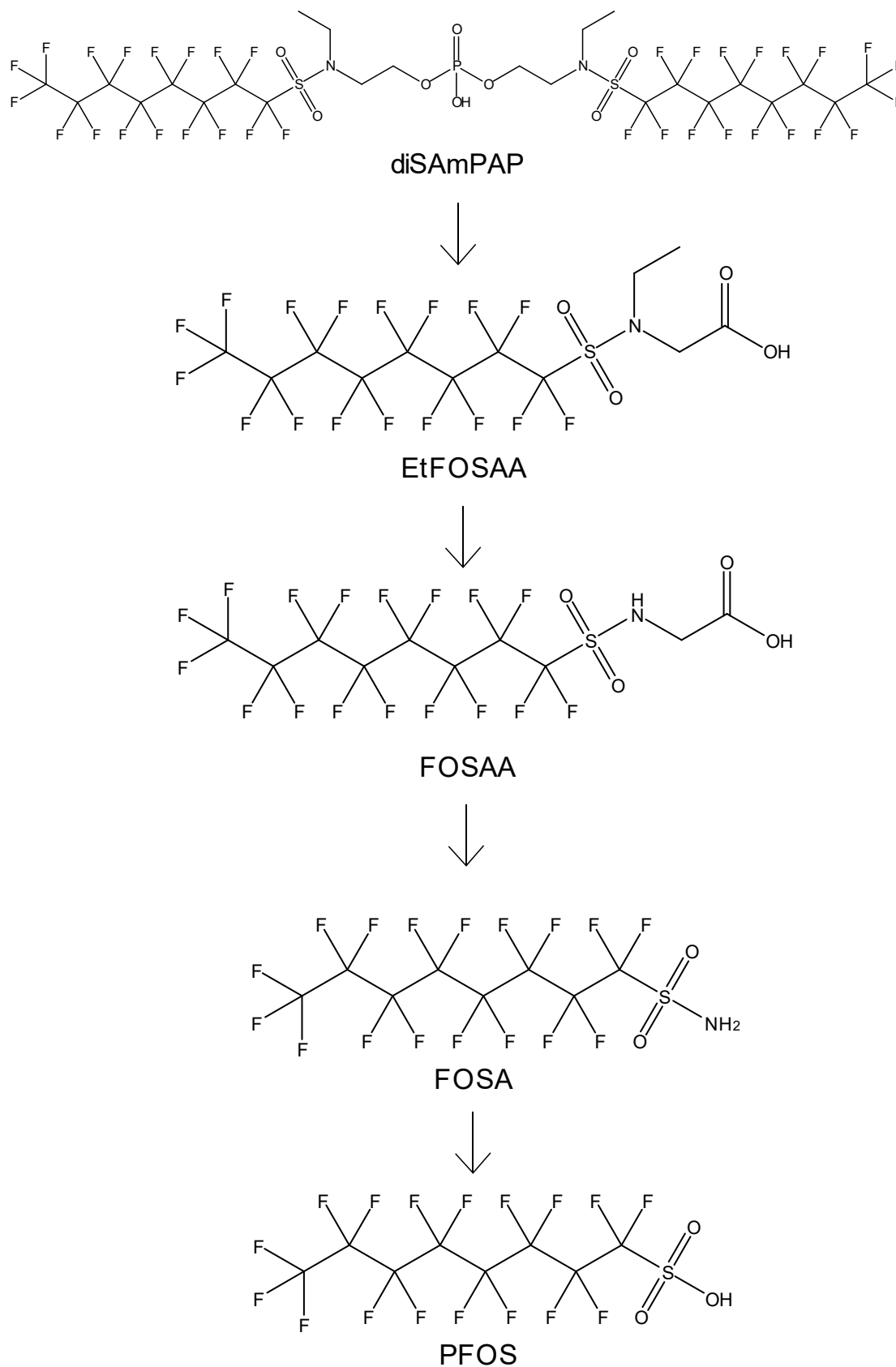
### Precursor classes, TP classes & suggested degradation schemes



**Figure S1:** 6:2/6:2 diPAP and the major TP perfluorohexanoic acid (PFHxA).



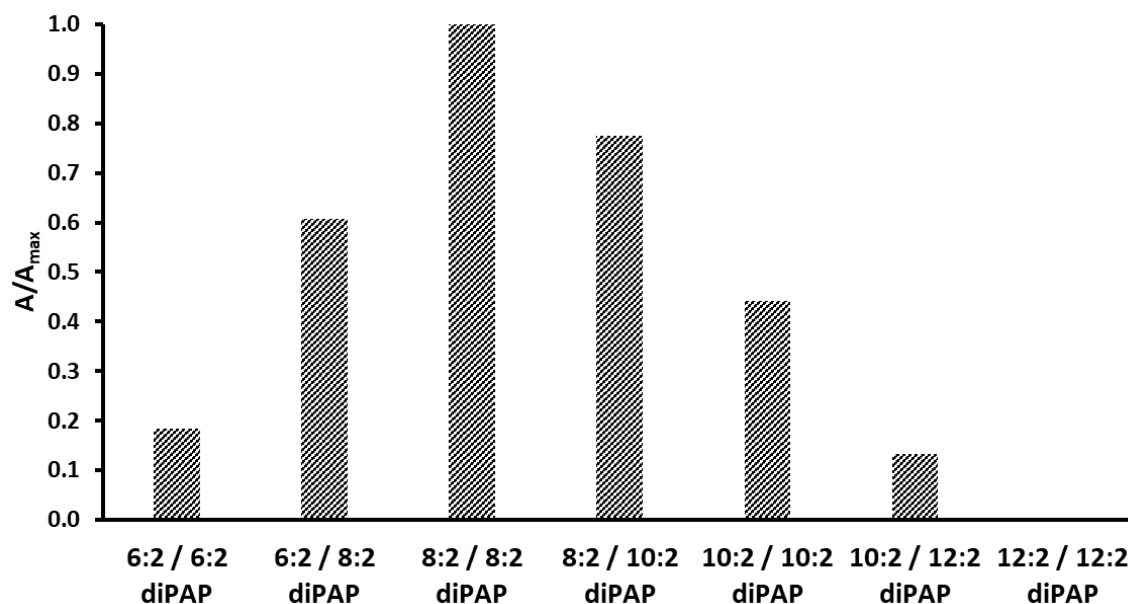
**Figure S2:** 6:2/6:2 FTMAP and the TP 6:2 FTSA.



**Figure S3:** diSAmPAP and the TPs EtFOSAA, FOSAA, FOSA and PFOS.

## Homologue patterns

Figure S4 shows the homologue pattern for diPAPs in soil sample S9. Relative signal intensities  $A$  are normalized by the signal intensity of 8:2/8:2 diPAP ( $A_{\max}$ ).



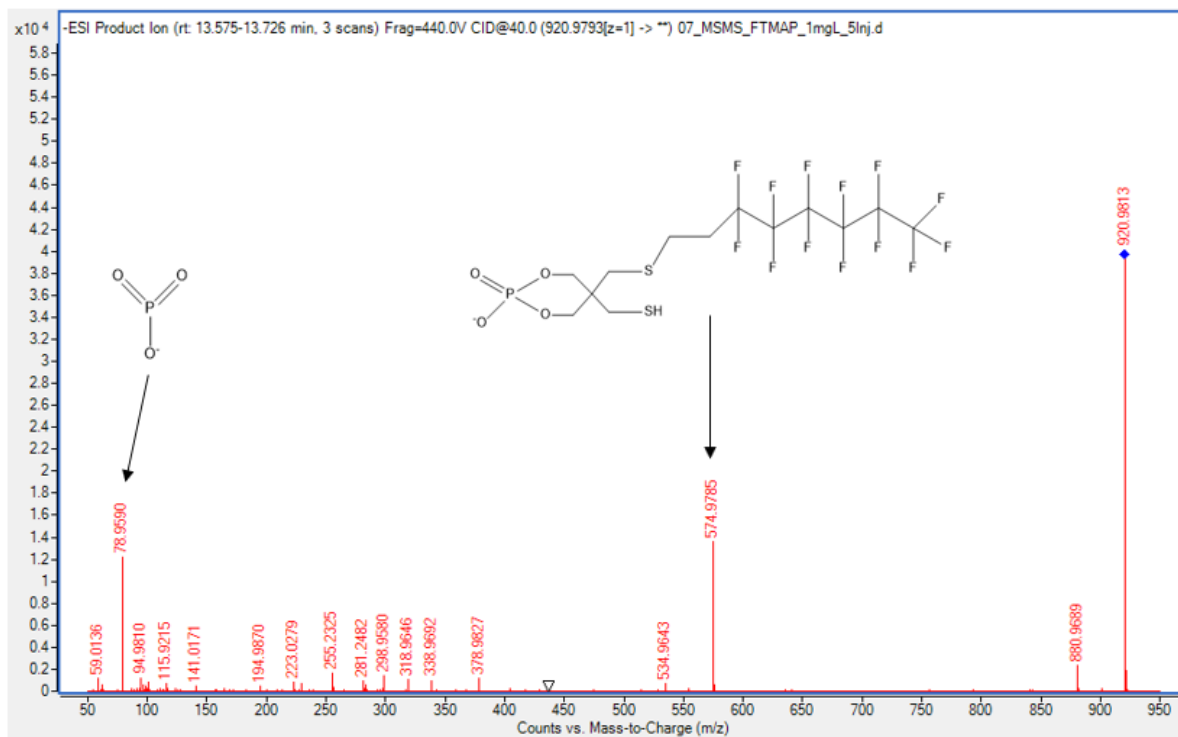
**Figure S4:** diPAP pattern in soil sample S9.

## Synthesis and identification of 6:2 FTMAP

6:2 FTMAP was synthesized according to the method supplied by Lee & Mabury (2011) [1]. Briefly, in the first step bis-(1H,1H,2H,2H-perfluorooctanethiolmethyl)-1,3-propanediol is obtained from a nucleophilic reaction of 1H,1H,2H,2H-perfluorooctanethiol with dibromopentyl glycol; the second reaction of bis-(1H,1H,2H,2H-perfluorooctanethiolmethyl)-1,3-propanediol with  $\text{POCl}_3$  yields the final white solid product which was recrystallized with m-xylene. The product was identified by  $^1\text{H}$ ,  $^{13}\text{C}$ ,  $^{31}\text{P}$  and  $^{19}\text{F}$  NMR and by high-resolution MS (targeted MS/MS, CE = 40 eV; 6550 QTOF-MS from Agilent Technologies).

## HRMS (spectrum in Fig. S5):

m/z 920.9813	[M-H] <sup>-</sup> (Δm 0.54 ppm)
m/z 880.9689	[M-H-2HF] <sup>-</sup> (Δm 0.5 ppm)
m/z 574.9785	[C <sub>13</sub> H <sub>13</sub> F <sub>13</sub> O <sub>4</sub> PS <sub>2</sub> ] <sup>-</sup> (Δm 1 ppm)
m/z 78.9590	[PO <sub>3</sub> ] <sup>-</sup> (Δm 0.7 ppm)



**Figure S5:** High resolution MS/MS fragmentation of the synthesized 6:2 FTMAP standard (1 mg/L; CE @ 40 eV).

## NMR

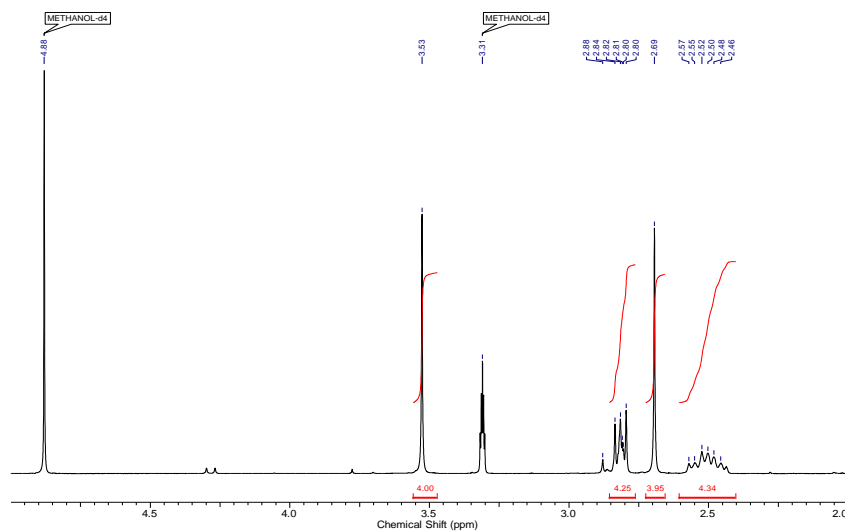
### $^1\text{H}$ ( $\text{CD}_3\text{OD}$ , 400 MHz)

$\delta = 2.46 - 2.57$  (m, 4H, CH<sub>2</sub>)

$\delta = 2.69$  (s, 4H, CH<sub>2</sub>)

$\delta = 2.8 - 2.88$  (m, 4H, CH<sub>2</sub>)

$\delta = 3.53$  (s, 4H, CH<sub>2</sub>)



**Figure S6:**  $^1\text{H}$  NMR spectrum of the synthesized 6:2 FTMAP standard (in  $\text{CD}_3\text{OD}$ , 400 MHz).

### $^{19}\text{F}$ ( $\text{CD}_3\text{OD}$ , 377 MHz)

$\delta = 82.5$  (CF<sub>3</sub>)

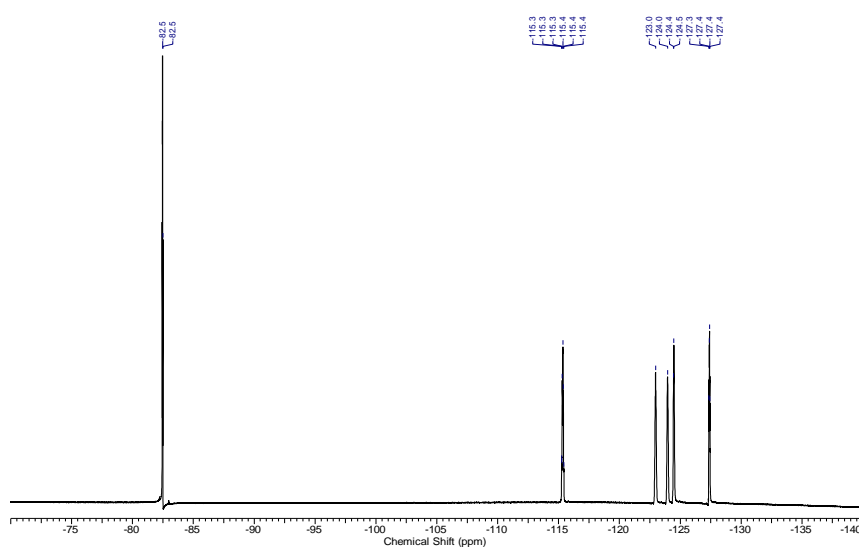
$\delta = 115.3-115.4$  (m, CF<sub>2</sub>)

$\delta = 123.0$  (s, CF<sub>2</sub>)

$\delta = 124.0$  (s, CF<sub>2</sub>)

$\delta = 124.4-124.5$  (d, CF<sub>2</sub>)

$\delta = 127.3-127.4$  (m, CF<sub>2</sub>)



**Figure S7:**  $^{19}\text{F}$  NMR spectrum of the synthesized 6:2 FTMAP standard (in  $\text{CD}_3\text{OD}$ , 377 MHz).

### $^{13}\text{C}$ ( $\text{CD}_3\text{OD}$ , 100 MHz)

$\delta = 25.17$

$\delta = 33.15$

$\delta = 33.36$

$\delta = 35.49$

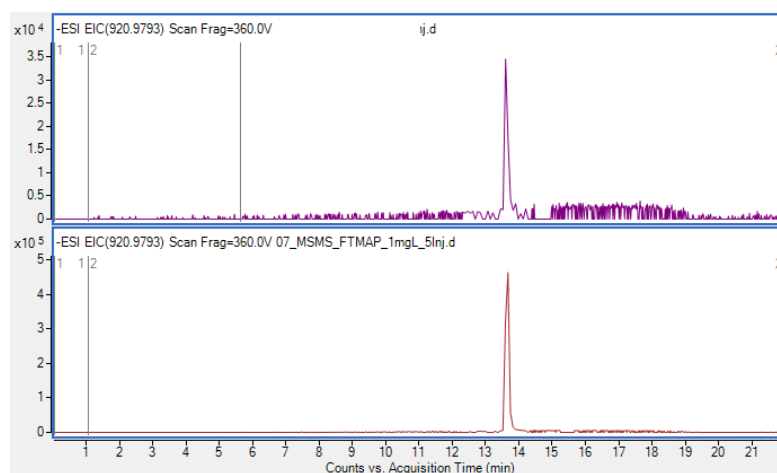
$\delta = 46.50$

$\delta = 63.88$

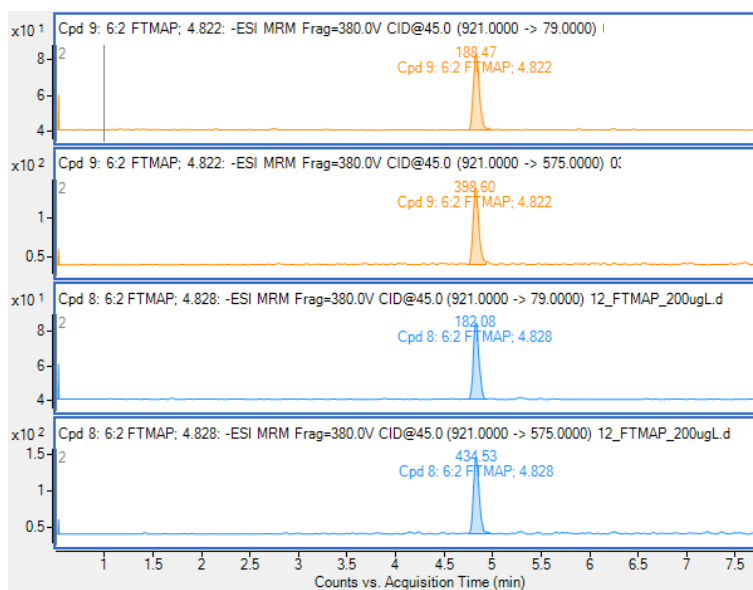
### $^{31}\text{P}$ ( $\text{CD}_3\text{OD}$ , 162 MHz)

$\delta = - 5.43$

### Identification of 6:2 FTMAP in paper and soil



**Figure S8:** Extracted ion chromatogram of  $m/z$  920.9793 (10 ppm) in soil sample S13 (top) and the synthesized 6:2 FTMAP standard (bottom)



**Figure S9:** MRM measurement of 6:2 FTMAP on a 6470 Agilent QqQ MS. Orange: Sample P2 (top:  $m/z$  921  $\rightarrow$   $m/z$  79; bottom:  $m/z$  921  $\rightarrow$   $m/z$  575), blue: FTMAP standard 200  $\mu\text{g/L}$  (top:  $m/z$  921  $\rightarrow$   $m/z$  79; bottom:  $m/z$  921  $\rightarrow$   $m/z$  575)

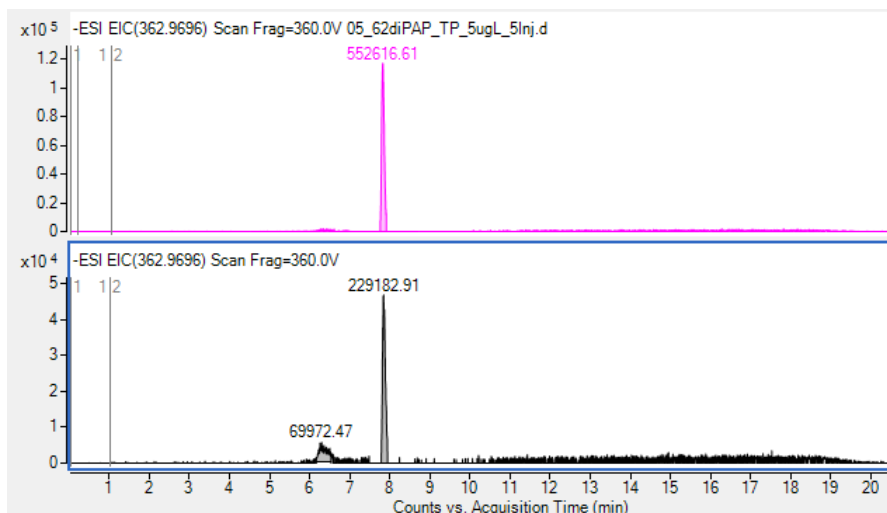
### Quantification of 6:2 FTMAP

6:2 FTMAP was quantified using a 1290 HPLC (Agilent Technologies, Waldbronn, Germany) coupled to a 6470 QqQ instrument. Eluent A (95:5 v/v  $\text{H}_2\text{O}/\text{MeOH}$ ) and eluent B (95:5 v/v  $\text{MeOH}/\text{H}_2\text{O}$ ), both with 2 mM  $\text{NH}_4\text{Ac}$ , were used for gradient elution. Mass transitions were measured in multiple reaction monitoring ( $m/z$  921  $\rightarrow$   $m/z$  575 @ 45 eV;  $m/z$  921  $\rightarrow$   $m/z$  79 @ 45 eV). A 6-point calibration curve ranging from 10  $\mu\text{g/L}$  up to 200  $\mu\text{g/L}$  ( $R^2 = 0.99$ ) was used to estimate the concentration in sample P2 to 9.2 mg /  $\text{m}^2$ .

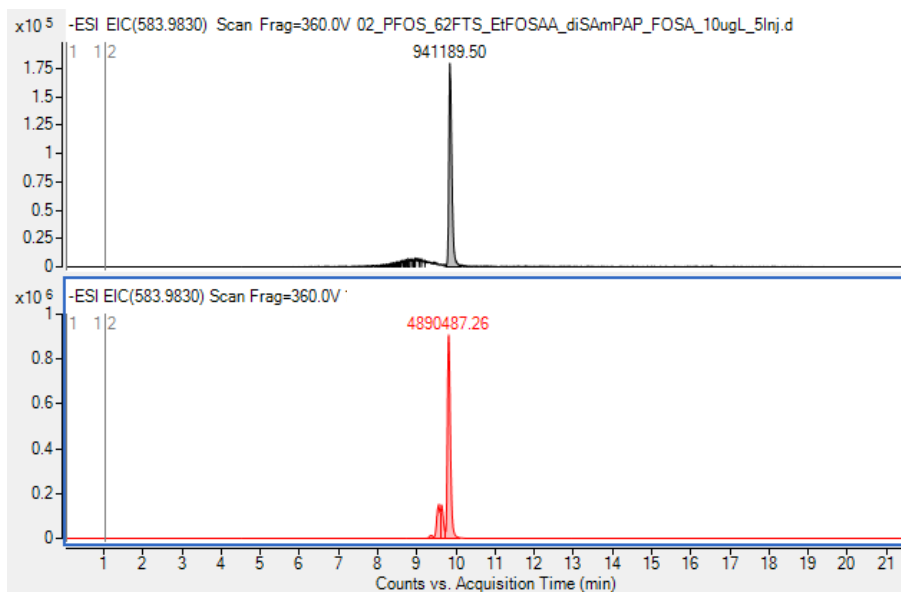


## PFAS identification by standards

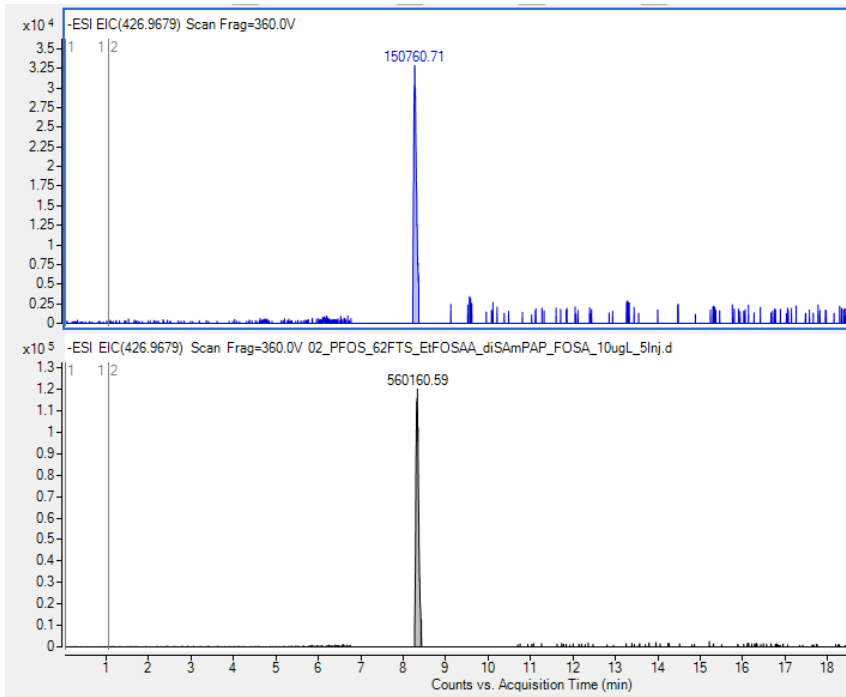
For mass deviations, see ESM2.xls.



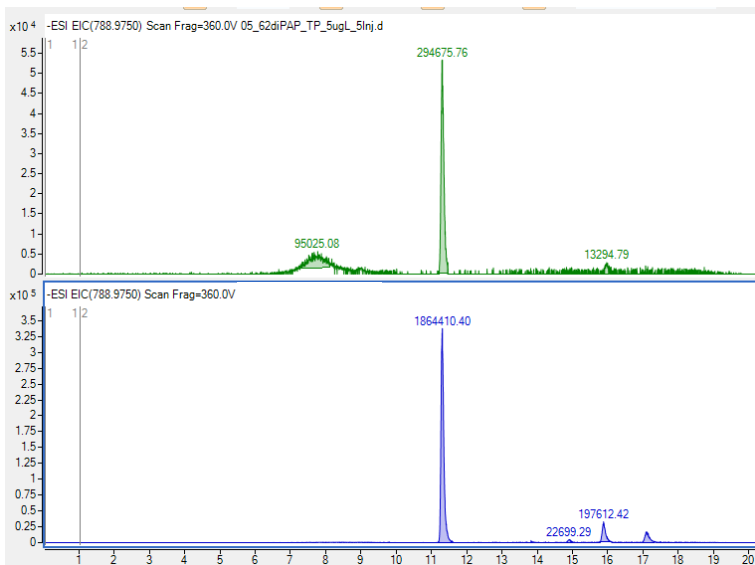
**Figure S10:** PFHpA in a standard solution (top, 5 µg/L) and in soil sample S12 (bottom).



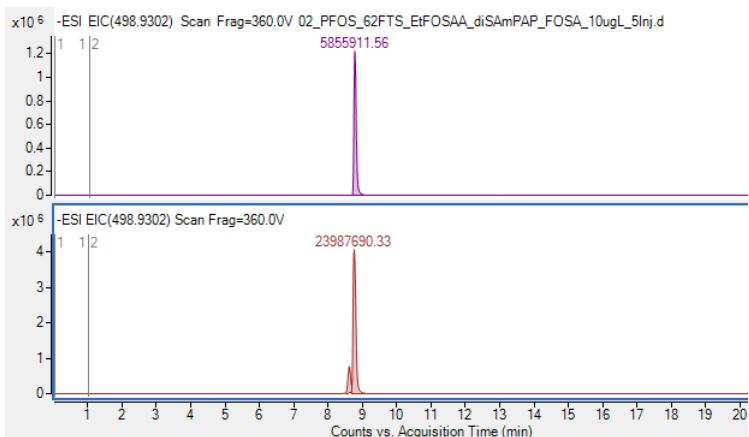
**Figure S11:** EtFOSAA in a standard solution (top, 10 µg/L) and in soil sample S12 (bottom).



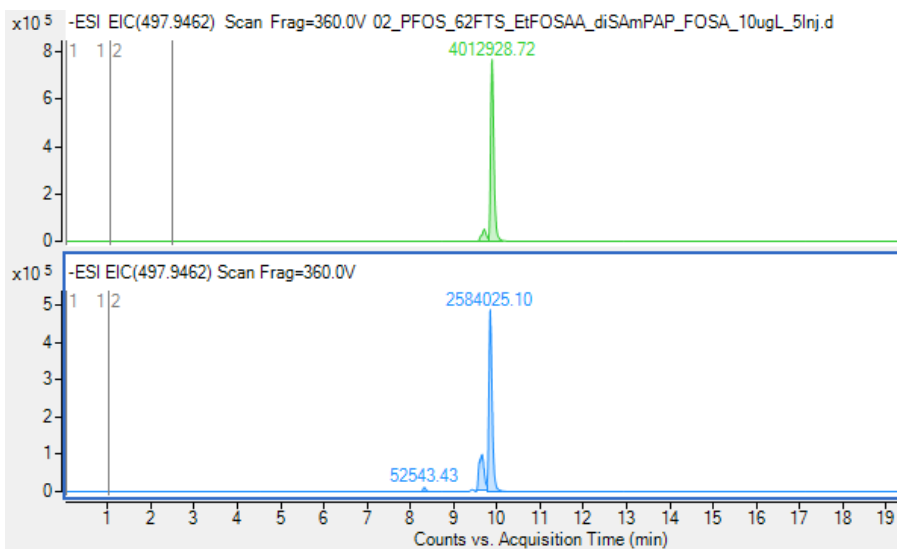
**Figure S12:** 6:2 FTSA in a standard solution (bottom, 10 µg/L) and in soil sample S13 (top).



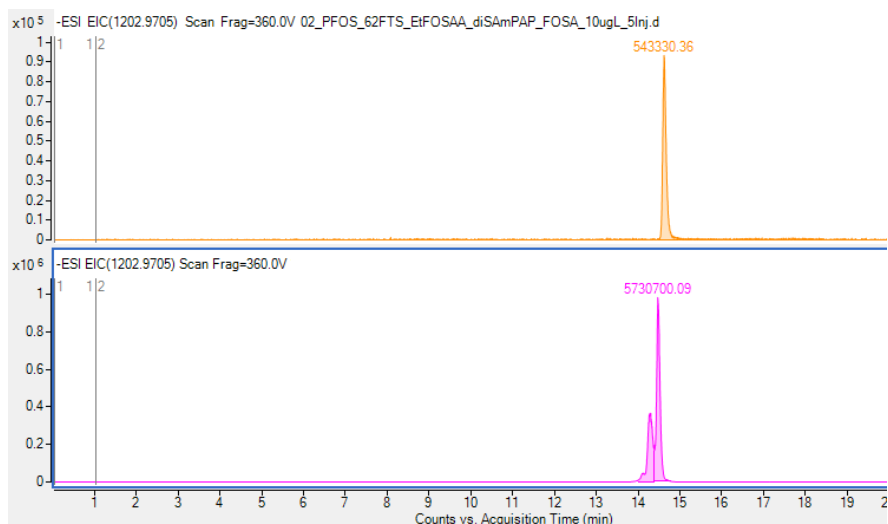
**Figure S13:** 6:2 diPAP in a standard solution (top, 5 µg/L) and in soil sample S12 (bottom).



**Figure S14:** PFOS in a standard solution (top, 10  $\mu\text{g/L}$ ) and in soil sample S12 (bottom). The double peak in soil sample S12 indicates branched isomers.



**Figure S15:** FOSA in a standard solution (top, 10  $\mu\text{g/L}$ ) and in soil sample S12 (bottom). The double peak in soil sample S12 indicates branched isomers.



**Figure S16:** diSAmPAP in a standard solution (top, 10  $\mu\text{g/L}$ ) and in soil sample S12 (bottom). The double peak in soil sample S12 indicates branched isomers.

## References

1. Lee, H.; Mabury, S. A., A pilot survey of legacy and current commercial fluorinated chemicals in human sera from United States donors in 2009. *Environmental Science & Technology* **2011**, *45*, (19), 8067-74.

**Chapter 10** – personal contribution

<b>Author</b>	<b>Author position</b>	<b>Scientific ideas %</b>	<b>Data generation %</b>	<b>Analysis &amp; interpretation %</b>	<b>Paper writing %</b>
Jonathan Zweigle	1	30	70	30	60
Boris Bugsel	2	30	20	30	10
Markus Schmitt	3	30	10	30	20
Christian Zwiener	4	10	0	10	10
Title of paper:	Electrochemical oxidation of 6:2 polyfluoroalkyl phosphate diester – transformation products and reactions kinetics with hydroxyl radicals				
Status in publication process:	Submitted for publication to: <i>Environmental Science &amp; Technology</i>				

## 10 Electrochemical oxidation of 6:2 polyfluoroalkyl phosphate diester – transformation products and reactions kinetics with hydroxyl radicals

Jonathan Zweigle<sup>1</sup>, Boris Bugsel<sup>1</sup>, Markus Schmitt<sup>1</sup>, Christian Zwiener<sup>1</sup>

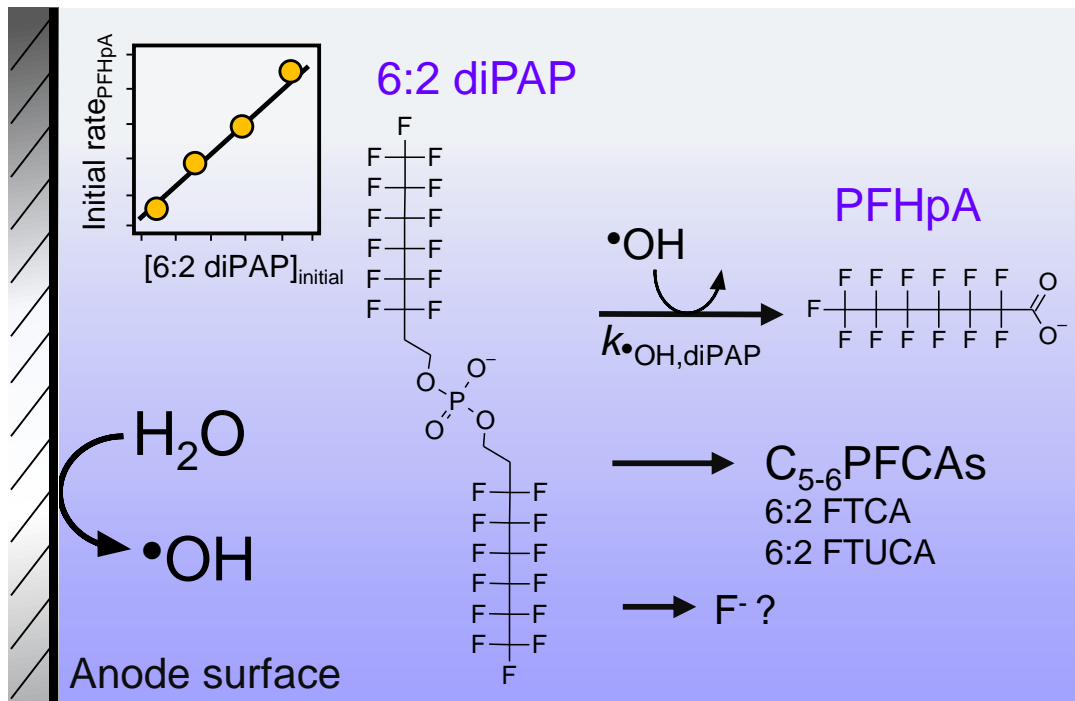
<sup>1</sup> Environmental Analytical Chemistry, Center for Applied Geoscience, University of Tübingen, Schnarrenbergstr. 94-96, 72076, Tübingen

Reproduced with permission from *Environmental Science & Technology*, submitted for publication. Unpublished work copyright 2021 American Chemical Society

## 10.1 Abstract

Per- and polyfluoroalkyl substances are widely used chemicals that often end in the environment. So far polyfluorinated precursors can be transformed into persistent perfluorinated end-products under environmental conditions. Electrochemical oxidation was used as a tool to characterize precursors and to simulate environmental transformation processes. 6:2 diPAP, as a representative PFCA precursor, was transformed to C<sub>5</sub>-C<sub>7</sub> PFCAs and two intermediates (6:2 FTCA and 6:2 FTUCA) at an applied potential  $\geq 2.5$  V (vs. Ag/AgCl). The potential intermediates 6:2 monoPAP and 6:2 FTOH showed similar TPs but with different ratios. The main product from 6:2 diPAP oxidation, PFHpA was formed in a pseudo first-order reaction from 6:2 diPAP by an OH-radical initiated reaction. Evidence for the  $\cdot\text{OH}$  reaction was obtained from quenching experiments with a decreasing formation of PFHpA with increasing 2-propanol concentration and pH. The steady-state  $\cdot\text{OH}$  concentrations were measured with terephthalic acid as  $\cdot\text{OH}$  probe and showed the same trends. An observed bimolecular rate constant for the formation of PFHpA during the reaction of 6:2 diPAP with  $\cdot\text{OH}$   $k_{\cdot\text{OH}, \text{diPAP}}^{\text{form PFHpA}} = 9.4 (\pm 1.4) \times 10^7 \text{ M}^{-1} \text{ s}^{-1}$  was estimated by an initial rate approach. The rate constant can be utilized to estimate environmental half-lives of 6:2 diPAP for the reaction with  $\cdot\text{OH}$  and the formation of persistent PFCAs.

# TOC Art, Graphical abstract





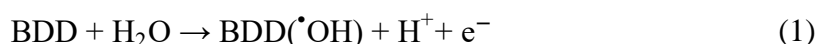
## 10.2 Introduction

Per- and polyfluoroalkyl substances (PFASs) are a diverse group of anthropogenic chemicals. Their fluorinated carbon backbone provides unique properties such as oil- and water repellency, thermal stability, and surfactant characteristics.<sup>1</sup> Therefore, PFAS are used in numerous industrial and household applications like fire-fighting foams, food contact materials, textiles, cosmetics, pesticides and as surfactants in industrial processing.<sup>2-5</sup> Due to their high persistence, some PFASs have distributed worldwide and were detected in water,<sup>6, 7</sup> air,<sup>8</sup> food,<sup>9</sup> soil,<sup>10</sup> wildlife<sup>11</sup> and in humans.<sup>12</sup> Especially perfluorooctanoic acid (PFOA) and perfluorooctanesulfonic acid (PFOS) have attracted early attention due to their widespread occurrence. Today, both are included in the Stockholm Convention on persistent organic pollutants (POPs)<sup>4, 13</sup> due to their high persistence, bioaccumulation, and toxicity (PBT).

Nowadays, the production and usage of individual legacy PFASs are regulated. However, many commercially used PFASs products which are still in use or not ultimately banned, can transform to persistent perfluorinated dead-end products such as perfluoroalkyl carboxylic- (PFCAs) and sulfonic acids (PFSA).<sup>14-18</sup> These commercially used products are often referred to as precursors.<sup>19, 20</sup> Precursors such as polyfluoroalkyl phosphate diesters (diPAPs) were identified in soils,<sup>21</sup> sewage sludge<sup>22</sup>, indoor environments,<sup>23</sup> consumer products,<sup>3</sup> and on human skin<sup>24</sup>, showing that they are ubiquitous. DiPAPs can transform oxidatively under environmental conditions to mobile PFCAs.<sup>14-16, 18, 25</sup> While diPAPs themselves are not mobile in the environment due to their hydrophobicity (6:2 diPAP:  $\log K_{ow} \approx 8.4$  and  $\log K_{oc} \approx 4.5$ ),<sup>26-29</sup> they can act as a long term source for groundwater contamination through degradation. This situation occurs in the region around Rastatt in southwest Germany where contaminated paper sludge was unintentionally applied on agricultural areas, leading to ground- and drinking water contamination.<sup>21</sup>

While biotic transformation of diPAPs was investigated in previous studies,<sup>14-16, 30-32</sup> little is known about abiotic transformation pathways in natural and technical systems. Electrochemical oxidation (EO) was successfully used to simulate biochemical transformation processes<sup>33, 34</sup> and oxidative processes in the environment.<sup>35, 36</sup> EO can be also used to generate environmental transformation products (TPs),<sup>37</sup> and to study environmental reactions with hydroxyl radicals ( $\cdot\text{OH}$ ).

The advantage of EO in contrast to microbial degradation experiments is the easy and accurate control of reaction parameters and the fast reaction kinetics, allowing rapid generation of relevant information. EO of organic molecules can be realized with non-active anodes, such as boron-doped diamond (BDD) electrodes,<sup>38</sup> and can be divided into direct and indirect processes.<sup>39</sup> By applying a certain potential, sorbed and free hydroxyl radicals ( $\cdot\text{OH}$ ) are generated by the oxidation of water on the BDD surface according to equation 1 and 2:



$\cdot\text{OH}$  can act as strong oxidants, which are also present in many natural environments, such as e.g. air, surface waters and soils.<sup>40-42</sup> Hence, environmental transformation and EO can show similar transformation products. Besides indirect oxidation via radicals, direct oxidation occurs when an organic compound R undergoes direct electron transfer with the anode surface at which it is oxidized to a product P:

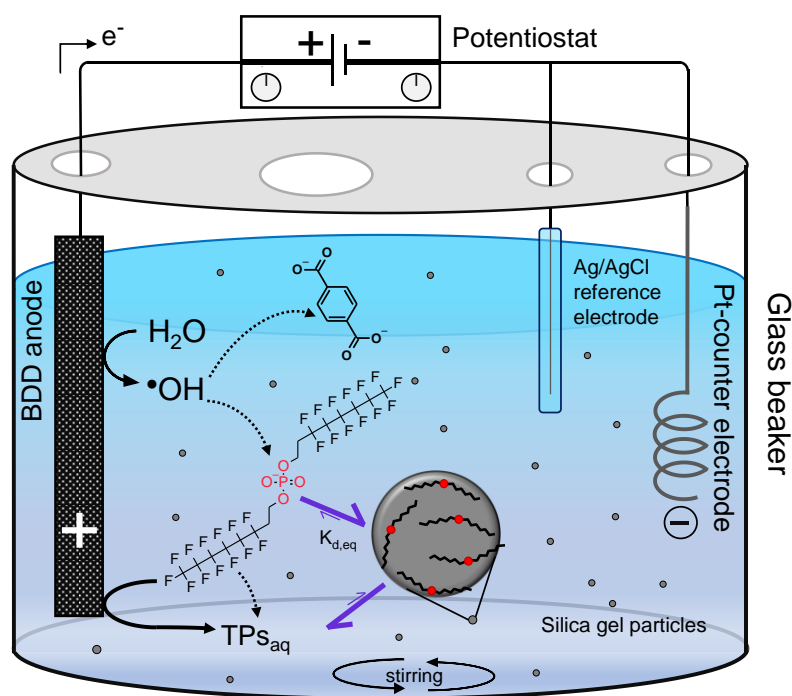


Since abiotic transformation of precursors such as diPAPs have not been investigated so far, the main scope of this study was to use EO to simulate the oxidation of 6:2 diPAP (structure in Figure 1), with a focus on the role of  $\cdot\text{OH}$  for the reaction. Due to the low water solubility of  $\sim 1 \mu\text{g/L}$ ,<sup>28</sup> a setup was used where 6:2 diPAP was sorbed to inert silica particles which served as reservoir and allowed concentrations above the water solubility in EO. This was necessary to generate TPs in sufficient concentrations for accurate detection. With terephthalic acid (TPA; structure in Figure 1) as  $\cdot\text{OH}$ -probe molecule, the role of  $\cdot\text{OH}$  during oxidation was elucidated. TPA only degrades via  $\cdot\text{OH}$  during EO and can, therefore, be used to study the role of indirect oxidation.<sup>43</sup> Different experimental parameters such as applied potential, initial 6:2 diPAP concentration, and pH were varied and combined with a kinetic approach to gain mechanistic insights into the transformation mechanism of 6:2 diPAP via  $\cdot\text{OH}$ . Furthermore, intermediates such as 6:2 fluorotelomer alcohol (6:2 FTOH), 6:2 monoPAP and perfluoroheptanoic acid (PFHpA) were oxidized electrochemically to complete the picture of this reaction.

### 10.3 Materials & Methods

**Chemicals and Reagents.** The specifications and origins of chemicals are shown in the SI (S1).

**Anodic oxidation.** EO experiments were performed in an in-house made electrochemical (EC) cell modified from Lege, et al.<sup>44</sup> based on a 100 mL glass beaker. A conductive boron-doped-diamond DIACHEM® electrode ( $A = 4.4 \text{ cm}^2$ ) with a 10  $\mu\text{m}$  diamond layer on Niobium base (CONDIAS, Germany) was used as working electrode. As a counter electrode, a 0.5 mm spiral Platinum wire from Alfa Aesar (Thermo Fisher) and as a reference electrode an Ag/AgCl electrode (3M, MF-2052, BASi, West Lafayette, USA) were used. All reported potentials are referenced vs. Ag/AgCl. The electrode spacing was 2.5 cm. Anodic oxidation was performed in 20 mM  $\text{NH}_4\text{FA}$  electrolyte (made from LC-MS grade water) under constant magnetic stirring. The electrolyte pH was adjusted by addition of  $\text{H}_3\text{PO}_4$  or NaOH.  $\text{NH}_4\text{FA}$  was used because it is volatile during the electrospray ionization (ESI), having the advantage that the samples can be directly injected without prior cleanup by e.g. solid phase extraction (SPE). Throughout an experiment, a constant voltage (2 V, 2.5 V, and 3 V) was applied by an Autolab PGSTAT 101 potentiostat from Metrohm. A scheme of the electrochemical setup is depicted in Figure 1.



**Figure 1:** Simplified scheme of the electrochemical cell used for anodic oxidation of 6:2 diPAP and other compounds, including the  $\cdot\text{OH}$ -probe TPA. Solid arrows indicate direct oxidation on the BDD surface, dotted arrows represent indirect oxidation via  $\cdot\text{OH}$ . Particles are suspended due to magnetic stirring. Note: While 6:2 diPAP is mainly sorbed to silica gel particles in equilibrium with the water phase (desorption), the degradation products are exclusively dissolved in the electrolyte.

In the case of 6:2 diPAP oxidation, 100 mg silica gel particles were weighed in the EC cell and mixed with 20 mL MeOH which was finally spiked with 4  $\mu\text{g}$  6:2 diPAP. In experiments with different initial 6:2 diPAP concentration, the amount was adjusted respectively. The solvent was evaporated under magnetic stirring overnight at room temperature to coat the particles. The coating procedure was performed to be able to include 6:2 diPAP above its low water solubility as a reservoir. Prior to oxidation, the electrolyte was spiked to a final TPA concentration of 10  $\mu\text{M}$  and 40 mL electrolyte was added to the dry particles. The cell was then ultrasonicated for 5 min to guarantee desorption of 6:2 diPAP to its solubility (equilibrium). During the experiment, 200  $\mu\text{L}$  samples for analysis of 6:2 diPAP and TPs were transferred to PP vials (water with suspended particles) at least as duplicates and for TPA analysis single samples were taken (glass vials). After anodic oxidation, residual 6:2 diPAP was extracted from the EC cell by adding 50 mL MeOH followed by 30 min sonication. After each experiment the cell was cleaned twice by ultrasonication with MeOH for 30 min followed by an

electrochemical cleaning step in  $\text{NH}_4\text{FA}$  with 150 pulses of alternating potentials (+2 V to -2 V) over 10 min. Regularly, the cell was also cleaned by electrolysis at a potential of 3 V for 20 min. Additionally, as quality control, an experiment without applying a voltage (0 V) and a blank experiment (3 V without 6:2 diPAP) were performed (Figure S1a-b). EO experiments with the intermediates 6:2 FTOH, 6:2 monoPAP and PFHpA were performed under identical conditions.

**Sample preparation.** Samples for analysis of 6:2 diPAP and TPs were diluted 50:50 with MeOH, centrifuged for 15 min (1800 relative centrifugal force (rcf)) and the supernatant was taken for subsequent measurement. TPA samples were centrifuged (15 min, 1800 rcf) and the supernatant was spiked with 3  $\mu\text{L}$  1:10 FA/ $\text{H}_2\text{O}$  per 100  $\mu\text{L}$  sample to adjust the pH for analysis. For 6:2 diPAP extraction after anodic oxidation, the electrolyte was filtered through a folded filter to separate the silica particles. The electrodes were rinsed with MeOH, which was directly collected in the EC cell together with the folded filter and the particles. The cell was then filled to a total volume of 50 mL with MeOH and sonicated for 30 min to guarantee desorption. A volume of 50 mL was used to guarantee that every part of the EC cell was covered with MeOH for extraction (40 mL electrolyte during oxidation). Additionally, extraction tests were performed which showed an extraction efficiency of  $88 \pm 3\%$  (Figure S2), and a second extraction step showed negligible 6:2 diPAP residues. The evaporation of MeOH during sonication was corrected gravimetrically. Finally, three aliquots were taken, centrifuged and diluted 50:50 with water for analysis.

**Cyclic voltammetry.** For details see SI (Figure S3).

**Compound analysis.** Suspect- and non-target screening for 6:2 diPAP TPs was performed by LC-QTOF-MS based on the accurate mass of the detected features followed by a molecular feature extraction algorithm. Extracted features were compared with a suspect list. Additionally, it was searched for features with negative to slightly positive mass defect (range from -0.25 to +0.1 Da) arising from the typical high fluorine content of PFASs.<sup>21</sup> The screening was performed using a 1260 Infinity HPLC (Agilent Technologies, Waldbronn, Germany) coupled to a 6550 QTOF-MS (Agilent Technologies, Santa Clara, USA). Details about chromatography and instrument parameters can be found in the SI (Section S2 and Table S1-2).

6:2 diPAP, C<sub>4</sub>-C<sub>7</sub> PFCAs, 6:2 and 5:3 fluorotelomer carboxylic acids (FTCAs) and 6:2 fluorotelomer unsaturated carboxylic acid (6:2 FTUCA) were quantified using a 1290 Infinity II HPLC (Agilent Technologies, Waldbronn, Germany) coupled to a tandem 6490 iFunnel Triple Quadrupole MS (Agilent Technologies, Santa Clara, USA) or the same HPLC system coupled to an Agilent 6470 TQ-MS. Details about chromatography and instrument parameters can be found in the SI (Section S2 and Table S1-3). Quantification was done with calibration curves of 7 different concentrations measured before and after a set of approximately 20 samples. Furthermore, in between the samples, quality standards were included. Each measurement contained two blanks. For data evaluation, the Agilent Mass Hunter Qualitative Analysis 10.0 and Quantitative Analysis 10.1 were used.

A 1260 Infinity HPLC (Agilent Technologies, Waldbronn, Germany) was used to separate TPA and to detect it with a diode array detector (DAD) at a wavelength of 245 nm (chromatographic details in SI Section S2). During each measurement series quality standards of TPA were included and used to verify the correct retention time (RT) of TPA in the samples.

**Data evaluation and quality control.** TPA was used as a  $\cdot\text{OH}$ -probe since it was shown to react selectively with  $\cdot\text{OH}$  during EO,<sup>45-49</sup> while it was not directly degraded on a BDD electrode surface.<sup>43</sup> The steady-state  $\cdot\text{OH}$  concentration  $[\cdot\text{OH}]_{\text{ss}}$  in mol/L was calculated for each experiments according to equation 4:

$$[\cdot\text{OH}]_{\text{ss}} = \frac{k_{\text{obs, TPA}}}{k_{\cdot\text{OH, TPA}}} \quad (4)$$

in which  $k_{\text{obs, TPA}}$  is the pseudo-first order rate constant in  $\text{s}^{-1}$  and  $k_{\cdot\text{OH, TPA}} = 4.4 \times 10^9 \text{ M}^{-1} \text{ s}^{-1}$  is the bimolecular reaction constant of TPA with  $\cdot\text{OH}$ .<sup>50</sup> For calculation of  $k_{\text{obs, TPA}}$ , TPA degradation was used, rather than the formation of the transformation product hydroxyterephthalate (hTPA), since it was further transformed during EO. The use of  $[\cdot\text{OH}]_{\text{ss}}$  is based on the assumption that other compounds present in the EC setup are in contact with the same  $\cdot\text{OH}$  as TPA.

To ensure reliable data quality sampling for TPs was always performed at least as duplicates and mostly as triplicates. The standard deviation was calculated for all detected compounds and is included in concentration time curves. For calculation of the error of rate constants the 95% confidence interval (CI) was calculated for linear

regressions, fitting of experimental data for rate constants was performed with Matlab R2018a (9.4.0.813654).

## 10.4 Results & Discussion

### **Electrochemical formation of TPs from 6:2 diPAP and effect of the potential.**

Selected samples of anodic oxidation experiments of 6:2 diPAP over 18 h in NH<sub>4</sub>FA (3 V; current density  $\approx 2 \text{ mA cm}^{-2}$ ) were screened by HPLC-QTOF for compounds present in a target list target and for features with negative mass defects typically for PFASs. The screening revealed PFCAs of different chain lengths, 6:2 FTCA and 6:2 FTUCA as relevant TPs, which were then quantified using a target method. PFHpA was a major TP which increased linearly over the first hours (Figure 2a). The concentrations of perfluorohexanoic acid (PFHxA) and PFPeA increased also over time but with a delay. Besides PFCAs, small amounts of 6:2 FTCA and 6:2 FTUCA could be quantified as TPs, which accumulated slowly with increasing oxidation time. PFBA and 5:3 FTCA were not detected during oxidation. The concentration of the precursor 6:2 diPAP could not be examined during EO since it is predominantly adsorbed on suspended particles and their aggregation prohibited representative sampling of the suspensions and hence quantification of 6:2 diPAP (for details see Figures S1 and S4). Therefore, 6:2 diPAP was extracted from the suspended particles after 18 h to quantify its residual amount, which will be discussed at the end of this section. Taking the results, mechanistic considerations and information from the literature into account, we propose a reaction scheme comprising intermediates (6:2 monoPAP, 6:2 FTOH, various PFAAs) and unknown products (Figure 3).

To get a better understanding of the transformation of 6:2 diPAP additional EO experiments with the potential intermediates 6:2 FTOH and 6:2 monoPAP (Figure 3) were performed under identical conditions (Figure 2b-c). The formation of 6:2 FTCA from 6:2 FTOH was fast and showed a typical maximum curve of an intermediate which is further degraded (probably to PFHpA) with a similar or a higher rate constant than that of its formation. Also 6:2 FTUCA shows this behavior at much lower concentration levels (1.7 nM at maximum) which is likely further oxidized to PFHxA. The formation of PFHpA was much faster than from 6:2 diPAP and shows a typical

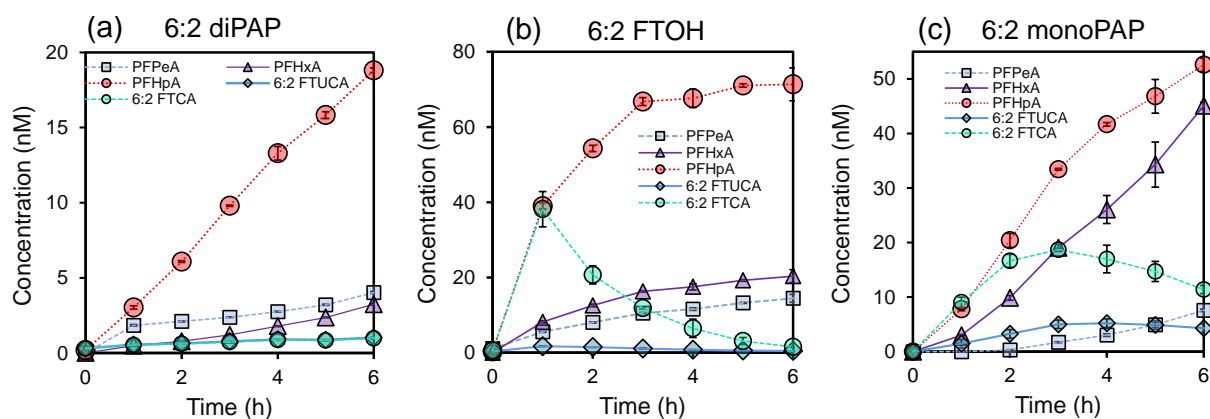
curve for end products of a consecutive reaction which levels off after 6 h. Also, PFHxA and PFPeA are typical end products.

Anodic oxidation of 6:2 monoPAP revealed the formation of similar transformation products as in case of 6:2 FTOH. PFHpA was the dominant TP and the formation of the intermediate 6:2 FTCA was fast with a similar or faster consecutive transformation. 6:2 FTCA and 6:2 FTUCA showed a similar behavior as during 6:2 FTOH oxidation, which is typical for intermediates. The formation of PFHxA was much faster than during 6:2 FTOH oxidation and PFPeA increased slower. Only during oxidation of 6:2 monoPAP PFBA was detected.

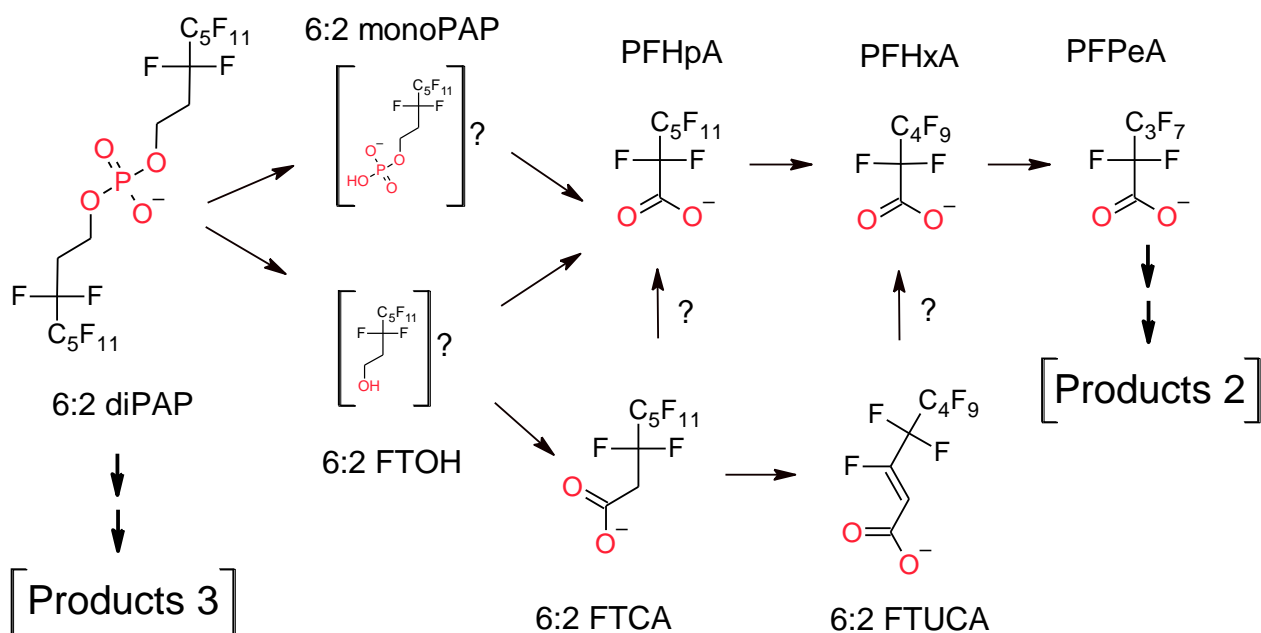
In comparison to 6:2 diPAP both 6:2 FTOH and 6:2 monoPAP showed different formation kinetics of TPs. Interestingly, more PFHxA than PFPeA was formed during EO of 6:2 FTOH and 6:2 monoPAP in contrast to 6:2 diPAP. This indicates that the EO of 6:2 diPAP is not exclusively proceeding via these intermediates which is further supported by the much lower formation of the intermediate 6:2 FTCA from 6:2 diPAP. It has also to be considered that particles with sorbed 6:2 diPAP on the electrode surface increase the importance of direct electrode reactions, which has an effect also on the kinetics of further downstream reactions.

After 18 h of oxidation the residual 6:2 diPAP was extracted from the setup. The extraction efficiency of  $88 \pm 3\%$  in control experiments without applied potential (Figure S2) showed that quantification of residual 6:2 diPAP was possible and showed low variability. After 18 h of oxidation 27% of the initial 6:2 diPAP amount was still present and about 50% of the mass balance is not covered by the above discussed TPs (Figure S5a). This shows that there are further processes which degrade 6:2 diPAP and TPs may not be detectable with the used analytical methods (discussed below).





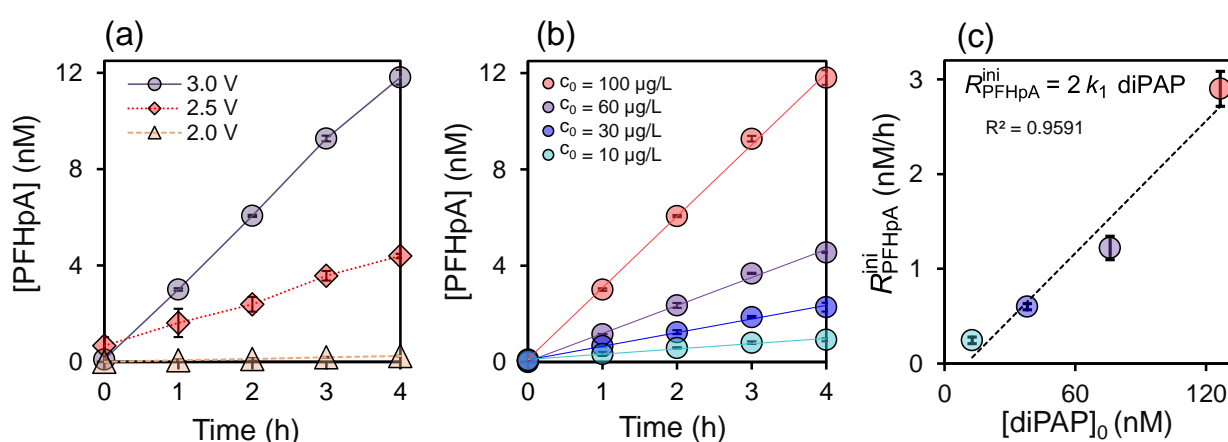
**Figure 2:** Formation of TPs from the precursors 6:2 diPAP (a), 6:2 FTOH (b) and 6:2 monoPAP (c) during anodic oxidation at a potential of 3 V with initial concentrations of 100  $\mu\text{g/L}$ . The error bars correspond to the standard deviation of triplicate measurements. For mass balance after 18 h of anodic oxidation see Figures S5a-c.



**Figure 3:** Reaction scheme for the anodic oxidation of 6:2 diPAP. Arrows represent direct electrode reactions and indirect oxidation via  $\cdot\text{OH}$ . Compounds in square brackets were not measured but are expected to occur as intermediates.

To investigate the role of the applied potential on the oxidation of 6:2 diPAP, 18 h experiments were conducted in  $\text{NH}_4\text{FA}$  electrolyte (pH 6) at 2 V, 2.5 V, and 3 V, and  $\text{C}_4$ - $\text{C}_7$  PFCAs were quantified as major TPs. During EO at 3 V, the concentration of PFHpA in the water phase increased over time, at 2.5 V the formation was slower and at a potential of 2 V no significant increase of PFHpA occurred (Figure 4a) and the

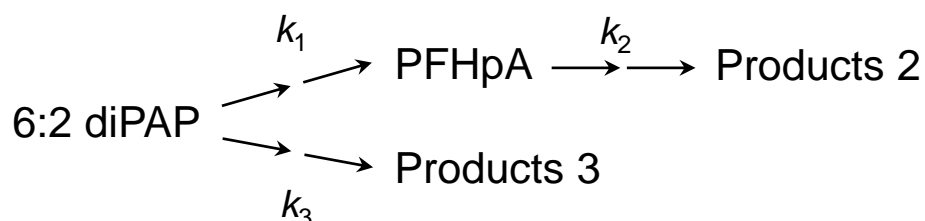
formation of other products was negligible. This is in good agreement with the mass balance at  $t_{18}$  (Figure S7). At 2 V oxidation almost all the initial 6:2 diPAP amount could be extracted at the end, showing that this potential is too low to degrade 6:2 diPAP. In case of 2.5 V and 3 V, besides PFHpA a delayed formation of PFHxA and PFPeA was also observed over time (complete degradation curves in Figure S8), which was influenced by the potential. PFBA was not detected. These experiments clearly show that PFCA formation from 6:2 diPAP is controlled by the applied potential. In case of 2.5 V and 3 V approximately 50% of the total fluorine mass balance after 18 h are not covered by 6:2 diPAP and C<sub>4</sub>-C<sub>7</sub>-PFCAs.



**Figure 4:** (a) Formation of PFHpA from anodic oxidation of 6:2 diPAP ( $c_0 = 100 \mu\text{g/L}$ ) at different applied potentials in  $\text{NH}_4\text{FA}$  electrolyte at pH 6. (b) Formation of PFHpA from anodic oxidation of 6:2 diPAP with different initial concentrations in  $\text{NH}_4\text{FA}$  electrolyte at a potential of 3 V at pH 6. Solid lines indicate linear regressions ( $R^2 < 0.99$ ). Error bars correspond to the standard deviation of triplicate samples (a) and duplicate samples (b). (c) Initial rates (see also equation 5) of PFHpA ( $R_{PFHpA}^{ini}$ ) dependency on the initial 6:2 diPAP concentration. Error bars are lower and upper 95% confidence intervals, resulting from the linear regressions.

**Kinetics of PFHpA formation from 6:2 diPAP.** A kinetic scheme was developed to describe PFHpA formation as the major TP from 6:2 diPAP with environmental concern due to its higher mobility. Based on the time sequence of the quantified TPs the following reaction pathway is proposed (Figure 5). The precursor 6:2 diPAP is oxidized to PFHpA, which is transformed to further products (Products 2), as indicated by a separate experiment with PFHpA as starting material (Figure S6). Since Products 2 would explain only less than 8% of the unknown fraction (SI Section S3), we included

a parallel transformation pathway of 6:2 diPAP which further yields unknown products (Products 3).



**Figure 5:** Proposed reaction scheme for the anodic oxidation of 6:2 diPAP comprising two parallel and consecutive reactions.

The proposed reaction can be described in a simplified way by four ordinary differential equations (ODEs) which can be solved analytically. Solving for the concentration of PFHpA over time yields the following analytical solution (for details and ODEs see SI Section S4):<sup>51</sup>

$$[\text{PFHpA}]_t = 2[\text{diPAP}]_0 \cdot \frac{k_1}{k_2 - k_1 - k_3} \cdot (e^{-(k_3 + k_1)t} - e^{-k_2 t}) \quad (5)$$

where  $[\text{PFHpA}]$  is the concentration of PFHpA in mol/L,  $[\text{diPAP}]_0$  corresponds to the initial 6:2 diPAP concentration,  $k_1$  is the (pseudo) first-order formation rate constant of PFHpA,  $k_2$  is the (pseudo) first-order decay constant of PFHpA and  $k_3$  is the first-order rate constant for the transformation of 6:2 diPAP to further products which can be further intermediates and end products. The processes underlying  $k_2$  and  $k_3$  cannot easily be quantified in our system, as only a fraction of the products was detectable. Moreover, the reaction conditions changed over time as observed after 18 h of anodic oxidation by a pH change of approximately one unit. Additionally, the formation of nitrate was observed by ion chromatography (data not shown) at a potential of 3 V showing that the electrolyte conditions are changing slightly. Probably ammonium is oxidized to nitrate under these conditions which accumulates in solution over time and potentially sorbs to the anode surface and may affect the oxidation reactions. Similar observations were made during EO of PFASs for sulfate and chloride.<sup>52-54</sup>

These observations in combination with little further decay of PFHpA during the experiment make the determination of rate-constants based on fitting the growth-decay curve challenging (eq. 5).

Interestingly, the initial formation within the first 4 h was always linear (Figure 4a and Figure S8 insets), which indicates that PFHpA was formed from 6:2 diPAP in a (pseudo) first order reaction and the PFHpA decay can be neglected during this time. Thus, these initial rates can be utilized to gain quantitative kinetic information without fitting the full formation curve with eq 5. The benefit is that only the rate constant of interest for the reaction of diPAP to PFHpA  $k_1$  has to be fitted in contrast to  $k_1$ ,  $k_2$ , and  $k_3$  in eq 5. With the initial rate approach one can determine  $k_1$  without knowledge about  $k_2$  and  $k_3$ , which can be expressed according to equation 6:

$$R_{\text{PFHpA}}^{\text{ini}} = 2 k_1 [\text{diPAP}]_0 \quad (6)$$

where  $k_1$  is the (pseudo) first-order rate constant in  $\text{s}^{-1}$  of the reaction of 6:2 diPAP to PFHpA and  $[\text{diPAP}]_0$  represents the initial 6:2 diPAP concentration in mol/L. The factor of 2 arises from the fact that one 6:2 diPAP molecule can be transformed into two PFHpA molecules.

This approach was already previously used in a different context when the kinetics of the precursor (in our case 6:2 diPAP) is unknown and only the kinetics of one initial product is known.<sup>55</sup>

To determine  $k_1$ , the initial concentration of 6:2 diPAP on the particles was varied during EO at a potential of 3 V to verify the effect on the initial rate of PFHpA according to eq 6. The formation of PFHpA clearly depends on the initial 6:2 diPAP concentration (Figure 4b; degradation curves including all detected PFCAs are shown in Figure S9). This observation suggests that the desorption kinetics of 6:2 diPAP from the silica particles is faster than its transformation to PFHpA. This is in good agreement with the fact that both 6:2 diPAP and the silica particle surface are negatively charged in the pH range of the experiments, which weakens sorption by electrostatic repulsion. Because the formation of PFHpA was linear over the first 4 h, the initial rates of formation  $R_{\text{PFHpA}}^{\text{ini}}$  in  $\text{mol L}^{-1}\text{s}^{-1}$  of PFHpA were determined by linear regressions. The linear regression of the initial rates over  $[\text{diPAP}]_0$  (Figure 4c) yielded a  $k_1$  of  $0.012 \pm 0.002 \text{ h}^{-1}$ .

Finally, the formation of PFHpA was fitted with eq. 5 to estimate  $k_3$  but with fixed rate constants  $k_1$  and  $k_2$  with data of three individual 3 V oxidation experiments (Figure S13). The outcome supports the idea that there must be a parallel reaction ( $k_3$  in Figure 5) to explain the decay of 6:2 diPAP after 18 h.

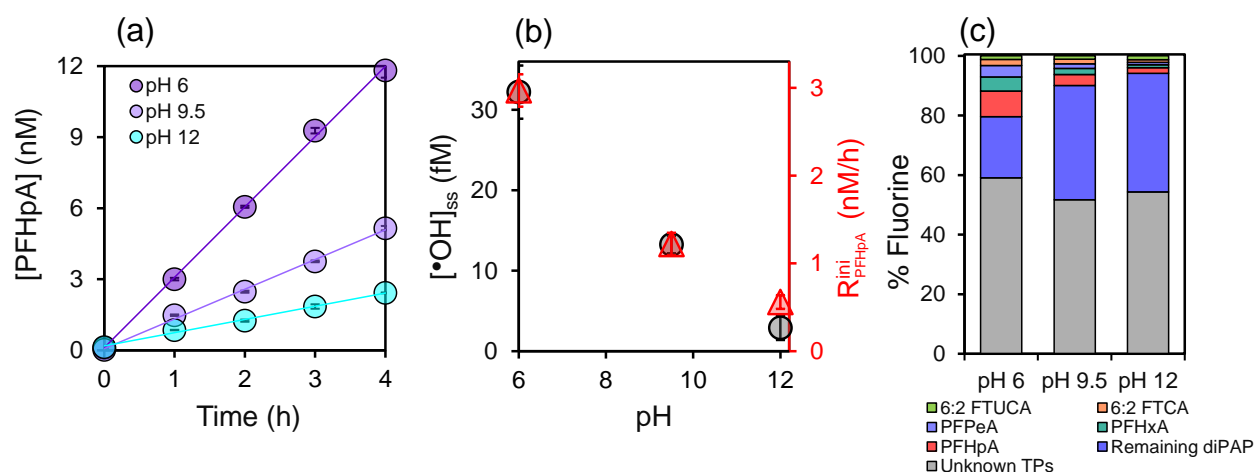
**PFHpA formation from 6:2 diPAP by  $\cdot\text{OH}$ .** To gain further insights into the mechanism of PFHpA formation from 6:2 diPAP the influence of the electrolyte pH was studied (pH 6, 9.5 and 12). The pseudo first-order decay constant of the  $\cdot\text{OH}$ -probe TPA ( $k_{\text{obs,TPA}}$ ) was strongly dependent on the pH showing that the steady-state OH-radical concentration  $[\cdot\text{OH}]_{\text{ss}}$  is directly correlated with the electrolyte pH (Figure S10a-b). The  $\cdot\text{OH}$  concentration decreased with increasing pH, which was also observed in other studies during anodic oxidation and presumably results from sorption of  $\text{OH}^-$  to the BDD surface leading to  $\text{O}_2$  evolution,<sup>56</sup> and suppression of  $\cdot\text{OH}$  formation at high pH. The formation of PFHpA, PFHxA and PFPeA were influenced to a similar extent (Figure S11). Especially  $R_{\text{PFHpA}}^{\text{ini}}$  showed a strong pH dependency (Figure 6a). When comparing  $[\cdot\text{OH}]_{\text{ss}}$  with  $R_{\text{PFHpA}}^{\text{ini}}$ , a linear relationship was observed over the pH range (Figure 6b). This outcome supports the idea that the reaction from 6:2 diPAP to PFHpA is caused by indirect oxidation via  $\cdot\text{OH}$ . Looking at the structure of 6:2 diPAP the  $\cdot\text{OH}$  can attack on the ether bond or directly at one  $\text{CH}_2$ -group of the fluorotelomer side chain. While this indirect oxidation step of diPAP can be caused by  $\cdot\text{OH}$ , the further transformation of PFCAs necessarily starts with an initial direct electron transfer on the anode surface,<sup>53</sup> and  $\cdot\text{OH}$  were shown to be too weak for PFCA mineralization.<sup>56, 57</sup> When considering the formation of TPs and the fraction that is not transformed to PFCAs and other detected TPs (Figure 6c, gray bars) after 18 h of oxidation it can be seen that this decline (gray bars) is mostly independent from the pH change, in contrast to the formation of PFCAs. Hence, it probably involves direct electron transfer reactions between the organic molecule and the anode surface and can be separated from  $\cdot\text{OH}$  chemistry. The mechanism of indirect oxidation was further investigated by a quenching experiment where 1% 2-propanol was added to the electrolyte during anodic oxidation at a potential of 3 V. 2-propanol is known to quench  $\cdot\text{OH}$ , and therefore removes them as potential oxidants from the system.<sup>58</sup> The addition of this quencher reduced  $R_{\text{PFHpA}}^{\text{ini}}$  in a similar way as  $k_{\text{obs,TPA}}$  to almost zero (Figure S12a-b). This supports the finding of indirect oxidation of PFHpA, however, at such high concentrations (1% 2-propanol) also the anode surface can be blocked and the direct oxidation pathway is potentially also influenced by the quencher. Nevertheless, in combination with the obvious pH dependency the experimental

findings provide good evidence for a reaction mechanism of 6:2 diPAP to PFHpA via  $\cdot\text{OH}$ .

Since the TPA decay and PFHpA formation correlated to each other, the assumption is reasonable that TPA and 6:2 diPAP were reacting with the same regime of  $\cdot\text{OH}$  and that a steady-state concentration of  $\cdot\text{OH}$  establishes. Furthermore, since they are both negatively charged, they are likely present in the vicinity of the anode surface where  $\cdot\text{OH}$  are generated. Based on the above-mentioned assumptions an overall second-order bimolecular rate constant  $k_{\cdot\text{OH}, \text{diPAP}}^{\text{form PFHpA}}$  for the reaction of 6:2 diPAP to PFHpA via  $\cdot\text{OH}$  can be calculated according to the following equation:

$$k_{\cdot\text{OH}, \text{diPAP}}^{\text{form PFHpA}} = \frac{k_1}{[\cdot\text{OH}]_{\text{ss}}} = (9.4 \pm 1.4) \times 10^7 \text{ M}^{-1} \text{ s}^{-1} \quad (7)$$

where  $k_1$  was calculated from the initial rates of PFHpA formation from 6:2 diPAP (Figure 4c) and  $[\cdot\text{OH}]_{\text{ss}}$  was determined via TPA degradation; the rate constant error results from the lower and upper 95% CI of the regression between  $R_{\text{PFHpA}}^{\text{ini}}$  and the initial 6:2 diPAP concentration. This bimolecular rate constant can be used to estimate the half-life of 6:2 diPAP in different environmental systems considering reactions with  $\cdot\text{OH}$ . Therefore,  $[\cdot\text{OH}]_{\text{ss}}$  needs to be known in the environmental system of interest. To our knowledge, this rate constant is reported for the first time in this study and provides an estimate about the relevance of abiotic transformation of 6:2 diPAP by  $\cdot\text{OH}$  to persistent and more mobile PFCAs in different natural and technical systems.



**Figure 6:** (a) Formation of PFHpA from anodic oxidation of 6:2 diPAP in  $\text{NH}_4\text{FA}$  electrolyte at a potential of 3 V at pH 6, pH 9.5 and pH 12. Solid lines through the PFHpA data correspond to linear regressions ( $R^2 > 0.99$ ). Error bar correspond to the standard deviation of triplicates (b) Steady-state  $\cdot\text{OH}$  concentration (black dots) calculated from pseudo-first order TPA

degradation TPA at the respective pH (left x-axis) vs the initial rate of formation of PFHpA (red triangles, right x-axis). Errorbars correspond to the lower and upper 95% CI. (c) % Fluorine of formed PFCAs, residual 6:2 diPAP and oxidation to unknown products after 18 h of anodic oxidation at pH 6, pH 9.5 and pH 12. Note: The residual 6:2 diPAP at pH 12 was corrected for a small fraction lost by hydrolysis.

## 10.5 Implications

During EO of 6:2 diPAP as a relevant environmental PFCA precursor the TPs 6:2 FTCA, 6:2 FTUCA, and C<sub>5</sub>-C<sub>7</sub> PFCAs were detected. PFHpA was the dominant TP of the reaction of 6:2 diPAP with  $\cdot\text{OH}$  (also for 6:2 FTOH and 6:2 monoPAP as precursors), showing that the length of the perfluorinated carbon chain does not change in this first reaction. This has implications for the use of EO to characterize unknown PFAS precursors, and to predict environmentally relevant TPs from abiotic processes. Shorter chain PFCAs were constantly less abundant than PFHpA but became more important after long oxidation times. While PFHxA and PFPeA together with the intermediates 6:2 FTUCA and 6:2 FTCA were also detected during biotransformation of telomer-based substances like diPAPs or FTOHs (6:2 and 8:2) in animals and microorganisms, some major differences became obvious.<sup>59</sup> During biodegradation, major TPs often were even numbered PFCAs which were typically one CF<sub>2</sub>-unit shorter than the precursor (PFHxA in case of a 6:2, PFOA in case of a 8:2 precursor).<sup>14, 30, 60</sup> Further metabolites from biodegradation like n:3 FTCAs have not been detected during EO. During reactions with  $\cdot\text{OH}$  however, the perfluorinated carbon chain remains unchanged. Odd numbered PFCAs were e.g. found in groundwater resulting from degradation of precursors at a contaminated site.<sup>27</sup> Therefore, the formation of large quantities of odd numbered PFCAs in relation to even numbered PFCAs from fluorotelomer precursors in the environment could be a potential indication for abiotic transformation processes, but should be investigated further.

With a kinetic approach a second-order bimolecular reaction rate constant for the reaction of 6:2 diPAP with  $\cdot\text{OH}$  was determined and can be used to estimate how fast 6:2 diPAP will be transformed in environmental systems if  $[\cdot\text{OH}]_{\text{ss}}$  is known.  $[\cdot\text{OH}]_{\text{ss}}$  is well known for surface water bodies with around  $10^{-16}$  M.<sup>61-63</sup> Whereas in soils  $[\cdot\text{OH}]_{\text{ss}}$  it is more difficult to predict, due to the dependency on several environmental

parameters such as soil moisture, pH, concentrations of humics, carbonate or other scavengers and difficulties to transfer laboratory results to the field conditions.

Reaction constants of PFASs with  $\cdot\text{OH}$  are scarce, however, for *N*-ethyl perfluorooctane sulfonamido acetate (*N*-EtFOSAA) a constant of  $1.7 \times 10^9 \text{ M}^{-1} \text{ s}^{-1}$  as an upper limit was determined.<sup>64</sup> This is approximately one order of magnitude higher than our reported constant for the reaction of 6:2 diPAP. Other studies found similar values for other perfluorooctane sulfonamide derivatives.<sup>65</sup> While the determined constants for precursors are high enough to be potentially relevant for environmental degradation, the reaction of PFOA or PFOS with  $\cdot\text{OH}$  is considered to be insignificant.<sup>64, 66</sup>

Further research is needed to evaluate the importance of  $\cdot\text{OH}$  for the environmental transformation of other PFAS precursors. In general, EO can be used as a fast method to get first information about the transformation behavior of PFAS precursors in terms of potential products and its kinetics with  $\cdot\text{OH}$ .

## Supporting information

Chemicals and reagents (S1); Details about analytical parameters (S2); LC-MS parameters (Table S1-3); blank- and 0 V experiment (Figure S1a-b); extraction efficiencies (Figure S2); CV (Figure S3); 6:2 diPAP at different potentials (Figure S4);  $t_{18}$  mass balance (Figure S5); PFHpA oxidation (Figure S6a-b);  $t_{18}$  mass balance at different potentials (Figure S7); formation of TPs at 2 V, 2.5 V and 3 V (Figure S8); formation of TPs with different  $\omega$  (Figure S9); TPA decay and  $[\cdot\text{OH}]_{\text{ss}}$  (Figure S10a-b); formation of TPs at different pH (Figure S11); quenching experiment (Figure S12a-b); Model (Figure S13 and equations M1-6); Calculations (S3), Equations and kinetic model (S4, Figure S14 and equations S1-8).

## Author information

Corresponding Authors:

\*Christian Zwiener – christian.zwiener@uni-tuebingen.de

\*Markus Schmitt – [markus.schmitt@uni-tuebingen.de](mailto:markus.schmitt@uni-tuebingen.de)



## **Notes**

The authors declare no competing financial interest.

## **Acknowledgements**

The authors acknowledge the state of Baden-Württemberg for funding of the project FluorTECH (BWPFC19010).

## 10.6 References

1. Lindstrom, A. B.; Strynar, M. J.; Libelo, E. L., Polyfluorinated compounds: past, present, and future. *Environ Sci Technol* **2011**, *45*, (19), 7954-61.
2. Buck, R. C.; Franklin, J.; Berger, U.; Conder, J. M.; Cousins, I. T.; de Voogt, P.; Jensen, A. A.; Kannan, K.; Mabury, S. A.; van Leeuwen, S. P., Perfluoroalkyl and polyfluoroalkyl substances in the environment: terminology, classification, and origins. *Integr Environ Assess Manag* **2011**, *7*, (4), 513-41.
3. Trier, X.; Granby, K.; Christensen, J. H., Polyfluorinated surfactants (PFS) in paper and board coatings for food packaging. *Environ Sci Pollut Res Int* **2011**, *18*, (7), 1108-20.
4. Wang, Z.; DeWitt, J. C.; Higgins, C. P.; Cousins, I. T., A Never-Ending Story of Per- and Polyfluoroalkyl Substances (PFASs)? *Environ Sci Technol* **2017**, *51*, (5), 2508-2518.
5. Nascimento, R. A.; Nunoo, D. B. O.; Bizkarguenaga, E.; Schultes, L.; Zabaleta, I.; Benskin, J. P.; Spano, S.; Leonel, J., Sulfluramid use in Brazilian agriculture: A source of per- and polyfluoroalkyl substances (PFASs) to the environment. *Environ Pollut* **2018**, *242*, (Pt B), 1436-1443.
6. Loos, R.; Gawlik, B. M.; Locoro, G.; Rimaviciute, E.; Contini, S.; Bidoglio, G., EU-wide survey of polar organic persistent pollutants in European river waters. *Environmental Pollution* **2009**, *157*, (2), 561-568.
7. Kaboré, H. A.; Vo Duy, S.; Munoz, G.; Méité, L.; Desrosiers, M.; Liu, J.; Sory, T. K.; Sauvé, S., Worldwide drinking water occurrence and levels of newly-identified perfluoroalkyl and polyfluoroalkyl substances. *Sci Total Environ* **2018**, *616-617*, 1089-1100.
8. Kim, S.-K.; Shoeib, M.; Kim, K.-S.; Park, J.-E., Indoor and outdoor poly- and perfluoroalkyl substances (PFASs) in Korea determined by passive air sampler. *Environmental Pollution* **2012**, *162*, 144-150.
9. Gebbink, W. A.; Ullah, S.; Sandblom, O.; Berger, U., Polyfluoroalkyl phosphate esters and perfluoroalkyl carboxylic acids in target food samples and packaging—method development and screening. *Environmental Science and Pollution Research* **2013**, *20*, (11), 7949-7958.
10. Houtz, E. F.; Higgins, C. P.; Field, J. A.; Sedlak, D. L., Persistence of perfluoroalkyl acid precursors in AFFF-impacted groundwater and soil. *Environ Sci Technol* **2013**, *47*, (15), 8187-95.
11. Sun, J.; Bossi, R.; Bustnes, J. O.; Helander, B.; Boertmann, D.; Dietz, R.; Herzke, D.; Jaspers, V. L. B.; Labansen, A. L.; Lepoint, G.; Schulz, R.; Sonne, C.; Thorup, K.; Tøttrup, A. P.; Zubrod, J. P.; Eens, M.; Eulaers, I., White-Tailed Eagle (*Haliaeetus albicilla*) Body Feathers Document Spatiotemporal Trends of Perfluoroalkyl Substances in the Northern Environment. *Environ Sci Technol* **2019**, *53*, (21), 12744-12753.

12. Fromme, H.; Midasch, O.; Twardella, D.; Angerer, J.; Boehmer, S.; Liebl, B., Occurrence of perfluorinated substances in an adult German population in southern Bavaria. *International Archives of Occupational and Environmental Health* **2006**, *80*, (4), 313-319.
13. (ENB), E. N. B., Summary of the Meetings of the Conferences of the Parties to the Basel, Rotterdam and Stockholm Conventions. **2019**.
14. D'Eon, J. C.; Mabury, S. A., Production of perfluorinated carboxylic acids (PFCAs) from the biotransformation of polyfluoroalkyl phosphate surfactants (PAPS): exploring routes of human contamination. *Environ Sci Technol* **2007**, *41*, (13), 4799-805.
15. Lee, H.; D'Eon, J.; Mabury, S. A., Biodegradation of polyfluoroalkyl phosphates as a source of perfluorinated acids to the environment. *Environ Sci Technol* **2010**, *44*, (9), 3305-10.
16. Liu, J.; Mejia Avendano, S., Microbial degradation of polyfluoroalkyl chemicals in the environment: a review. *Environ Int* **2013**, *61*, 98-114.
17. Houtz, E. F.; Sutton, R.; Park, J. S.; Sedlak, M., Poly- and perfluoroalkyl substances in wastewater: Significance of unknown precursors, manufacturing shifts, and likely AFFF impacts. *Water Res* **2016**, *95*, 142-9.
18. Eriksson, U.; Haglund, P.; Karrman, A., Contribution of precursor compounds to the release of per- and polyfluoroalkyl substances (PFASs) from waste water treatment plants (WWTPs). *J Environ Sci* **2017**, *61*, 80-90.
19. Taxvig, C.; Rosenmai, A. K.; Vinggaard, A. M., Polyfluorinated alkyl phosphate ester surfactants - current knowledge and knowledge gaps. *Basic Clin Pharmacol Toxicol* **2014**, *115*, (1), 41-4.
20. Xiao, F., Emerging poly- and perfluoroalkyl substances in the aquatic environment: A review of current literature. *Water Res* **2017**, *124*, 482-495.
21. Bugsel, B.; Zwiener, C., LC-MS screening of poly- and perfluoroalkyl substances in contaminated soil by Kendrick mass analysis. *Anal Bioanal Chem* **2020**.
22. D'Eon, J. C.; Crozier, P. W.; Furdui, V. I.; Reiner, E. J.; Libelo, E. L.; Mabury, S. A., Observation of a commercial fluorinated material, the polyfluoroalkyl phosphoric acid diesters, in human sera, wastewater treatment plant sludge, and paper fibers. *Environ Sci Technol* **2009**, *43*, (12), 4589-94.
23. De Silva, A. O.; Allard, C. N.; Spencer, C.; Webster, G. M.; Shoeib, M., Phosphorus-containing fluorinated organics: polyfluoroalkyl phosphoric acid diesters (diPAPs), perfluorophosphonates (PFPA), and perfluorophosphinates (PFPIAs) in residential indoor dust. *Environ Sci Technol* **2012**, *46*, (22), 12575-82.
24. Poothong, S.; Padilla-Sánchez, J. A.; Papadopoulou, E.; Giovanoulis, G.; Thomsen, C.; Haug, L. S., Hand Wipes: A Useful Tool for Assessing Human Exposure to Poly- and

Perfluoroalkyl Substances (PFASs) through Hand-to-Mouth and Dermal Contacts. *Environmental Science & Technology* **2019**, 53, (4), 1985-1993.

25. Liu, C.; Liu, J., Aerobic biotransformation of polyfluoroalkyl phosphate esters (PAPs) in soil. *Environ Pollut* **2016**, 212, 230-237.

26. Söhlmann, R.; Striegel, G.; Lange, F. T., Die Anwendung der Summenparameter EOF und AOF bei der Untersuchung der Tiefenverlagerung von Perfluoralkyl- und Polyfluoralkylverbindungen (PFAS) in belasteten Böden in Mittelbaden. *Mitt Umweltchem Ökotox* **2018**.

27. Janda, J.; Nodler, K.; Scheurer, M.; Happel, O.; Nurenberg, G.; Zwiener, C.; Lange, F. T., Closing the gap - inclusion of ultrashort-chain perfluoroalkyl carboxylic acids in the total oxidizable precursor (TOP) assay protocol. *Environ Sci Process Impacts* **2019**.

28. Wang, Z.; MacLeod, M.; Cousins, I. T.; Scheringer, M.; Hungerbühler, K., Using COSMOtherm to predict physicochemical properties of poly- and perfluorinated alkyl substances (PFASs). *Environmental Chemistry* **2011**, 8, (4).

29. Chen, M.; Wang, Q.; Shan, G.; Zhu, L.; Yang, L.; Liu, M., Occurrence, partitioning and bioaccumulation of emerging and legacy per- and polyfluoroalkyl substances in Taihu Lake, China. *Sci Total Environ* **2018**, 634, 251-259.

30. D'Eon J, C.; Mabury, S. A., Exploring indirect sources of human exposure to perfluoroalkyl carboxylates (PFCAs): evaluating uptake, elimination, and biotransformation of polyfluoroalkyl phosphate esters (PAPs) in the rat. *Environ Health Perspect* **2011**, 119, (3), 344-50.

31. Lee, H.; Tevlin, A. G.; Mabury, S. A.; Mabury, S. A., Fate of polyfluoroalkyl phosphate diesters and their metabolites in biosolids-applied soil: biodegradation and plant uptake in greenhouse and field experiments. *Environ Sci Technol* **2014**, 48, (1), 340-9.

32. Rosenmai, A. K.; Nielsen, F. K.; Pedersen, M.; Hadrup, N.; Trier, X.; Christensen, J. H.; Vinggaard, A. M., Fluorochemicals used in food packaging inhibit male sex hormone synthesis. *Toxicol Appl Pharmacol* **2013**, 266, (1), 132-42.

33. Johansson, T.; Weidolf, L.; Jurva, U., Mimicry of phase I drug metabolism--novel methods for metabolite characterization and synthesis. *Rapid Commun Mass Spectrom* **2007**, 21, (14), 2323-31.

34. Yuan, T.; Permentier, H.; Bischoff, R., Surface-modified electrodes in the mimicry of oxidative drug metabolism. *TrAC Trends in Analytical Chemistry* **2015**, 70, 50-57.

35. Kotthoff, L.; Keller, J.; Lorchner, D.; Mekonnen, T. F.; Koch, M., Transformation Products of Organic Contaminants and Residues-Overview of Current Simulation Methods. *Molecules* **2019**, 24, (4).

36. Hoffmann, T.; Hofmann, D.; Klumpp, E.; Kuppers, S., Electrochemistry-mass spectrometry for mechanistic studies and simulation of oxidation processes in the environment. *Anal Bioanal Chem* **2011**, *399*, (5), 1859-68.
37. Tisler, S.; Zwiener, C., Formation and occurrence of transformation products of metformin in wastewater and surface water. *Sci Total Environ* **2018**, *628-629*, 1121-1129.
38. Radjenovic, J.; Sedlak, D. L., Challenges and Opportunities for Electrochemical Processes as Next-Generation Technologies for the Treatment of Contaminated Water. *Environ Sci Technol* **2015**, *49*, (19), 11292-302.
39. Martinez-Huitle, C. A.; Ferro, S., Electrochemical oxidation of organic pollutants for the wastewater treatment: direct and indirect processes. *Chem Soc Rev* **2006**, *35*, (12), 1324-40.
40. Zafiriou, O. C.; Jousot-Dubien, J.; Zepp, R. G.; Zika, R. G., Photochemistry of natural waters. *Environmental Science & Technology* **1984**, *18*, (12), 358A-371A.
41. Vione, D.; Falletti, G.; Maurino, V.; Minero, C.; Pelizzetti, E.; Malandrino, M.; Ajassa, R.; Olariu, R. I.; Arsene, C., Sources and sinks of hydroxyl radicals upon irradiation of natural water samples. *Environ Sci Technol* **2006**, *40*, (12), 3775-81.
42. Georgiou, C. D.; Sun, H. J.; McKay, C. P.; Grintzalis, K.; Papapostolou, I.; Zisimopoulos, D.; Panagiotidis, K.; Zhang, G.; Koutsopoulou, E.; Christidis, G. E.; Margiolaki, I., Evidence for photochemical production of reactive oxygen species in desert soils. *Nat Commun* **2015**, *6*, 7100.
43. Jing, Y.; Chaplin, B. P., Mechanistic Study of the Validity of Using Hydroxyl Radical Probes To Characterize Electrochemical Advanced Oxidation Processes. *Environ Sci Technol* **2017**, *51*, (4), 2355-2365.
44. Lege, S.; Eisenhofer, A.; Heras, J. E. Y.; Zwiener, C., Identification of transformation products of denatonium - Occurrence in wastewater treatment plants and surface waters. *Sci Total Environ* **2019**, *686*, 140-150.
45. Liu, J.; Lagger, G.; Tacchini, P.; Girault, H. H., Generation of OH radicals at palladium oxide nanoparticle modified electrodes, and scavenging by fluorescent probes and antioxidants. *Journal of Electroanalytical Chemistry* **2008**, *619-620*, 131-136.
46. Liao, W.; Murugananthan, M.; Zhang, Y., Electrochemical degradation and mechanistic analysis of microcystin-LR at boron-doped diamond electrode. *Chemical Engineering Journal* **2014**, *243*, 117-126.
47. He, Y.; Huang, W.; Chen, R.; Zhang, W.; Lin, H., Enhanced electrochemical oxidation of organic pollutants by boron-doped diamond based on porous titanium. *Separation and Purification Technology* **2015**, *149*, 124-131.

48. He, Y.; Dong, Y.; Huang, W.; Tang, X.; Liu, H.; Lin, H.; Li, H., Investigation of boron-doped diamond on porous Ti for electrochemical oxidation of acetaminophen pharmaceutical drug. *Journal of Electroanalytical Chemistry* **2015**, *759*, 167-173.
49. Guo, L.; Jing, Y.; Chaplin, B. P., Development and Characterization of Ultrafiltration TiO<sub>2</sub> Magneli Phase Reactive Electrochemical Membranes. *Environ Sci Technol* **2016**, *50*, (3), 1428-36.
50. Page, S. E.; Arnold, W. A.; McNeill, K., Terephthalate as a probe for photochemically generated hydroxyl radical. *J Environ Monit* **2010**, *12*, (9), 1658-65.
51. Espenson, J. H., Chemical kinetics and reaction mechanisms. *New York: McGraw-Hill* **1995**, Vol. 102.
52. Zhuo, Q.; Li, X.; Yan, F.; Yang, B.; Deng, S.; Huang, J.; Yu, G., Electrochemical oxidation of 1H,1H,2H,2H-perfluorooctane sulfonic acid (6:2 FTS) on DSA electrode: operating parameters and mechanism. *J Environ Sci (China)* **2014**, *26*, (8), 1733-9.
53. Niu, J.; Li, Y.; Shang, E.; Xu, Z.; Liu, J., Electrochemical oxidation of perfluorinated compounds in water. *Chemosphere* **2016**, *146*, 526-38.
54. Schaefer, C. E.; Andaya, C.; Burant, A.; Condee, C. W.; Urtiaga, A.; Strathmann, T. J.; Higgins, C. P., Electrochemical treatment of perfluorooctanoic acid and perfluorooctane sulfonate: Insights into mechanisms and application to groundwater treatment. *Chemical Engineering Journal* **2017**, *317*, 424-432.
55. Schmitt, M.; Erickson, P. R.; McNeill, K., Triplet-State Dissolved Organic Matter Quantum Yields and Lifetimes from Direct Observation of Aromatic Amine Oxidation. *Environ Sci Technol* **2017**, *51*, (22), 13151-13160.
56. Zhuo, Q.; Deng, S.; Yang, B.; Huang, J.; Wang, B.; Zhang, T.; Yu, G., Degradation of perfluorinated compounds on a boron-doped diamond electrode. *Electrochimica Acta* **2012**, *77*, 17-22.
57. Vecitis, C. D.; Park, H.; Cheng, J.; Mader, B. T.; Hoffmann, M. R., Kinetics and mechanism of the sonolytic conversion of the aqueous perfluorinated surfactants, perfluorooctanoate (PFOA), and perfluorooctane sulfonate (PFOS) into inorganic products. *J Phys Chem A* **2008**, *112*, (18), 4261-70.
58. Zhou, S.; Bu, L.; Yu, Y.; Zou, X.; Zhang, Y., A comparative study of microcystin-LR degradation by electrogenerated oxidants at BDD and MMO anodes. *Chemosphere* **2016**, *165*, 381-387.
59. Wang, N.; Szostek, B.; Buck, R. C.; Folsom, P. W.; Sulecki, L. M.; Gannon, J. T., 8-2 fluorotelomer alcohol aerobic soil biodegradation: pathways, metabolites, and metabolite yields. *Chemosphere* **2009**, *75*, (8), 1089-96.

60. Bizkarguenaga, E.; Zabaleta, I.; Prieto, A.; Fernandez, L. A.; Zuloaga, O., Uptake of 8:2 perfluoroalkyl phosphate diester and its degradation products by carrot and lettuce from compost-amended soil. *Chemosphere* **2016**, *152*, 309-17.
61. Russi, H.; Kotzias, D.; Korte, F., Photoinduzierte hydroxylierungsreaktionen organischer chemikalien in natürlichen Gewässern - Nitrate als potentielle OH-radikalquellen. *Chemosphere* **1982**, *11*, (10), 1041-1048.
62. Brezonik, P. L.; Fulkerson-Brekken, J., Nitrate-Induced Photolysis in Natural Waters: Controls on Concentrations of Hydroxyl Radical Photo-Intermediates by Natural Scavenging Agents. *Environmental Science & Technology* **1998**, *32*, (19), 3004-3010.
63. Lam, M. W.; Tantuco, K.; Mabury, S. A., PhetoFate: a new approach in accounting for the contribution of indirect photolysis of pesticides and pharmaceuticals in surface waters. *Environ Sci Technol* **2003**, *37*, (5), 899-907.
64. Plumlee, M. H.; McNeill, K.; Reinhard, M., Indirect photolysis of perfluorochemicals: hydroxyl radical-initiated oxidation of N-ethyl perfluorooctane sulfonamido acetate (N-EtFOSAA) and other perfluoroalkanesulfonamides. *Environ Sci Technol* **2009**, *43*, (10), 3662-8.
65. Nguyen, T. V.; Reinhard, M.; Gin, K. Y., Rate laws and kinetic modeling of N-ethyl perfluorooctane sulfonamidoethanol (N-EtFOSE) transformation by hydroxyl radical in aqueous solution. *Water Res* **2013**, *47*, (7), 2241-50.
66. Javed, H.; Lyu, C.; Sun, R.; Zhang, D.; Alvarez, P. J. J., Discerning the inefficacy of hydroxyl radicals during perfluorooctanoic acid degradation. *Chemosphere* **2020**, *247*, 125883.

## 10.7 Supporting Information

### Section 1 Chemicals and Reagents

Water, methanol (MeOH), ammonium acetate (NH<sub>4</sub>Ac), and formic acid (FA) were LC-MS grade and purchased from Fisher scientific. Sodium hydroxide solution (NaOH) and ammonium formate (NH<sub>4</sub>FA) were obtained from Honeywell Fluka. The PFCA reference standards (perfluorobutanoic- (PFBA), pentanoic- (PFPeA), hexanoic- (PFHxA), and heptanoic acid (PFHpA)), 6:2 FTOH and 85% H<sub>3</sub>PO<sub>4</sub> were from Sigma Aldrich. 6:2 and 5:3 fluorotelomer carboxylic acids (FTCAs) and 6:2 unsaturated fluorotelomer carboxylic acid (6:2 FTUCA) were purchased from Wellington Laboratories. 6:2/6:2 diPAP and 6:2 monoPAP came from Toronto Research Chemicals (TRC). Sodium terephthalate (TPA) was purchased from Tokyo Chemical Industry (TCI). Silicagel 60 for column chromatography (particle diameter: 63 – 200 µm) was purchased from Merck Germany.

### Section 2 Details on analytical parameters

#### **HPLC-QTOF-MS:**

For compound separation, a Poroshell 120 EC-C<sub>18</sub> column (2.1 mm × 100 mm) with a particle size of 2.7 µm and a flow rate of 0.35 mL/min at 40 °C was used. A gradient elution of eluent A (95/5 H<sub>2</sub>O/MeOH + 2 mM NH<sub>4</sub>Ac) and B (95/5 MeOH/H<sub>2</sub>O + 2 mM NH<sub>4</sub>Ac) was applied and the analytes were ionized with negative ESI. The QTOF-MS was operated in scan mode with a scan rate of 3 spectra/s in a range from m/z 110 to 1700.

#### **HPLC-QqQ-MS:**

To separate the target analytes, a Waters Acquity BEH C<sub>18</sub> column (2.1 mm × 100 mm) with a particle size of 1.7 µm and a flow rate of 0.4 mL/min at 60 °C was used with identical eluent composition as during QTOF-screening but with a different gradient (for details see Table S1-2). The ionization was operated in negative ESI mode and all analytes were measured with two



mass transitions except for perfluorobutanoic- (PFBA) and perfluoropentanoic acid (PFPeA) (in case of the 6470 QqQ) for which only one product ion was formed (for details see Table S3).

### HPLC-UV:

Separation of TPA was carried out on a Phenomenex column (150 mm × 3 mm, particle size 4 μm, Synergi 4n polar RP 80 Å) at 40 °C with a flow rate of 0.5 mL/min using an isocratic method with eluent A (90/10 H<sub>2</sub>O/MeOH + FA, pH 3) and B (MeOH) (80/20).

**Table S 1:** Summary of instrument and scan source parameters used for HPLC-QTOF- and HPLC-QqQ-MS measurements.

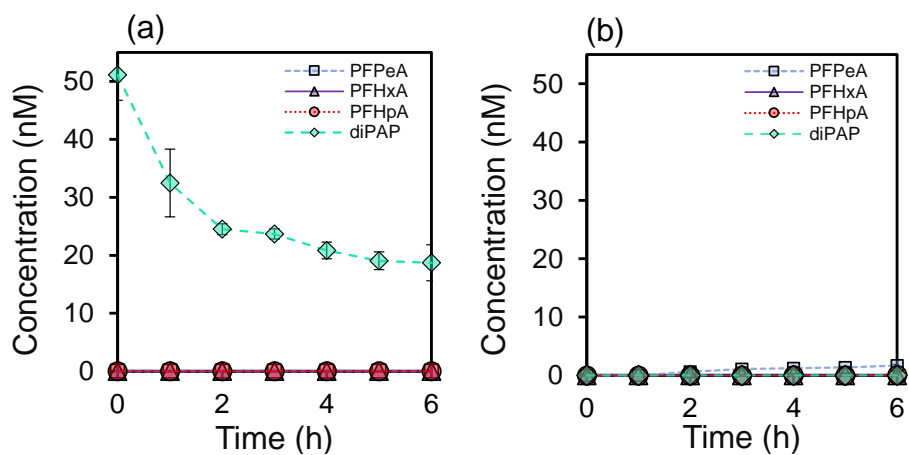
	6550 QTOF	6490 QqQ	6470 QqQ
<b>Instrument Parameters</b>			
Gas Temp (°C)	150	150	230
Gas Flow (L/min)	16	16	4
Nebulizer pressure (psig)	35	45	15
Sheath gas temperature (°C)	380	380	350
Sheath gas flow (L/min)	12	12	12
<b>Scan Source Parameter</b>			
Capillary voltage (V)	3000	3000	4000
Nozzle voltage (V)	300	0	-

**Table S 2:** Gradient elution of the HPLC-QTOF and the HPLC-QqQ method. A = 95/5 H<sub>2</sub>O/MeOH + 2 mM NH<sub>4</sub>Ac and B = 95/5 MeOH/H<sub>2</sub>O + 2 mM NH<sub>4</sub>Ac.

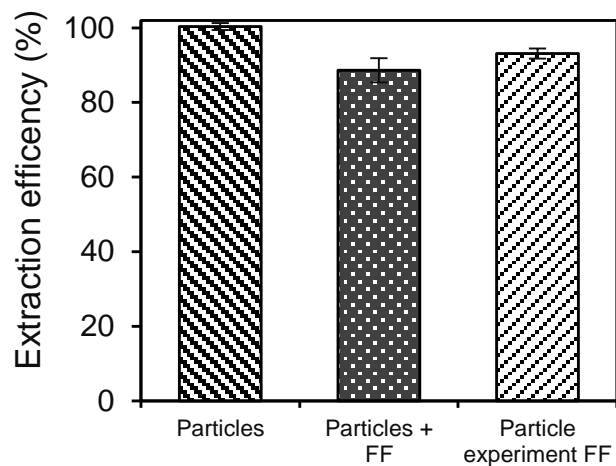
6550 QTOF			6490 QqQ			6470 QqQ		
Time (min)	A (%)	B (%)	Time (min)	A (%)	B (%)	Time (min)	A (%)	B (%)
0	85	15	0	60	40	0	40	60
8	0	100	1.0	40	60	1.0	40	60
13	0	100	1.5	0	100	3.5	0	100
13.1	85	15	4.5	0	100	6.0	0	100
20	85	15	4.6	60	40	6.1	60	40
			7.0	60	40	7.5	60	40

**Table S 3:** Parameters used during MRM for the target compounds: precursors and the corresponding product ions with respective collision energies (CE setpoint in V) and fragmentor voltages (FV). The dwell time used during MRM was 15 ms.

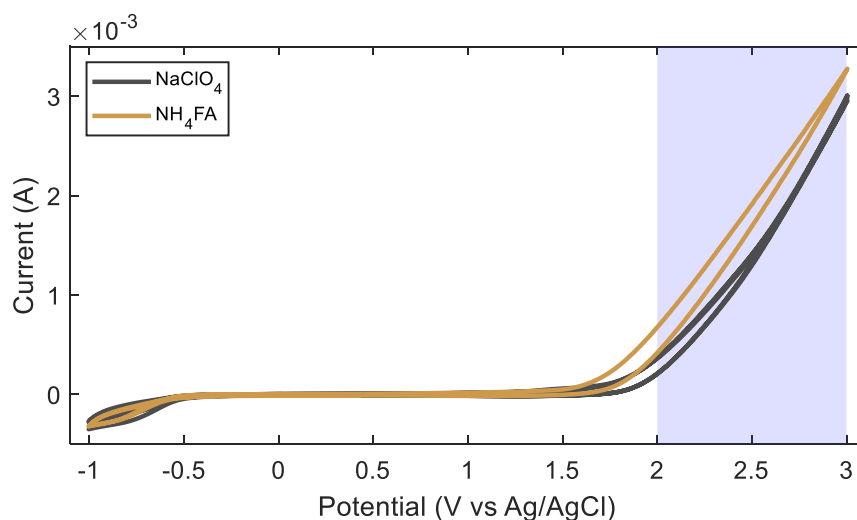
Compound name	Precursor ion	Product ion	Agilent 6490 QqQ		Agilent 6470 QqQ	
			FV (V)	CE (V)	FV (V)	CE (V)
6:2 diPAP	789	443	380	30	135	30
6:2 diPAP	789	97	380	30	135	30
6:2 FTCA	377	292.7	380	20	80	15
6:2 FTCA	377	63	380	5	80	6
5:3 FTCA	341	236.9	380	10	140	15
5:3 FTCA	341	216.8	380	25	140	15
6:2 FTUCA	357	293	380	10	70	15
6:2 FTUCA	357	243	380	40	70	15
PFHpA	362.8	318.8	380	5	72	0
PFHpA	362.8	168.7	380	15	72	12
PFHxA	312.9	268.9	380	5	70	8
PFHxA	312.9	119	380	25	70	18
PFPeA	262.9	219	380	5	60	8
PFPeA	262.9	68.8	380	45	-	-
PFBA	212.9	168.8	380	5	60	8



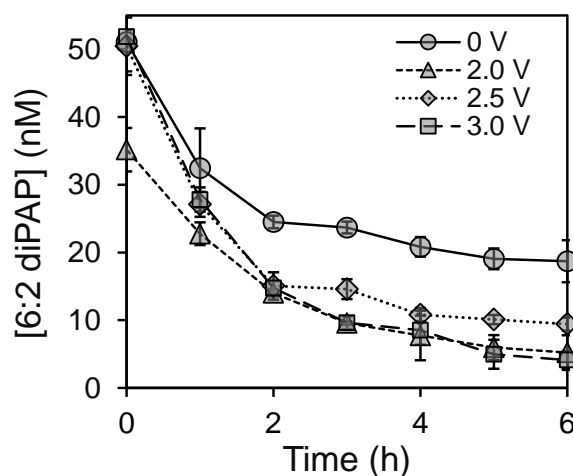
**Figure S 1:** (a) Behavior of diPAP in suspension in the electrochemical cell without any potential (0 V) applied. Hourly samples of the suspension were taken by a pipette. (b) Blank experiment for anodic oxidation of a pure solution with  $\text{NH}_4\text{FA}$  electrolyte at 3 V and pH 6 (without any 6:2 diPAP added). Error bars correspond to the standard deviation of triplicates.



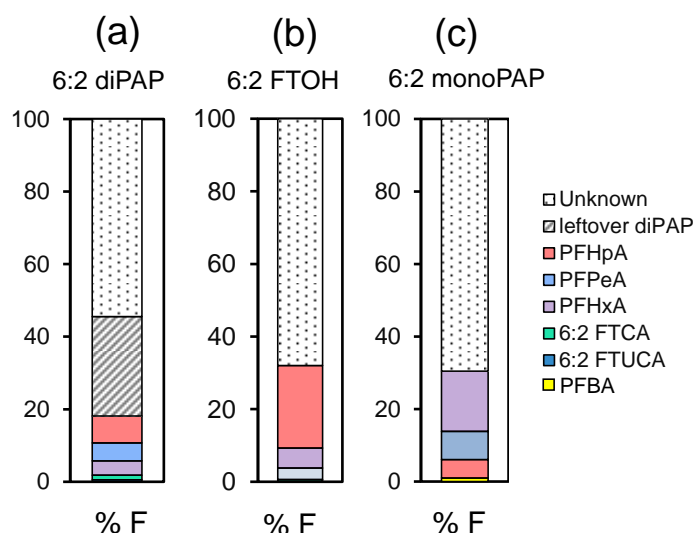
**Figure S 2:** Extraction efficiency of 6:2 diPAP from silica particles, from silica particles and the folded filter (FF) and after 4 h of stirring in  $\text{NH}_4\text{FA}$  electrolyte, simulating an anodic oxidation experiment. Error bars are calculated from triplicates using the gaussian error propagation.



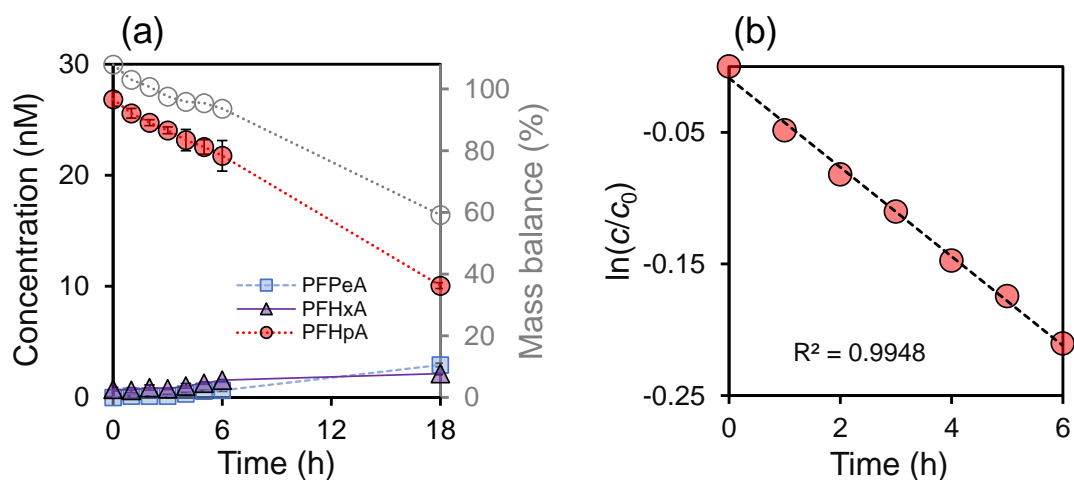
**Figure S 3:** In order to characterize the BDD anode, cyclic voltammetry (CV) was conducted in the identical EC cell with an electrolyte volume of 10 mL. This was done for characterization of the domain of  $\bullet\text{OH}$  formation at a scan rate of 10 mV/s in a range from -1 V to 3 V. CV was performed in 20 mM  $\text{NH}_4\text{FA}$  and 20 mM  $\text{NaClO}_4$  electrolyte at pH 6 in two cycles.  $\text{NaClO}_4$  was used as a reference, since it is a typical electrolyte used during electrochemical oxidation. The blue area highlights the range of potentials where anodic oxidation experiments were performed.



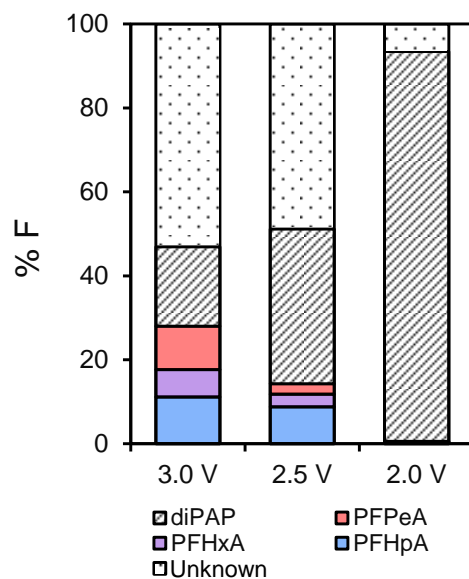
**Figure S 4:** Concentration of 6:2 diPAP over time during anodic oxidation in  $\text{NH}_4\text{FA}$  electrolyte (pH = 6) at applied potentials of 0 V, 2 V, 2.5 V and 3 V. Error bars correspond to the standard deviation of triplicates. The concentration of the precursor 6:2 diPAP on the suspended particles was examined over time. The suspension was taken as a liquid sample (water + particles). However, the measured initial concentration was lower than the actual spiked initial concentration (approximately 50 nM instead of 126 nM), showing that 6:2 diPAP was not equally distributed in the EC cell. This could result either from an unequal distribution of the suspended particles or from sorption of 6:2 diPAP to the glass wall or to the BDD anode due to its hydrophobicity. Furthermore, 6:2 diPAP decreased in the control experiment (0 V), where no transformation products were detected (Figure S1a). This observation shows that particle aggregation might have occurred over time and the decrease cannot be explained exclusively by oxidation, showing that this sampling method is not representative for 6:2 diPAP.



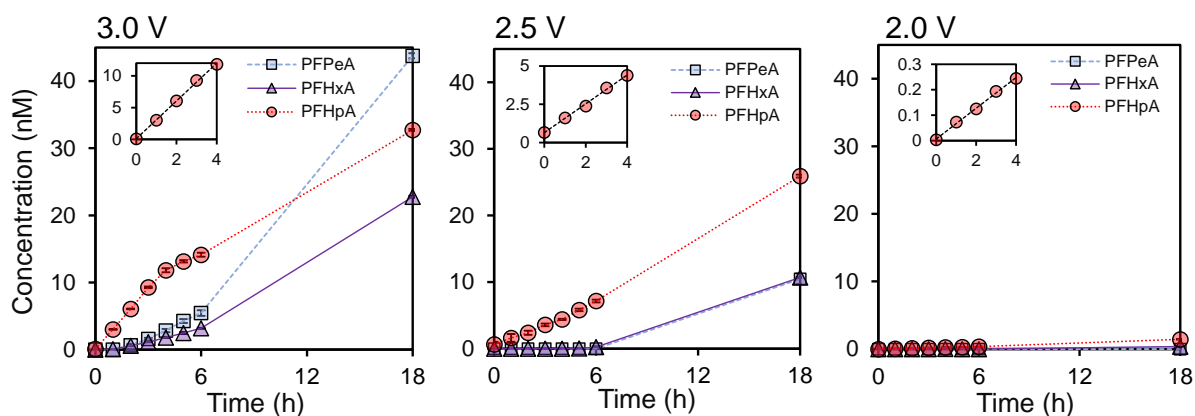
**Figure S 5:** Percent fluorine (%F) (mol fluorine per molecule divided by initial mol fluorine in precursor) of 6:2 diPAP (18 h) (a), 6:2 FTOH (6 h) (b), and 6:2 monoPAP (18 h) (c) for all detected TPs after anodic oxidation at an applied potential of 3 V in  $\text{NH}_4\text{FA}$  electrolyte. Note: PFBA only detected in the 6:2 monoPAP oxidation experiment. In the 6:2 diPAP experiment leftover 6:2 diPAP were extracted after 18 h.



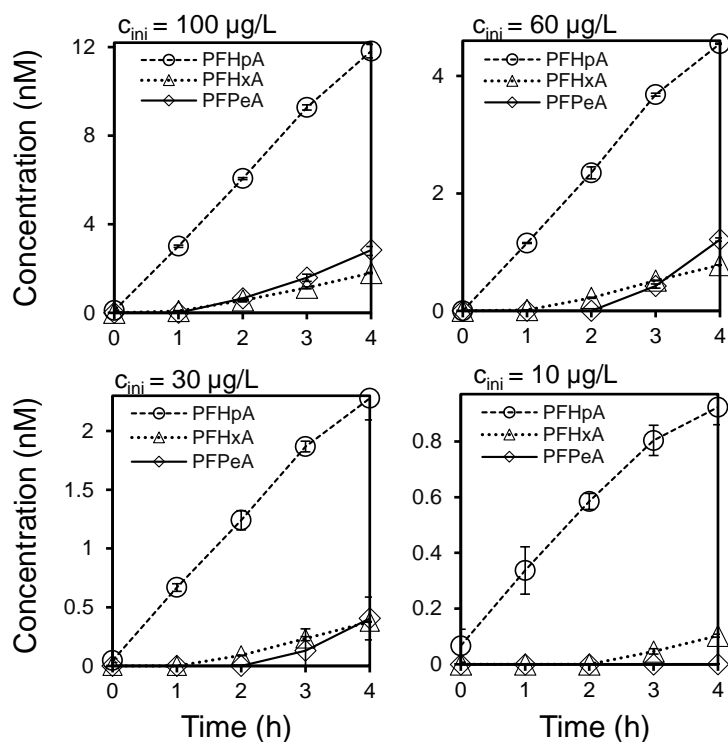
**Figure S 6:** (a) Anodic oxidation of PFHpA at a potential of 3 V in  $\text{NH}_4\text{FA}$  buffer over 18 h ( $c_0 = 10$  nM). The mass balance (gray circles) was calculated with molar concentrations according to  $\text{MB} = \Sigma([\text{C}_4\text{-C}_7 \text{ PFCAs}]) / [\text{PFHpA}]_{\text{initial}}$ . Error bars correspond to the standard deviation of triplicates. (b) First-order decay of PFHpA ( $k_{\text{obs,PFHpA}} = 0.034 \text{ h}^{-1}$ ) over the first 6 h.



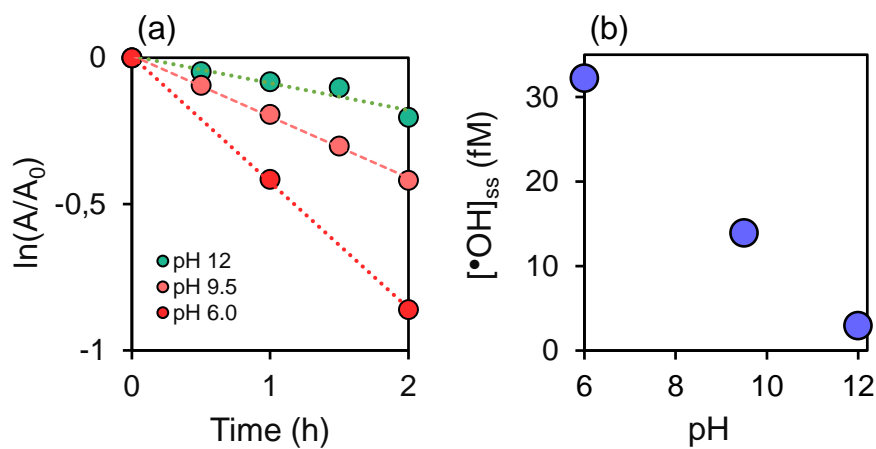
**Figure S 7:** Fluorine fraction (mol fluorine per molecule divided by initial mol fluorine in 6:2 diPAP) in percent of PFHpA, PFHxA, PFPeA, and 6:2 diPAP after 18 h of anodic oxidation at potentials of 3 V, 2.5 V and 2 V in  $\text{NH}_4\text{FA}$  electrolyte. Note: PFBA was not detected during anodic oxidation.



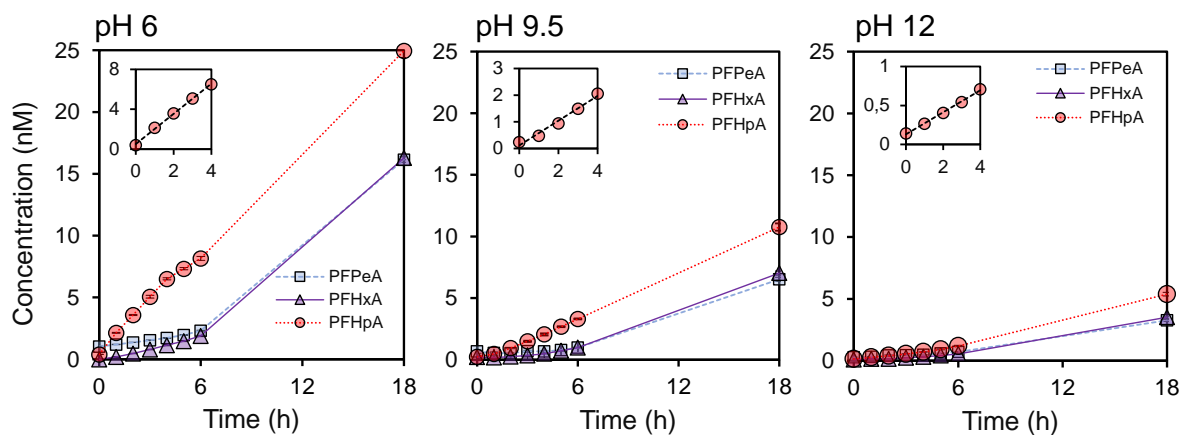
**Figure S 8:** Anodic oxidation of 6:2 diPAP over 18 h at potentials of 3 V, 2.5 V and 2 V in  $\text{NH}_4\text{FA}$  electrolyte at pH 6. Error bars correspond to the standard deviation of triplicates. Inlets are showing the linear behavior of PFHpA formation in the first four hours.



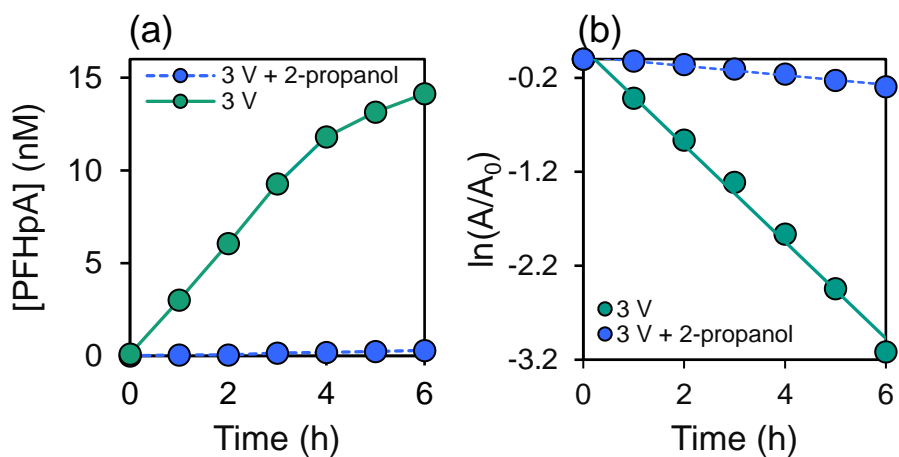
**Figure S 9:** Formation of PFHpA, PFHxA and PFPeA from anodic oxidation of 6:2 diPAP at different initial concentrations at a potential of 3 V in  $\text{NH}_4\text{FA}$  electrolyte at pH 6. PFBA was not detected. Error bars correspond to the standard deviation of duplicates. Note: The x-axes are scaled to PFHpA.



**Figure S 10:** (a) Pseudo first-order degradation of TPA during anodic oxidation at different pH-values. (b) Calculated steady state  $\cdot\text{OH}$  concentration vs electrolyte pH.

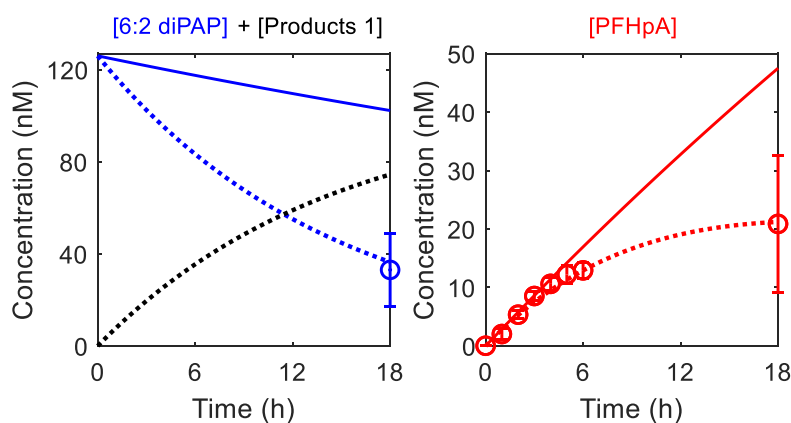


**Figure S 11:** Anodic oxidation of 6:2 diPAP over 18 h at a potential of 3 V at pH 6, pH 9.5 and pH 12 in  $\text{NH}_4\text{FA}$  electrolyte. Error bars correspond to the standard deviation of triplicates. Inlets highlight the linear behavior of PFHpA formation in the first four hours.



**Figure S 12:** (a) Formation of PFHpA from anodic oxidation of 6:2 diPAP at a potential of 3 V in  $\text{NH}_4\text{FA}$  electrolyte at pH 6 with and without 1% 2-propanol. (b) Degradation of TPA with and without 2-propanol.





**Figure S 13:** Results from the kinetic model of 6:2 diPAP and PFHpA during anodic oxidation at a potential of 3 V. Dots are experimental concentrations of three individual oxidation experiments, (left): extraction of leftover 6:2 diPAP, (right) PFHpA concentration. Error bars correspond to the standard deviation of the three individual experiments. Lines correspond to modeled concentrations over time. The first model (straight lines) assumes, that 6:2 diPAP is exclusively oxidized to PFHpA with the determined rate constant  $k_1 = 0.012 \text{ h}^{-1}$ . (eq. M1-2) Obviously, the 6:2 diPAP decay is too slow, while the formation of PFHpA does not match the experimental data showing, that there must be another process leading to degradation of 6:2 diPAP. Model 2 (dotted lines) is the model described by eq. M3-6 (for details see also SI section Equations. The rate constant  $k_3$  is calculated from curve fitting of the PFHpA data with eq. M4 using Matlab.  $k_1 = 0.012 \text{ h}^{-1}$  and  $k_2 = 0.034 \text{ h}^{-1}$  (determined from the PFHpA degradation experiment, see Figure S6b). This model can predict the experimental data much better (6:2 diPAP in extracts and PFHpA formation). However, since the PFHpA concentration after 18 h was not robust the initial rates approach was used instead.

#### Model 1

$$[\text{diPAP}]_t = [\text{diPAP}]_0 \cdot e^{-k_1 t} \quad (\text{M1})$$

$$[\text{PFHpA}]_t = 2 [\text{diPAP}]_0 \cdot (1 - e^{-k_1 t}) \quad (\text{M2})$$

#### Model 2

$$[\text{diPAP}]_t = [\text{diPAP}]_0 \cdot e^{-(k_1+k_3)t} \quad (\text{M3})$$

$$[\text{PFHpA}]_t = 2[\text{diPAP}]_0 \cdot \frac{k_1}{k_2 - k_1 - k_3} \cdot (e^{-(k_3+k_1)t} - e^{-k_2 t}) \quad (\text{M4})$$

$$[\text{P3}]_t = [\text{diPAP}]_0 \cdot \frac{k_3}{k_3+k_1} \cdot (1 - e^{-(k_3+k_1)t}) \quad (\text{M5})$$

$$[\text{P2}]_t = 2[\text{diPAP}]_0 - 2[\text{diPAP}]_t - [\text{P3}]_t - [\text{PFHpA}]_t \quad (\text{M6})$$

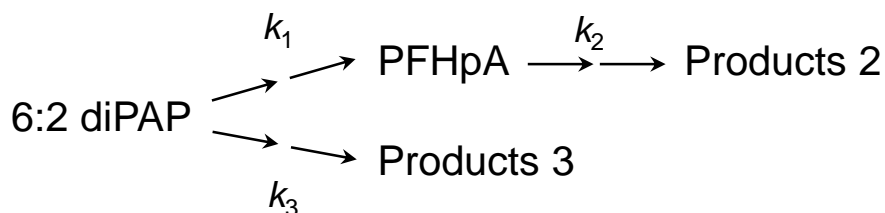
### Section S3 Calculations

For the calculation of products 2 after 18 h ( $[P2]_{18h}$ ) with the assumption of no parallel reaction pathway ( $k_3 = 0$ ) (see Figure 3) the following equations and a mass balance equation were used:

$$[\text{diPAP}]_t = [\text{diPAP}]_0 \cdot e^{-(k_1+k_3)t}$$
$$[\text{PFHpA}]_t = 2[\text{diPAP}]_0 \cdot \frac{k_1}{k_2 - k_1 - k_3} \cdot (e^{-(k_3+k_1)t} - e^{-k_2t})$$
$$[P2]_t = 2[\text{diPAP}]_0 - 2[\text{diPAP}]_t - [\text{PFHpA}]_t$$

With the experimental rate constants  $k_1$  and  $k_2$  from the separate PFHpA oxidation experiment (Figure S6a)  $[P2]_{18h}$  yields 5.5 nmol fluorine. This covers only 7.6% of the unknown part (Figure S5a) from the mass balance after 18 h of a typical anodic oxidation experiment of 6:2 diPAP at a potential of 3 V. Therefore, there must be a parallel reaction leading to the observed 6:2 diPAP decay.

## Section S4 Equations



**Figure S 14:** Proposed reaction scheme of the parallel and consecutive reactions during anodic oxidation of 6:2 diPAP.

All equations were set up according to Espenson<sup>1</sup>.

Differential equations:

$$\frac{d[\text{diPAP}]}{dt} = -k_1[\text{diPAP}] - k_3[\text{diPAP}] \quad (\text{S1})$$

$$\frac{d[\text{PFHpA}]}{dt} = 2k_1[\text{diPAP}] - k_2[\text{PFHpA}] \quad (\text{S2})$$

$$\frac{d[\text{P3}]}{dt} = k_3[\text{diPAP}] \quad (\text{S3})$$

$$\frac{d[\text{P2}]}{dt} = k_2[\text{PFHpA}] \quad (\text{S4})$$

Analytical solutions:

$$[\text{diPAP}]_t = [\text{diPAP}]_0 \cdot e^{-(k_1+k_3)t} \quad (\text{S5})$$

$$[\text{PFHpA}]_t = 2[\text{diPAP}]_0 \cdot \frac{k_1}{k_2 - k_1 - k_3} \cdot (e^{-(k_3+k_1)t} - e^{-k_2t}) \quad (\text{S6})$$

$$[\text{P3}]_t = [\text{diPAP}]_0 \cdot \frac{k_3}{k_3+k_1} \cdot (1 - e^{-(k_3+k_1)t}) \quad (\text{S7})$$

$$[\text{P2}]_t = 2[\text{diPAP}]_0 - 2[\text{diPAP}]_t - [\text{P3}]_t - [\text{PFHpA}]_t \quad (\text{S8})$$

- $[\text{diPAP}]$  = concentration of 6:2 diPAP ( $\text{mol L}^{-1}$ )
- $[\text{PFHpA}]$  = concentration of PFHpA ( $\text{mol L}^{-1}$ )
- $[\text{P3}]$  = concentration of product 3 ( $\text{mol L}^{-1}$ )
- $[\text{P2}]$  = concentration of product 2 ( $\text{mol L}^{-1}$ )
- $k_1, k_2, k_3$  = first-order rate constants ( $\text{s}^{-1}$ )
- $[\text{diPAP}]_0$  = initial 6:2 diPAP concentration ( $\text{mol L}^{-1}$ )

Note: In this model one mole 6:2 diPAP is transformed to one mole P3 and two moles PFHpA.

## References

1. Espenson, J. H., Chemical kinetics and reaction mechanisms. New York: McGraw-Hill **1995**, Vol. 102.

**Chapter 11 – personal contribution**

<b>Author</b>	<b>Author position</b>	<b>Scientific ideas %</b>	<b>Data generation %</b>	<b>Analysis &amp; interpretation %</b>	<b>Paper writing %</b>
Boris Bugsel	1	40	70	65	80
Oliver Nied	2	5	10	5	0
Markus Schmitt	3	35	20	30	0
Christian Zwiener	4	20	0	0	20
Title of paper:		Photochemical degradation of the perfluoroalkyl carboxylic acid precursor 6:2 diPAP			
Status in publication process:		Unpublished manuscript			

# 11 Photochemical degradation of the perfluoroalkyl carboxylic acid precursor 6:2 polyfluorinated dialkylated phosphate diester (6:2 diPAP) on mineral surfaces

Boris Bugsel<sup>1</sup>, Markus Schmitt<sup>1</sup>, Oliver Nied<sup>1</sup>, Christian Zwiener<sup>1</sup>

<sup>1</sup> Environmental Analytical Chemistry, Center for Applied Geoscience, University of Tübingen, Schnarrenbergstr. 94-96, 72076, Tübingen

Unpublished manuscript

## 11.1 Abstract

Per- and polyfluorinated substances are chemicals with widespread applications that have led to numerous contaminated field sites globally. In this work, the photochemical behavior under simulated sunlight of the PFCA precursor 6:2 diPAP sorbed on mineral phases (SiO<sub>2</sub>, SiO<sub>2</sub> (anatase and rutile) and FeOOH) which are typical components in soils was studied in aqueous suspensions. 6:2 diPAP was transformed by all three mineral phases. A pure suspension of FeOOH did not transform 6:2 diPAP, but the addition of 500 μM oxalate as electron donor activated the photo-Fenton process which led to a transformation of 6:2 diPAP. In all mineral phases, the first detected TP was 6:2 FTCA which could be further oxidized to PFCAs. The anatase suspension transformed 80 % of the initially introduced 6:2 diPAP to C<sub>5</sub>-C<sub>7</sub> PFCAs (C<sub>7</sub>>C<sub>6</sub>>C<sub>5</sub>) after 6 h of irradiation. Due to a relatively simple system and no chain shortening of the generated PFCAs, anatase suspensions are proposed as alternative method to characterize PFAS contaminations.

## 11.2 Introduction

The contamination of the environmental compartments such as groundwater, lakes and soil with hazardous, persistent chemicals is a major challenge. In the past years, the substance class of per- and polyfluorinated alkyl substances (PFAS) has gained attention due to its use in the industry and consumer products [1-3]. PFAS is a collective term for compounds which bear an alkyl chain where hydrogen atoms were either fully or partially replaced by fluorine atoms. The strong C-F bond makes PFAS thermally and chemically stable [4]. For the industry, those properties are very desirable as they make PFAS very durable. However, the combination of their heavy use in a variety of products with their longevity has resulted in a global distribution of PFAS in various compartments in the environment [5-8].

A major environmental contamination with PFAS is the region around Rastatt/Baden-Baden in southwest Germany. Several hundreds of hectares are contaminated with various PFAS. The contamination originates from the application of paper sludge that contained PFAS impregnated papers onto arable land. Over time, the PFAS have

migrated into groundwater, drinking water and plants [9-11]. In one of our earlier studies, we investigated the contaminants in four different soil samples from the region and found more than 61 PFAS from twelve different compound classes [12]. Among the contaminant substance classes were N-ethyl perfluorooctane sulfonamido ethanol diester (diSAmPAP), polyfluorinated phosphate diesters (diPAPs), perfluorinated carboxylic acids (PFCAs) and perfluorinated sulfonic acids (PFSAs).

From an environmental perspective, clustering PFAS into two subgroups is suggestive. The first subgroup contains all so-called precursors, i.e. PFAS that under environmental conditions can break down and form transformation products (TPs). If PFAS are considered non-degradable in the environment, they fall in the second subgroup of dead-end products. Among the dead-end products are the well-known PFAS classes PFCAs and PFSAs.

PFAS which fall into the precursor category are for example n:2 fluorotelomer sulfonic acids (FTSA) [13], n:2 fluorotelomer alcohols (FTOH) [14], diSAmPAP [15] and diPAPs [16] which were all shown to break down in the environment. However, the majority of these studies investigated the microbial transformation of precursors while their photochemical behavior as a further important transformation process in the environment remains unclear. A variety of studies have investigated the photochemical behavior of PFCAs under various conditions [17-19] and also a few precursors such as fluorotelomer alcohols (FTOHs) [20], fluorotelomer sulfonic acids (n:2 FTS) [21] and N-ethyl perfluorooctane sulfonamido acetate (EtFOSAA) [22], a TP of diSAmPAP [15]. The photochemical behavior of diPAPs, one of the major contaminants in the region in Rastatt/Baden-Baden, however was not investigated so far. Hence, the goal of this study is to investigate if photochemical processes on mineral surfaces play a role in the transformation of the precursor compound 6:2 diPAP. To the best of our knowledge, this is the first study to evaluate the photochemical behavior of 6:2 diPAP.

The photochemical decomposition of organic compounds in soil largely depends on the soil composition. Organic matter and inorganic species such as iron or manganese may act as quencher or sensitizer and can to a large extent affect photochemical reactions [23]. In this work, the photolysis on soil particles and on the pure mineral phases goethite (FeOOH), silicium dioxide (SiO<sub>2</sub>), anatase (TiO<sub>2</sub>) and rutile (TiO<sub>2</sub>)



was investigated in aqueous solutions to evaluate their possible individual contribution on the transformation of 6:2 / 6:2 diPAP. Silicium dioxide is a widespread mineral in soil and was previously reported as a photochemical catalyst for the removal of micropollutants [24]. Goethite was selected as it has been found to be the most abundant iron mineral in soils [25] and is known to be photochemically active [26]. TiO<sub>2</sub> was selected due to its high known photocatalytic activity [27-29] and an overall widespread occurrence, as Philippe et al. (2018) [30] determined concentrations of  $0.36 \pm 0.19$  mass percent TiO<sub>2</sub> in eight soils (minimum 0.07 and maximum 0.6 mass percent).

Both TiO<sub>2</sub> and goethite, the latter under the addition of a reducing agent such as oxalate, are known to form hydroxyl radicals (<sup>•</sup>OH) among other reactive oxygen species (ROS) in irradiated aqueous suspensions [31, 32] which can play a crucial role in environmental transformation processes [33].

All experiments were therefore performed in aqueous suspensions to achieve reliable and comparable results. We are aware that reactions in suspensions may greatly differ from those on dry or moist layers. However, a homogeneous distribution of the mineral or soil phases with an evenly distributed layer thickness during irradiation is crucial to achieve reliable results. Instead, we simplified the system and used aqueous suspensions that are easier to handle and are expected to produce more comparable results between different mineral phases.

Terephthalic acid (TPA) was introduced as an <sup>•</sup>OH probe molecule in every experiment. TPA is known to selectively react with <sup>•</sup>OH to hydroxyterephthalic acid (hTPA) and can hence be used to study the influence of <sup>•</sup>OH [34].

### 11.3 Material & Methods

#### **Chemicals and reagents**

Optima LC-MS grade methanol (MeOH), ammonium acetate (NH<sub>4</sub>Ac), formic acid (FA) and water were purchased from Fisher Scientific. Sodium dihydrogen phosphate (NaH<sub>2</sub>PO<sub>4</sub>) and titanium dioxide (TiO<sub>2</sub>, anatase and rutile) were obtained from Merck (Darmstadt, Germany). The authentic reference standard of bis[2-(perfluorohexyl)ethyl]phosphate (6:2/6:2 diPAP) was obtained from Toronto Research

Chemicals (North York, Ontario, Canada). Goethite (Bayferrox 920 Z) was purchased from Lanxess (Cologne, Germany) and washed with LC-MS grade water for five times. Terephthalic acid (TPA) was purchased from TCI.

### **Sample preparation**

All photochemical experiments were performed in the artificial sunlight chamber UVACUBE 400 (Hoenle UV Technology, Gräfeling, Germany). The chamber was equipped with a SOL 500 RF 2 light source and an H2 filter glass.

The mineral phase (20 mg) and soil (100 mg) were weighed into 100 mL glass vessels. To coat the particles, 20 mL of a 2.5 mg/L 6:2 diPAP solution were prepared in a volumetric flask. An aliquot of 10  $\mu$ L were withdrawn out of this solution, mixed with 990  $\mu$ L 90/10 MeOH/H<sub>2</sub>O (v/v) and diluted 100-fold which results in a theoretical concentration of 250 ng/L. The actual measured concentration was used to estimate the expected amount of TPs (see section data evaluation).

The rest of the volumetric flask was poured over the mineral phase/soil and the MeOH was evaporated by placing the vessel in an ultrasonic bath. Once the MeOH was fully evaporated, 100 mL Milli-Q water containing 10  $\mu$ M TPA was poured over the coated mineral phase and the vessel was again sonicated for 10 minutes. The resulting suspension was then stirred with a magnetic stirrer, the pH value adjusted with 0.1 and 1 M HCl/NaOH and allowed to equilibrate for 30 minutes in the darkness. The vessel was then placed in the artificial sunlight chamber and continuously irradiated and stirred with a magnetic stirrer. Since the evaporation in the sunlight simulator is considerable due to elevated temperature (29 °C), the evaporated water was gravimetrically determined and refilled before every sampling. The suspension was subsequently allowed to equilibrate for a minimum of two minutes.

For PFAS samples, 100  $\mu$ L of the suspension were mixed with 900  $\mu$ L MeOH in a 2 mL polypropylene (PP) tube. All samples were taken in duplicates. For TPA samples, 180  $\mu$ L were mixed with 20  $\mu$ L 10 mM NaH<sub>2</sub>PO<sub>4</sub> in a 200  $\mu$ L PP microinlet vial.

In order to correctly quantify the leftover precursor concentrations after 6 hours of irradiation, the vessels were placed in an oven at 70 °C overnight to evaporate the water. 100 mL 90/10 MeOH/H<sub>2</sub>O (v/v) were then poured on the dried particles and the vessel was sealed with aluminum foil and sonicated for 60 minutes in order to desorb

any precursors that might have sorbed to the particles or the glass. An aliquot was taken and diluted 1:100 with 90/10 MeOH/H<sub>2</sub>O (v/v). These samples are referred to as “t<sub>end</sub> extracts” in the results.

Both PFAS and TPA samples were centrifuged at maximum speed (PFAS samples: 13 000 rpm, 15 minutes; TPA samples: 8400 rpm, 15 minutes) prior to analysis, PFAS samples were furthermore diluted 1:10 with 90/10 MeOH/H<sub>2</sub>O (v/v).

### **TPA sample analysis**

TPA was measured with a 1260 HPLC on a diode array detector (DAD) (Agilent Technologies, Waldbronn, Germany). Chromatographic separation of TPA was achieved with a Phenomenex column (150 mm × 3 mm, particle size 4 μm, Synergi 4n polar RP 80 Å) with a flow rate of 0.5 mL/min using an isocratic method with eluent A (90/10 H<sub>2</sub>O/MeOH + FA, pH 3) and B (MeOH) (80/20).

### **PFAS sample analysis (target screening)**

6:2 diPAP and its TPs were quantified using a 1290 Infinity II HPLC (Agilent Technologies, Waldbronn, Germany) coupled to a 6470 triple quadrupole mass spectrometer operated in negative electrospray ionization mode (Agilent Technologies, Santa Clara, USA). To separate the analytes, a Waters Acquity UPLC BEH C18 column (2.1 mm x 100 mm) with a particle size of 1.7 μm and a flow rate of 0.4 mL/min was used. The column compartment was set to 60 °C. Eluent A (95/5 H<sub>2</sub>O/MeOH + 2 mM NH<sub>4</sub>Ac) and eluent B (5/95 H<sub>2</sub>O/MeOH + 2 mM NH<sub>4</sub>Ac) were used for gradient elution. The gradient started with 40% B, followed by a linear increase to 60% B after 1 min and another linear increase to 100% B after 3.5 min. 100% B were held until 6 min, the column was afterwards equilibrated until 7.5 min. 5 μL of the sample were injected. Mass transitions and collision energies of the analytes are given in Table S1.

### **PFAS sample analysis (non-target screening)**

All samples were also screened for possible TPs by high resolution mass spectrometry (HRMS). Here, a 1260 HPLC (Agilent Technologies, Waldbronn, Germany) was used coupled to a 6550 QTOF (Agilent Technologies, Santa Clara, USA) using negative electrospray ionization. Further details on the measurement including gradient and

source parameters are given in the supporting information. A screening method that was described in one of our earlier publications (Bugsel & Zwiener, 2020 [12]) was used to determine unknown PFAS. Briefly, the molecular feature extraction (MFE) algorithm of the qualitative analysis B10.0 software from Agilent Technologies was used to determine 1) homologous series with -CF<sub>2</sub>- repeating units and 2) PFAS that are present in the OECD database by comparing their exact masses with the measured accurate masses. However, no other compounds than the ones quantified using the target screening approach were detected.

### Data evaluation

The product curves show the formation of the quantified TPs as individual lines (colored circles), the maximum theoretical concentration as black dotted line (2-fold the initial measured molar diPAP concentration), the sum of all TPs (white circles) and for the last time point the sum of all TPs plus 2-fold the extracted diPAP concentration as a red dot. Due to the double chain structure, one mole diPAP can produce two mole single-chained TPs. The difference between the red dot and the black dotted line hence can be regarded as the unexplained fraction.

Steady-state •OH concentrations •[OH]<sub>ss</sub> were calculated according to

$$[\bullet OH]_{ss} = \frac{k_{obs,TPA}}{k_{\bullet OH,TPA}}$$

where  $k_{obs,TPA}$  is the observed pseudo first order rate constant from the TPA degradation and  $k_{\bullet OH,TPA} = 4.4 \cdot 10^9 \text{ M}^{-1}\text{s}^{-1}$  is the bimolecular reaction constant of TPA with •OH [34].

### 6:2 diPAP sampling

6:2 diPAP is very hydrophobic with a water solubility of about 1 µg/L [35], the precursor is hence expected to be dominantly sorbed to the mineral phase. A correct quantification of 6:2 diPAP throughout the experiment would therefore require a consistent sampling of the suspension. Regardless if the samples were irradiated or not, a decline of the 6:2 diPAP concentration could be observed in pre-experiments

over time (shown as an example for the goethite mineral phase in the supporting information).

In order to gain insights on the influence from the irradiation, dark control experiments were performed and showed a significant decline in the 6:2 diPAP concentration over time. However, no transformation products could be observed. This decline could be a result of a) either degradation with undetermined TPs in the dark or b) aggregation processes of the mineral particles over time, resulting in less samples particles and therefore a lower concentration. To verify whether this decline was due to degradation or physical sedimentation processes, the correct diPAP concentration at the end of the experiment (“ $t_{\text{end}}$  extracts”) needed to be determined. We therefore determined and optimized recovery efficiencies for the used mineral phases by coating the mineral phase with 50  $\mu\text{g}$  6:2 diPAP and extracted the particles subsequently without irradiation. Best recoveries (89 %) were achieved with 90/10 MeOH/H<sub>2</sub>O (v/v) as extraction solvent. In all recovery tests, 90/10 MeOH/H<sub>2</sub>O (v/v) yielded higher recoveries than pure MeOH (data shown in supporting information).

With this improved recovery technique, 82 % of the initially spiked 6:2 diPAP could be recovered. This value lies in the same range as the recovery verification without irradiation (86.4 %  $\pm$  5.8 %, tested in triplicates). We therefore conclude that a) the observed decline of the diPAP concentration is only due to physical processes such as agglomeration or sedimentation that lead to less sampled particles and b) a decline of the diPAP concentration over time is not meaningful. We therefore focused on the  $t_{\text{end}}$  extracts only to measure the concentration of 6:2 diPAP. However, due to a much higher water solubility of possible TPs because of their single-chain structure, we do not expect this behavior to be true for TPs. Performing the experiment with perfluoroheptanoic acid (PFHpA) instead of 6:2 diPAP in combination with a mineral phase confirmed this as identical concentrations throughout the experiment were observed (for further information, see supporting information).

## 11.4 Results & Discussion

### Experiment overview

The following Table 1 gives a brief overview on the setups of the performed experiments and calculated  $[\bullet\text{OH}]_{ss}$ . The individual experiments are discussed in detail subsequently.

Table 1: Overview of performed experiments and detected steady-state  $[\bullet\text{OH}]$  concentrations

Mineral phase	Anatase	Rutile	Goethite	Goethite	SiO <sub>2</sub>	SiO <sub>2</sub>
concentration of mineral phase	20 mg / 100 mL	20 mg / 100 mL	20 mg / 100 mL	20 mg / 100 mL	100 mg/100 mL	100 mg/100 mL
$c_0$ diPAP	500 $\mu\text{g/L}$	500 $\mu\text{g/L}$	500 $\mu\text{g/L}$	500 $\mu\text{g/L}$	500 $\mu\text{g/L}$	500 $\mu\text{g/L}$
pH	6	6	4	4	6	6
Oxalate	-	-	500 $\mu\text{M}$	-	-	-
H <sub>2</sub> O <sub>2</sub>	-	-	-	-	-	10 mM
$k_{\text{TPA}}$ [ $\text{s}^{-1}$ ]	2.85E-3	7.50E-4	4.08E-4	2.78E-6	1.31E-5	1.04E-3
$[\bullet\text{OH}]_{ss}$ [M]	6.5E-13	1.7E-13	9.3E-14	6.3E-16	3.0E-15	2.4E-13

### Titanium dioxide particles as mineral phase

Photodegradation on TiO<sub>2</sub> particles showed an efficient and fast transformation of 6:2 diPAP for both anatase and rutile crystalline types (50  $\mu\text{g}$  6:2 diPAP on 20 mg TiO<sub>2</sub>, 10  $\mu\text{M}$  TPA, pH 6). High transformation rates for TPA confirmed the photocatalytic activity for both crystalline types ( $[\bullet\text{OH}]_{ss} = 6.5 \cdot 10^{-13}$  for anatase and  $[\bullet\text{OH}]_{ss} = 1.7 \cdot 10^{-13}$  for rutile). It is in good agreement with the literature that anatase has a higher activity than rutile as for example also determined by Zhang & Nosaka (2014) [29].

6:2 FTCA, 6:2 FTUCA, PFHpA, PFHxA and PFPeA were detected as 6:2 diPAP TPs. The product curves of anatase and rutile are shown in Figure 1 and Figure 2, respectively. In both crystalline types, 6:2 FTCA reached its maximum concentration after 1 h (anatase: 100 % transformation; rutile: 112 % transformation). The subsequent behavior of 6:2 FTCA however is considerably different: Once the maximum 6:2 FTCA concentration was reached after 1h, 6:2 FTCA is only slowly degraded in the rutile suspension, but almost fully degraded after 2 h in the anatase

suspension. We expect this behavior to be a result of the hydrophobic properties and cluster and film formation that we observed in the rutile suspension but not in the anatase suspension. When irradiated,  $\bullet\text{OH}$  are generated directly on the surface of the  $\text{TiO}_2$  particles [29]. Since 6:2 diPAP was coated directly on the surface, a high fraction of  $\bullet\text{OH}$  is expected to react with 6:2 diPAP. The resulting oxidation product is then released into the bulk solution where it can only further react in the direct proximity to  $\text{TiO}_2$  particles. The homogeneous distribution of anatase particles in the bulk solution is expected to release  $\bullet\text{OH}$  more evenly than the rutile suspension, leading to a higher transformation of TPs which are located in the bulk solution. Furthermore, the cluster and film formation on the surface may lead to shading of the suspension.

Since for both anatase and rutile transformation rates  $\geq 100\%$  from 6:2 diPAP to 6:2 FTCA were achieved, TPs that are produced subsequently are necessarily an oxidation product of 6:2 FTCA. This needs to involve two chain-shortening steps to produce PFPeA. To investigate if this chain shortening takes place before or after the production of PFHpA, we performed the same experiment (20 mg anatase, pH 6) without 6:2 diPAP but PFHpA instead. Over 6 hours of irradiation, the concentration of PFHpA was stable and no PFHxA could be detected (data shown in supporting information). This confirms that PFCA chains are not shortened and different pathways produce PFHpA, PFHxA and PFPeA from 6:2 FTCA. The large gap between the maximum TPs and the sum of all TPs from the anatase experiment after 2 h furthermore suggests that an intermediate product between 6:2 FTCA and the PFCAs is not captured by our target and non-target analysis. After 6 h, the mass balance could be 82 % closed in the anatase experiment.

It needs to be considered that the TP curve in the rutile experiment interestingly exceeds the possible amount significantly (120 % 6:2 FTCA / 149 % total TPs after 1 h). This could be due to non-representative sampling of the initial diPAP concentration or a too high diPAP concentration in the glass vessel due to contamination. Even though all glassware and stirrers were always cleaned with methanol prior to the experiment, carryover due to the strong sorption of 6:2 diPAP to glassware might have happened here. The increased initial 6:2 diPAP concentration would then allow more TPs than expected.

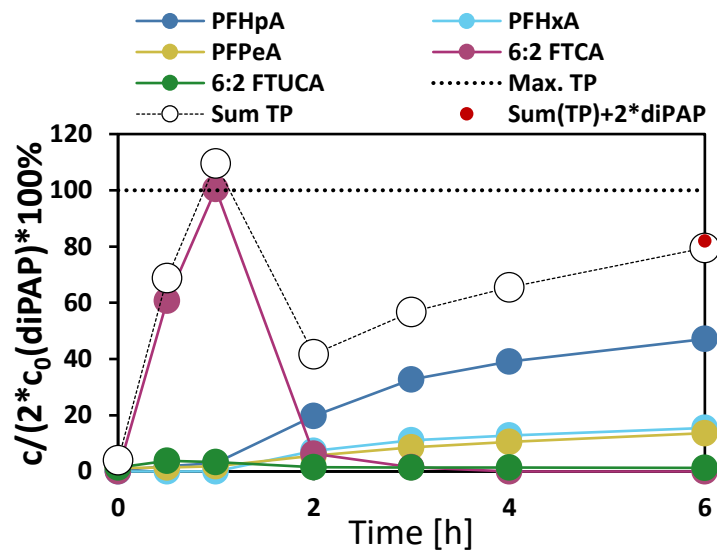


Figure 1: Degradation of 50 µg 6:2 / 6:2 diPAP on 20 mg anatase mineral phase.

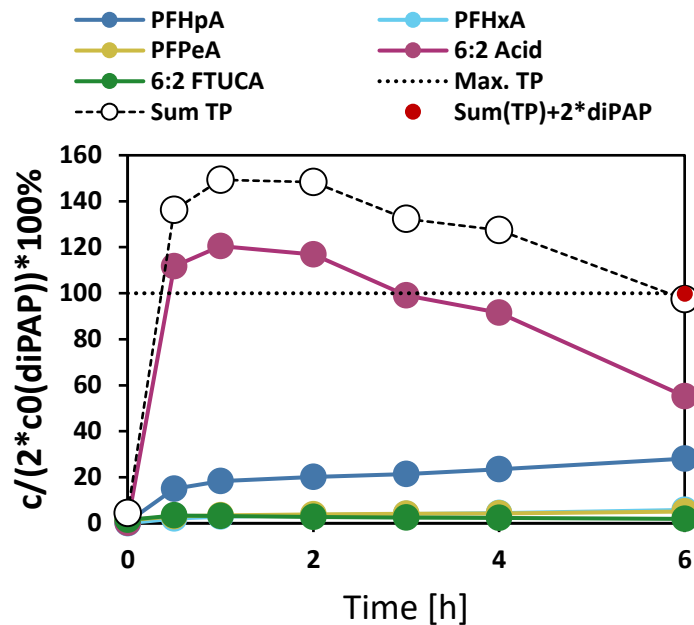


Figure 2: Degradation of 50 µg 6:2 / 6:2 diPAP on 20 mg rutile mineral phase.

### Goethite particles as mineral phase

Goethite experiments were performed with 50 µg 6:2 diPAP coated on 20 mg goethite particles at pH 4. After 24 hours of irradiation, no TPs could be observed and 83 % of the initially spiked 6:2 diPAP could be extracted in the  $t_{\text{end}}$  extract. The same setup without irradiation did not results in detectable TPs either and 84 % of the initially spiked 6:2 diPAP was determined in the  $t_{\text{end}}$  extract (data shown in supporting information). This clearly indicates that a pure suspension of goethite is not reactive



and a transformation of 6:2 diPAP does not take place. The absence of  $\bullet\text{OH}$  was also confirmed by virtually no degradation of TPA ( $k_{\text{TPA}} \approx 0.01 \text{ h}^{-1}$ ).

We therefore performed the same experiment again but added 500  $\mu\text{M}$  oxalate to the system. Oxalate is well known to form a complex with Fe(III) where it acts as an electron donor and initiates the photo-Fenton process [32, 36], producing a variety of ROS. This setup resulted in a considerably higher transformation of TPA ( $k_{\text{TPA}} = 1.47 \text{ h}^{-1}$ ), indicating the presence of  $\bullet\text{OH}$  at  $[\bullet\text{OH}]_{\text{SS}} = 9.3 * 10^{-14} \text{ mol/L}$  and a formation of TPs from 6:2 diPAP.

Figure 3 shows the quantified TPs and the  $t_{\text{end}}$  diPAP extract for the setup with 50  $\mu\text{g}$  6:2 diPAP coated on 20 mg goethite, pH4, 500  $\mu\text{M}$  oxalate in 100 mL suspension for a total experiment duration of 24 h. The predominantly observed TP here was 6:2 FTCA, reaching its maximum concentration after 6 hours of irradiation. Further identified TPs are 6:2 FTUCA, PFHpA and PFHxA. The subsequent decline of 6:2 FTCA indicates a further oxidation with unidentified intermediate products: None of the other TPs is directly produced from 6:2 FTCA as the sum of all TPs declines after 6 h as well. Furthermore, after 24 h irradiation, the sum of all TPs account for 10 % of the initially spiked 6:2 diPAP concentration only. In combination with the  $t_{\text{end}}$  extracts, 43 % of the initially spiked 6:2 diPAP can be explained by the target analytes. We can hence conclude that a) a significant amount of TPs was produced as a further oxidation product from 6:2 FTCA and b) that significant amounts (33.4 %) of the initial 6:2 diPAP concentration were recovered in the  $t_{\text{end}}$  extract and therefore no full transformation occurred.

A repetition of the same setup at pH 6 confirms a strong pH dependency which is in good agreement with the findings from Mazellier & Sulzberger (2001) [37] who found that at pH 4 the highest sorption of oxalate on goethite was achieved. For TPA, we found half-life times of approximately 1 h at pH 4 and 6 h and pH 6 (data shown in supporting information) which confirms that much less  $\bullet\text{OH}$  are present at pH 6.

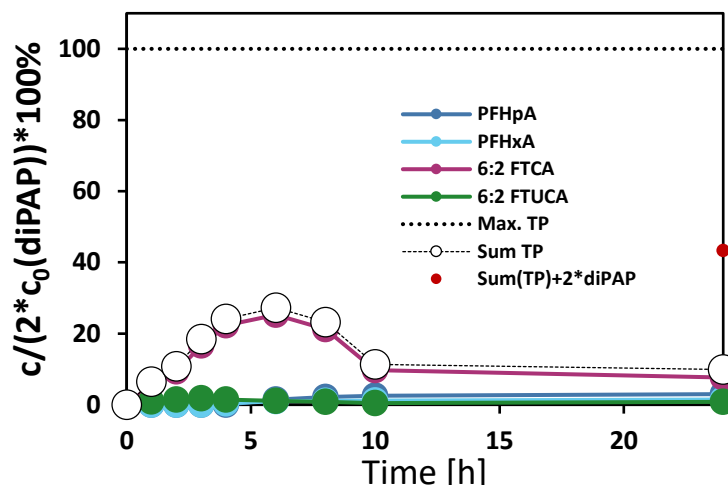


Figure 3: Product curves from the degradation of 50 µg 6:2 diPAP on 20 mg goethite mineral phase (pH 4, 10 µM TPA, 500 µM oxalate in 100 mL suspension. Note that after the 10 h sample, the glass vessel was covered with a watch glass to prevent excessive evaporation).

### Silicium dioxide particles as mineral phase

Figure 4 a) shows the 6:2 FTCA production from 50 µg 6:2 diPAP on 100 mg silica particles at pH 6. Over 6 h, 45 % 6:2 diPAP are transformed to 6:2 FTCA. No other TPs were detected. We afterwards repeated the experiment with the same setup but added 10 mM H<sub>2</sub>O<sub>2</sub> to the system to investigate the influence of •OH. H<sub>2</sub>O<sub>2</sub> is known to photolytically degrade to •OH with wavelengths < 370 nm according to  $H_2O_2 + h\nu \rightarrow 2 \cdot OH$  [38]. This overlaps with the generated sunlight spectrum (see supporting information). The addition of 10 mM hydrogen peroxide to the experiment hence yielded a much higher production of •OH ( $[•OH]_{ss} = 3 \cdot 10^{-15}$  without H<sub>2</sub>O<sub>2</sub> and  $[•OH]_{ss} = 2.4 \cdot 10^{-13}$  with 10 mM H<sub>2</sub>O<sub>2</sub>). This significantly higher steady-state concentration of •OH is does however not significantly affect the transformation of 6:2 diPAP as the production of 6:2 FTCA is not affected (see Figure 2).

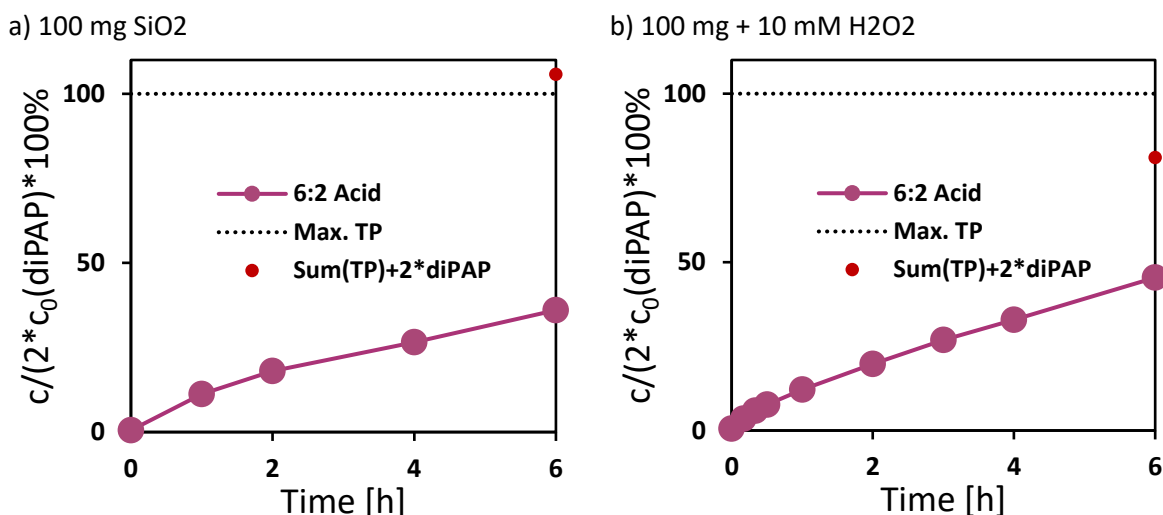


Figure 4: Formation of 6:2 FTCA from 50 µg 6:2 diPAP on 100 mg silica gel in 100 mL suspension at pH 6 (a) and the same setup with 10 mM H<sub>2</sub>O<sub>2</sub> (b)

From this behavior we can conclude that a) either •OH are not the main species which are responsible for the transformation of 6:2 diPAP since a higher [•OH]<sub>ss</sub> would then lead to a higher transformation of 6:2 diPAP or that b) 6:2 diPAP and TPA are not equally affected by the generated •OH. In the experiment with added H<sub>2</sub>O<sub>2</sub>, this can be explained as follows: With pKa values of 3.5 and 4.5, respectively, TPA is expected to be within the bulk solution since the experiment was performed at pH 6. The precursor 6:2 diPAP is sorbed on the silica particles where it therefore might be much less affected by the photogenerated •OH than TPA. This is different from the •OH which are produced by the mineral phases themselves, since they are produced directly on the surface they are expected to have a much larger effect on the 6:2 diPAP which are sorbed on the surface.

### Comparison of the investigated mineral phases

In all setups with an observed transformation of 6:2 diPAP the first generated TP was 6:2 FTCA. Further oxidation of 6:2 FTCA significantly occurred in both TiO<sub>2</sub> suspensions and to a smaller extent in the goethite suspension. Due to the slow reaction kinetics in SiO<sub>2</sub> suspensions, the experiment run time was insufficient to show if further oxidation of 6:2 FTCA would have occurred.

The results suggest that the photochemical degradation pathway of 6:2 diPAP on the investigated mineral phases produces 6:2 FTCA as a major intermediate TP which then can be further oxidized to produce dead-end PFCAs.

## **Antase suspension as a tool for PFAS characterization?**

The efficient and fast decomposition of 6:2 diPAP with anatase in a relatively simple system might be promising in the characterization of PFAS contaminations. After an oxidation time of 6 h, 82 % of the initial 6:2 diPAP could be recovered as TPs. As shown with an experiment using PFHpA instead of 6:2 diPAP, the produced PFCAs do not exhibit a chain-shortening. In this setup, we used a known precursor with a known concentration to produce TPs. The results look promising that this technique can also be applied to other (unknown) precursors. Here, we used an authentic standard to coat the particles, this could however as well be done with extracts from contaminated samples. Often times, PFAS contaminations are known, but an identification of the contaminants is lacking. Methods such as the extractable organic fluorine (EOF) or total oxidizable precursor (TOP) assay to estimate the overall contaminations exist and are well established, but do not always allow to conclude the chain length of precursors [39]. For example, Janda et al. (2019) [39] reported the production of C2-C9 PFCAs from the oxidation of 8:2 diPAP after the TOP assay. Here, we present a technique that produced C5-C7 PFCAs only from the oxidation of 6:2 diPAP. The applicability to other precursors needs to be verified in further experiments, that however is beyond the scope of this work.

## **Conclusions**

In this work, we presented the decomposition of 6:2 diPAP on various mineral phases. Under simulated sunlight, all investigated phases were able to decompose the precursor in aqueous suspensions. The comparability to moist and dry soil layers is currently investigated in our laboratories, however, the decomposition in the environment is expected to be slow and significantly vary depending on conditions such as soil composition, pH, moisture content and lighting conditions. Here, we showed that typical components of soil are able to degrade the precursor 6:2 diPAP under sunlight conditions in aqueous suspensions.

## **Acknowledgement**

The authors thank the state of Baden-Württemberg for funding the FluorTECH project.

## 11.5 References

1. Fujii, Y., K.H. Harada, and A. Koizumi, *Occurrence of perfluorinated carboxylic acids (PFCAs) in personal care products and compounding agents*. Chemosphere, 2013. **93**(3): p. 538-44.
2. Trier, X., K. Granby, and J.H. Christensen, *Polyfluorinated surfactants (PFS) in paper and board coatings for food packaging*. Environmental Science and Pollution Research, 2011. **18**(7): p. 1108-1120.
3. Lang, J.R., et al., *Release of Per- and Polyfluoroalkyl Substances (PFASs) from Carpet and Clothing in Model Anaerobic Landfill Reactors*. Environmental Science & Technology, 2016. **50**(10): p. 5024-32.
4. Buck, R.C., et al., *Perfluoroalkyl and polyfluoroalkyl substances in the environment: terminology, classification, and origins*. Integrated Environmental Assessment and Management, 2011. **7**(4): p. 513-41.
5. Janda, J., et al., *Robust trace analysis of polar (C 2-C 8) perfluorinated carboxylic acids by liquid chromatography-tandem mass spectrometry: method development and application to surface water, groundwater and drinking water*. Environmental Science and Pollution Research, 2019. **26**(8): p. 7326-7336.
6. Ingelido, A.M., et al., *Biomonitoring of perfluorinated compounds in adults exposed to contaminated drinking water in the Veneto Region, Italy*. Environment International, 2018. **110**: p. 149-159.
7. Strynar, M., et al., *Identification of novel perfluoroalkyl ether carboxylic acids (PFECAs) and sulfonic acids (PFESAs) in natural waters using accurate mass time-of-flight mass spectrometry (TOFMS)*. Environmental Science & Technology, 2015. **49**(19): p. 11622-11630.
8. Pan, Y., et al., *Worldwide Distribution of Novel Perfluoroether Carboxylic and Sulfonic Acids in Surface Water*. Environmental Science & Technology, 2018. **52**(14): p. 7621-7629.
9. Brendel, S., et al., *Short-chain perfluoroalkyl acids: environmental concerns and a regulatory strategy under REACH*. Environmental Sciences Europe, 2018. **30**(1): p. 9.

10. Biegel-Engler, A., et al., *Mitteilungen des Umweltbundesamtes zu per- und polyfluorierten Chemikalien (PFC) in Trinkwasser*. Bundesgesundheitsblatt Gesundheitsforschung Gesundheitsschutz, 2017. **60**(3): p. 341-346.
11. Muschket, M., et al., *Determination of transformation products of per-and polyfluoroalkyl substances at trace levels in agricultural plants*. Journal of Chromatography A, 2020: p. 461271.
12. Bugsel, B. and C. Zwiener, *LC-MS screening of poly-and perfluoroalkyl substances in contaminated soil by Kendrick mass analysis*. Analytical and Bioanalytical Chemistry, 2020. **412**: p. 4797-4805.
13. Wang, N., et al., *6:2 fluorotelomer sulfonate aerobic biotransformation in activated sludge of waste water treatment plants*. Chemosphere, 2011. **82**(6): p. 853-8.
14. Wang, N., et al., *8-2 fluorotelomer alcohol aerobic soil biodegradation: pathways, metabolites, and metabolite yields*. Chemosphere, 2009. **75**(8): p. 1089-96.
15. Benskin, J.P., et al., *Biodegradation of N-ethyl perfluorooctane sulfonamido ethanol (EtFOSE) and EtFOSE-based phosphate diester (SAmPAP diester) in marine sediments*. Environmental Science & Technology, 2013. **47**(3): p. 1381-9.
16. Liu, C. and J. Liu, *Aerobic biotransformation of polyfluoroalkyl phosphate esters (PAPs) in soil*. Environmental Pollution, 2016. **212**: p. 230-237.
17. Hori, H., et al., *Efficient decomposition of environmentally persistent perfluorocarboxylic acids by use of persulfate as a photochemical oxidant*. Environmental Science & Technology, 2005. **39**(7): p. 2383-2388.
18. Vaalgamaa, S., et al., *Photochemical reactivity of perfluorooctanoic acid (PFOA) in conditions representing surface water*. Science of The Total Environment, 2011. **409**(16): p. 3043-8.
19. Wang, Y., et al., *Photochemical degradation of environmentally persistent perfluorooctanoic acid (PFOA) in the presence of Fe(III)*. Chinese Chemical Letters, 2008. **19**(3): p. 371-374.
20. Gauthier, S.A. and S. Mabury, *Aqueous Photolysis of 8:2 Fluorotelomer Alcohol*. Environmental Toxicology and Chemistry, 2005.

21. Jin, L., C. Jiang, and P. Zhang, *Photochemical decomposition of 1H, 1H, 2H, 2H-perfluorooctane sulfonate (6: 2FOTS) induced by ferric ions*. *Journal of Environmental Sciences*, 2017. **51**: p. 120-127.
22. Plumlee, M.H., K. McNeill, and M. Reinhard, *Indirect photolysis of perfluorochemicals: hydroxyl radical-initiated oxidation of N-ethyl perfluorooctane sulfonamido acetate (N-EtFOSAA) and other perfluoroalkanesulfonamides*. *Environmental Science & Technology*, 2009. **43**(10): p. 3662-3668.
23. Balmer, M.E., K.-U. Goss, and R.P. Schwarzenbach, *Photolytic Transformation of Organic Pollutants on Soil Surfaces An Experimental Approach*. *Environmental Science & Technology*, 2000. **34**(7): p. 1240-1245.
24. Qu, R., et al., *Hydroxyl radical based photocatalytic degradation of halogenated organic contaminants and paraffin on silica gel*. *Environmental Science & Technology*, 2018. **52**(13): p. 7220-7229.
25. Scheinost, A.C., *Metal oxides*, in *Encyclopedia of Soils in the Environment*. 2005, Elsevier Academic Press. p. 428-438.
26. Mazellier, P. and M. Bolte, *Heterogeneous light-induced transformation of 2, 6-dimethylphenol in aqueous suspensions containing goethite*. *Journal of Photochemistry and Photobiology A: Chemistry*, 2000. **132**(1-2): p. 129-135.
27. Moma, J. and J. Baloyi, *Modified Titanium Dioxide for Photocatalytic Applications*, in *Photocatalysts-Applications and Attributes*. 2018, IntechOpen.
28. Linsebigler, A.L., G. Lu, and J.T. Yates Jr, *Photocatalysis on TiO<sub>2</sub> surfaces: principles, mechanisms, and selected results*. *Chemical Reviews*, 1995. **95**(3): p. 735-758.
29. Zhang, J. and Y. Nosaka, *Mechanism of the OH radical generation in photocatalysis with TiO<sub>2</sub> of different crystalline types*. *The Journal of Physical Chemistry C*, 2014. **118**(20): p. 10824-10832.
30. Philippe, A., et al., *Characterization of the natural colloidal TiO<sub>2</sub> background in soil*. *Separations*, 2018. **5**(4): p. 50.
31. Hirakawa, T. and Y. Nosaka, *Properties of O<sub>2</sub><sup>•-</sup>-and OH<sup>•</sup> formed in TiO<sub>2</sub> aqueous suspensions by photocatalytic reaction and the influence of H<sub>2</sub>O<sub>2</sub> and some ions*. *Langmuir*, 2002. **18**(8): p. 3247-3254.

32. Balmer, M.E. and B. Sulzberger, *Atrazine degradation in irradiated iron/oxalate systems: effects of pH and oxalate*. Environmental Science & Technology, 1999. **33**(14): p. 2418-2424.
33. Lee, Y. and U. Von Gunten, *Oxidative transformation of micropollutants during municipal wastewater treatment: Comparison of kinetic aspects of selective (chlorine, chlorine dioxide, ferrate VI, and ozone) and non-selective oxidants (hydroxyl radical)*. Water Research, 2010. **44**(2): p. 555-566.
34. Page, S.E., W.A. Arnold, and K. McNeill, *Terephthalate as a probe for photochemically generated hydroxyl radical*. Journal of Environmental Monitoring, 2010. **12**(9): p. 1658-65.
35. Wang, Z., et al., *Using COSMOtherm to predict physicochemical properties of poly-and perfluorinated alkyl substances (PFASs)*. Environmental Chemistry, 2011. **8**(4): p. 389-398.
36. Zuo, Y. and J. Hoigne, *Formation of hydrogen peroxide and depletion of oxalic acid in atmospheric water by photolysis of iron (III)-oxalato complexes*. Environmental Science & Technology, 1992. **26**(5): p. 1014-1022.
37. Mazellier, P. and B. Sulzberger, *Diuron degradation in irradiated, heterogeneous iron/oxalate systems: the rate-determining step*. Environmental Science & Technology, 2001. **35**(16): p. 3314-3320.
38. Bianco, A., et al., *Photochemistry of the Cloud Aqueous Phase: A Review*. Molecules, 2020. **25**(2): p. 423.
39. Janda, J., et al., *Closing the gap - inclusion of ultrashort-chain perfluoroalkyl carboxylic acids in the total oxidizable precursor (TOP) assay protocol*. Environmental Science: Processes & Impacts, 2019. **21.11**: p. 1926-1935.



## 11.6 Supporting Information

### Mass transitions in target Analysis

Table S 1: Mass transitions and collision energies in HPLC-QqQ method

Compound name	Precursor m/z	Fragment 1	CE 1	Fragment 2	CE 2
5:3 FTCA	341	236.9	15	216.8	15
6:2 FTCA	377	293	15	63	6
6:2 diPAP	789	443	30	97	30
6:2 FTUCA	357	293	15	243	15
PFBA	213	168.9	8	-	-
PFHpA	362.9	319	0	169	12
PFHxA	313	268.9	8	119	18
PFPeA	263	218.9	8	-	-

### Photochemical degradation experiments

Figure S 1 shows the measured spectrum in the used simulated sunlight generator

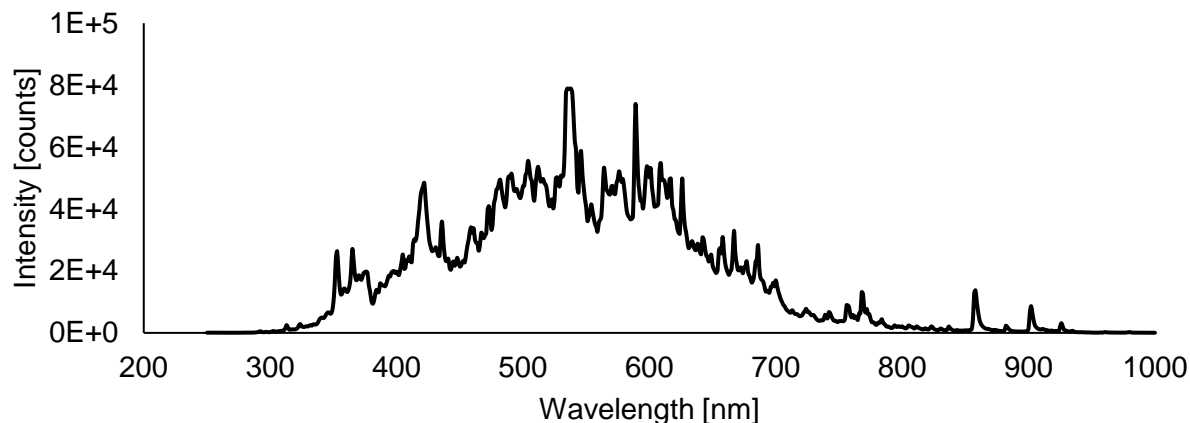


Figure S 1: Wavelength distribution of the light generated by the sunlight generator UVACUBE 400

### Recovery efficiencies

Figure S 2 shows the investigated recovery efficiencies for non-irradiated TiO<sub>2</sub> suspensions. 50 µg 6:2 diPAP on 20 mg TiO<sub>2</sub> were used to determine the recovery. Among the tested solvents and extraction techniques, 90/10 MeOH/H<sub>2</sub>O showed the highest recovery and was therefore used for further experiments. A second extraction step was also tested but did not produce higher recovery efficiencies. For the goethite suspension, the recovery efficiency with 90/10 MeOH/H<sub>2</sub>O was 86.4% ± 5.8%.

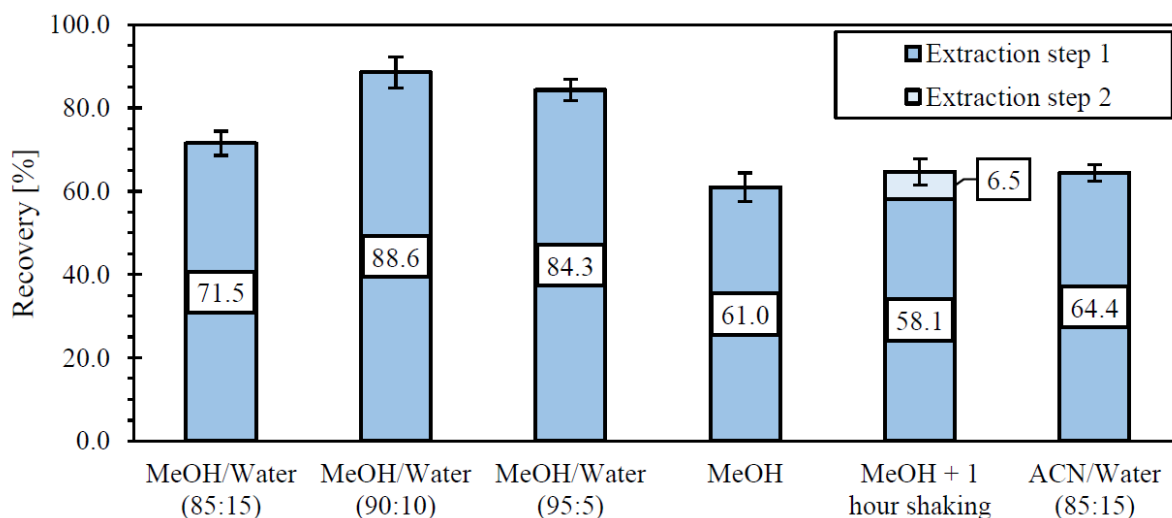


Figure S 2: Recovery efficiencies in from non-irradiated TiO<sub>2</sub> suspensions

### pH dependance with goethite

Figure S 3 shows the formation of TPs from 6:2 diPAP at pH values 4 and 6 (left) as well as the degradation of TPA at pH 4 and 6 (right)

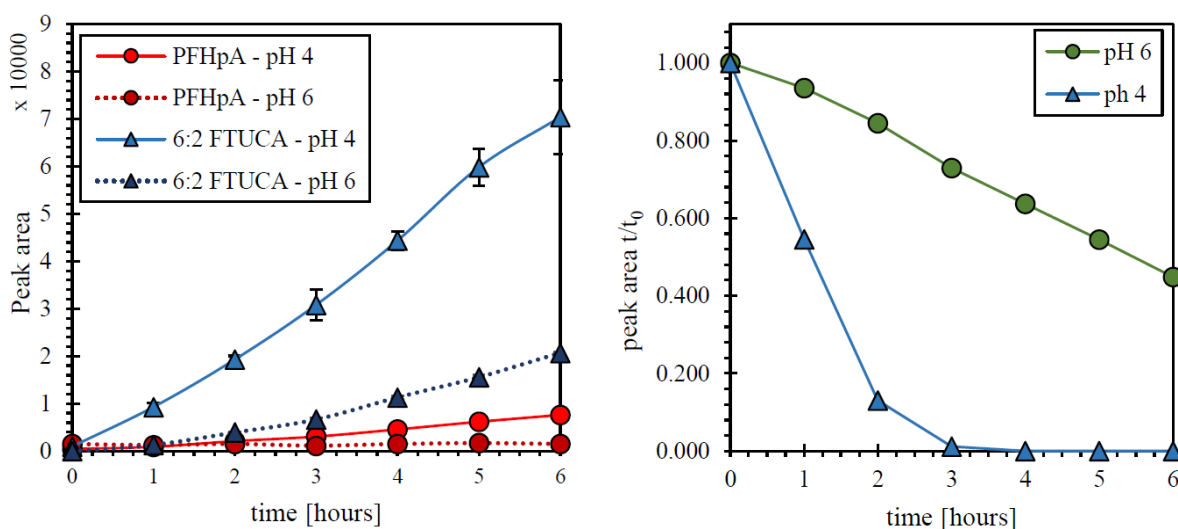


Figure S 3: Formation of TPs from 6:2 diPAP (left) and degradation of TPA (right) at pH 4 and pH 6 in the goethite experiment (error bars: s=1, n=3)

### Experiment with PFHpA (TiO<sub>2</sub>, pH 6)

Figure S4 shows  $c/c_0$  for PFHpA of an experiment with 20 mg TiO<sub>2</sub> and PFHpA ( $C_0 = 6.3 \mu\text{g/L}$ ) over 6 hours.

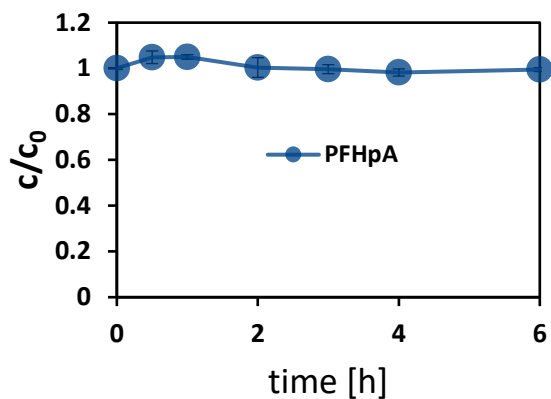


Figure S 4: PFHpA in TiO<sub>2</sub> suspension at pH 6

### diPAP concentration over time in goethite

Figure S5 shows the measured concentrations of 6:2 diPAP in an irradiated and dark control experiment with goethite (with no oxalate added). All TPs were < LOQ formed in both experiments.

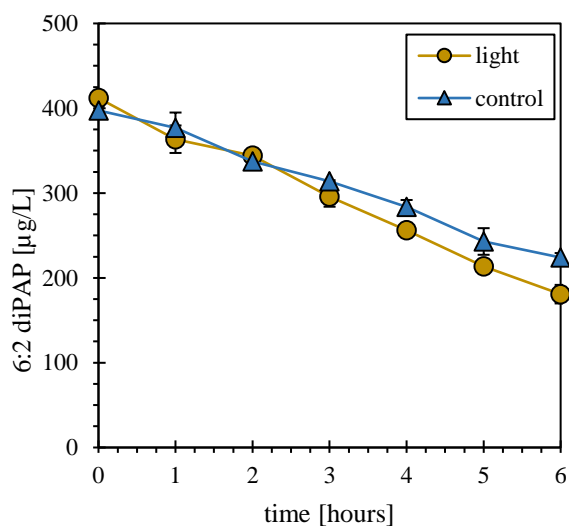


Figure S 5: Measured concentration of 6:2 diPAP in goethite experiments without oxalate (error bars:  $s=1$ ,  $n=3$ )